Damage Tolerant Design for Additive Manufacturing

An experimental study on the fatigue behaviour of stretch dominated AlSi10Mg multiple load path structures

M. Hofwegen

TUDelft   nlr

Damage Tolerant Design for Additive Manufacturing

An experimental study on the fatigue behaviour of stretch dominated AlSi10Mg multiple load path structures

by

M. Hofwegen

to obtain the degree of Master of Science
at the Delft University of Technology.
to be defended publicly on Tuesday March 30, 2021 at 13:00.

An electronic version of this thesis is available at `http://repository.tudelft.nl/`.

Preface

With this MSc. thesis I conclude my studies at the TU Delft. The last year in which I wrote this thesis has been an interesting and challenging period. Not only because of the circumstances, but also because of the many directions in which research on the damage tolerance of additive manufactured structures is possible. I am relieved to present this thesis, in which a contribution to this interesting topic is made. I therefore would like to thank my supervisors, Calvin Rans from TU Delft and Emiel Amsterdam from NLR, for their guidance, support and for pushing me in the right direction. I furthermore like to thank all colleagues from the NLR who helped me with the manufacturing and testing of the specimens. Without their help I would not be able to run such a complete and precise experimental programme.

I want to thank my parents for their support and understanding throughout my entire studies. They supported me in my decisions, which made me experience a lot and made my time in Delft unforgettable. I finally want to thank my family, friends, fellow-students and everyone I met on the way, for these amazing years.

M. Hofwegen
Delft, March 2021

Summary

To expand the use of additive manufacturing in aerospace towards more critical and more optimised applications, it is required to design parts in a damage tolerant context. Multiple load path structures are suitable for this, since these structures are likely to provide for damage tolerance through gradual failure. Moreover, the geometrical freedom offered by AM makes it possible to produce these parts. The use of multiple load paths fits in the framework of currently used design processes.

The goal of this thesis is to assess the damage tolerance of additive manufactured multiple load path structures by analysing the fatigue life and damage propagation of components with increasing redundancy. An experimental approach is chosen, whereby three types of AlSi10Mg specimens with 1, 9 and 81 parallel struts are fatigue tested and analysed for their fatigue life and failure characteristics. The specimens have an equal total cross-sectional area, meaning that the more redundant structures have thinner struts. Manufacturing related effects are analysed through the fatigue testing of an additional set of single struts, which makes comparison of different diameter single struts possible. The expected damage propagation mechanism is investigated by testing damaged specimens and through modelling the step-wise failure of the redundant structures.

The main findings of this study are as follows. A decreased fatigue life is found for multiple load path specimens with more but thinner struts. This shorter fatigue life is attributed to manufacturing related effects. The use of a smaller diameter leads to a shorter fatigue life, corresponding to the AM size effect. This is also shown with the fatigue testing of single struts. Also, production parameters play a role in the fatigue performance of single struts. Any effects originating from different crack growth lifes, cross-sectional deviations and the statistical size effect in fatigue were considered, but were found to be not prominent enough to explain the observed decrease in fatigue life for the more redundant structures.

The failure of the multiple load path structures showed a step-wise pattern, which was random throughout the cross-section of the specimens. With increasing number of struts, the time between the first visible and overall failure of the part increases, up to 45% of the total fatigue life for the specimens with 81 struts. The step-wise failure, fatigue life and crack growth period could be accurately modelled with the so-called cascading damage model, showing that statistical differences are the origin of this gradual failure pattern. Upon combining multiple struts, the scatter in the overall fatigue life of the structure decreases. This increases the predictability of the fatigue life. Testing specimens with initial damages furthermore showed a lower sensitivity to initial damages for the specimens with more struts.

Multiple load path structures are thus more damage tolerant due to the more gradual failure, less sensitivity to initial damages and increased predictability of the fatigue life. However, due to the decreased total fatigue life, the advantage over single load path elements with a high design margin, is not distinct in the design of aerospace parts.

Contents

List of Figures

List of Tables

List of Symbols and Abbreviations

Abbreviations

2D	Two-dimensional
3D	Three-dimensional
AM	Additive manufacturing
ASTM	American Society for Testing and Materials
CAD	Computer aided design
CPU	Central processing unit
CT	Computer tomography
DCPD	Direct current potential drop
DED	Direct energy deposition
DFAM	Design for additive manufacturing
DFM	Design for manufacturing
DT	Damage tolerance
EBM	Electron beam melting
FEM	Finite element method
FGM	Functionally graded materials
GD	Generative design
GP	Grace period
GR	Grace ratio
HIP	Hot isostatic pressing
ID	Specimen identifier
L-PBF	Laser powder bed fusion
LENS	Laser engineered net shaping
MILP	Mixed integer linear programming
MSD	Multiple site damage
NLR	Royal Netherlands Aerospace Centre
PDF	Probability density function
PBF	Powder bed fusion
SEM	Scanning electron microscope
SIMP	Solid isotropic material with penalty
SLM	Selective laser melting
SLS	Selective laser sintering
STD	Standard deviation
TO	Topology optimisation
UTS	Ultimate tensile strength
WAAM	Wire and arc additive manufacturing
YTS	Yield tensile strength

Symbols

a	Crack length [mm]
a_0	Initial crack length [mm]
A	Cross-sectional area [mm^2]
b	Power law exponent [-]
c	Power law constant [-]
C	Paris' law constant [m/(cycle MPa m$^{0.5}$)]
d	Diameter [mm]
D	Damage [-]
E	Young's modulus [GPa]
F	Force [kN]
I	Current [A]
K	Stress intensity factor [MPa m$^{0.5}$]
K_T	Stress concentration factor [-]
L	Length [mm]
m	Paris' law exponent [-]
M	Number of iterations [-]
n	Number of struts [-]
N	Number of cycles [cycles]
r	Voltage ratio [-]
R	Resistance [Ω]
S	Stress [MPa]
t	Thickness [mm]
V	Voltage [V]
$\varnothing$	Diameter [mm]
β	Geometry correction factor [-]
ε	Strain [-]
v	Poisson's ratio [-]
ρ	Resistivity [Ω m]

1

Introduction

In recent years, additive manufacturing (AM) has been gaining more attention for application in the aerospace industry and is used to produce final metal parts [1, 2]. This technique is promising for aerospace applications, since certain manufacturing constraints are removed. Because of this new geometrical freedom, more complex shaped parts can be created that satisfy the challenging load and weight requirements that are usual in the aerospace industry. Because parts can be better optimised for their function, lighter parts can be designed. Furthermore, the development of metal AM processes makes it possible to create these parts with high structural properties.

Although these lighter and more optimised geometries, of which an example is shown in figure 1.1, are a large advantage in terms of weight and material waste, it has led to a wide range of new design processes. Besides, the material properties in AM are different from those of the same alloys used in conventional manufacturing and can even vary throughout one part. The nature of the layer-wise production is responsible for this and has also led to different and new types of defects in AM parts [3]. Because of this and the relatively novelty of metal additive manufacturing, the behaviour of AM parts is not sufficiently known yet. As a consequence, the current use of AM parts in aircraft is limited to non-critical applications and high design margins are applied [3].
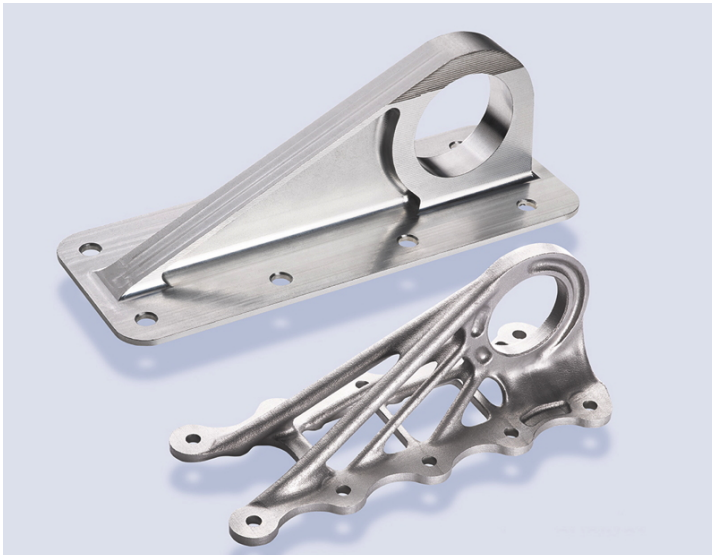
Figure 1.1: Redesigned Airbus A350 titanium cabin bracket (from GE [1])

---

[1]GE, *Laser Metalz: Bionic Design Is The Next Frontier For 3D Printing* [website], https://www.ge.com/news/reports/laser-metalz-bionic-design-next-frontier-3d-printing, accessed: 09/03/2021

To take full advantage of the possibilities of AM in aerospace, the use of AM parts should be expanded towards more critical and already more optimised structures, such as the primary aircraft structure. This shift in application is furthermore expected, seen the positive business case of AM parts in aerospace. Because of the lower part weight, possibility to decrease the number of parts in a structure due to higher part complexity, the decrease of scrap material and the investments done by large companies, the wide use of AM is of advantage for the aerospace industry [3].

The shift towards applications of AM in critical areas leads to structural integrity concerns. Failure in these critical areas of the aircraft structure can have catastrophic consequences. These safety concerns are even further increased because of the manufacturing-dependent material behaviour and new types of defects in AM. From a geometrical standpoint, the complexity of the parts designed for AM is increased. Structural optimisation has led to relatively thin and thus highly loaded elements, as visible in figure 1.1. Because of this, these parts are expected to have a lower tolerance with respect to damages. To safely operate aircraft that are equipped with these parts, future AM parts need to be designed such that the structural integrity is ensured.

Although extensive research is done in the fields of structural optimisation and the material and process parameters for AM, little attention is given to structural integrity through damage tolerance (DT) in the design for AM structures. Damage tolerant design of AM structures is thus a relatively new field. This is even more the case, since conventional approaches of DT do not directly apply for AM due to the production-dependent material behaviour and large variety of design methods.

The often observed trend of having a multistage structural optimisation scheme in design for AM, combined with the geometrical freedom offered by AM, however allows for the use of highly redundant structures. This is for example shown with the use of lattice and truss-like structures. These types of multiple load path structures have a potential to provide for structural integrity through a fail-safe mechanism. It is therefore needed to investigate whether these type of structures are more damage tolerant than conventional AM structures, and whether they can be made suitable to apply by using currently used design methods.

The aim of this thesis is to assess the damage tolerance of additive manufactured multiple load path structures, as more damage tolerant counterparts of single load path ligaments that are currently used in the design for AM. Therefore, the fatigue life and damage propagation of structures with increasing redundancy will be analysed in this thesis. An experimental procedure is used, which includes the testing and analysis of specimens with increasing number of parallel struts. Single elements are analysed to find the manufacturing related influences that occur upon splitting up a certain cross-sectional area into multiple load paths. A numerical model is used to test the theoretical damage propagation mechanisms, which can be compared to the individual failure events observed in the experiments. From the results of the experiments and model, the damage tolerance of multiple load path structures will be commented.

2

Literature Review

In order to assess the damage tolerance of additive manufactured multiple load structures, it is needed to understand the basic behaviour of AM material and the concept of damage tolerance. Therefore, the literature on the fatigue behaviour of AM specimens is reviewed. Moreover, the currently used design processes for AM are reviewed, since the new geometries and processes lead to new and different ways to apply damage tolerance. It is shown that in the currently used methods, damage tolerance does not play a major role. Multiple load path structures however have a potential for improved damage tolerance, due to their gradual failure in fatigue, increasing the time between visible damage and overall failure of the part. These multiple load path structure can be applied in the design for AM, by splitting up the cross-section of a single load path in multiple elements. The sections hereafter provide the reasoning behind the application of multiple load paths and the fit of this concept in currently used methods, next to the other above-mentioned points.

2.1. Additive Manufacturing Characteristics

Additive manufacturing is a set of manufacturing techniques that add material in a step-wise manner to create final products. It is different from classic manufacturing processes, where material is in general removed from a larger piece of material, also called subtractive manufacturing processes [4]. The term 3D-printing is also often used for AM, however not applicable to all possible AM production techniques. Key in the development of AM techniques is the use of computers, on which models can be created that define where material should be present and which can be sent to the machines to produce the part. Multiple AM techniques exist, which share certain characteristics, but also have fundamental differences, as described in section 2.1.1. As a result of these new manufacturing techniques, material properties also change, as described in this section. The design methods also differ from the methods used in conventional design, which will be discussed in section 2.2.

2.1.1. Production Methods

Various AM processes are developed in the last decades. These processes are subdivided into seven categories according to the ASTM standard F2792 [4]. These categories are binder jetting, direct energy deposition, material extrusion, material jetting, powder bed fusion, sheet lamination and vat photopolymerisation. These are applicable for metal, polymers or both. In the aerospace industry, powder bed fusion (PBF) and directed energy deposition (DED) are the most frequently used processes for metal parts [5, 6]. Metal material that is used in these processes and which is of interest for aerospace applications include aluminium, titanium and super alloys such as Inconel.

PBF systems melt a layer of powder selectively by using an energy beam [7]. After this, a new full layer of powder is added on top. Parts of this new layer are melted again, which are added to the part in process. Selective laser sintering (SLS), selective laser melting (SLM) and electron beam melting (EBM) are widely used techniques, with a difference in the degree of heating, resulting in sintering or melting, or the energy source [8, 9]. DED methods concentrate the energy source on a stream of material that is then melted and added to the part. Both powder and wire supplies can be used. Used techniques are laser engineered net shaping (LENS) and wire and arc AM (WAAM) [8, 9].

2.1.2. AM Fatigue Properties

Due to the production process, additive manufactured material behaves differently as compared to conventionally produced material. Reasons for this are amongst others the layer-wise production, different thermal histories and different surface smoothness. The mechanical properties of AM manufactured material are described by Yadollahi and Shamsaei [10]. They state that for bulk material, the mechanical properties for AM material are the same, as compared to specimens produced with the same material and using conventional manufacturing. The fatigue life is however lower for the specimens produced using AM. The degree in which the fatigue properties are lower for AM material differs throughout the literature, with Edwards et al. mentioning a 77% lower fatigue life for AM titanium alloy [11], whereas Spierings et al. state that the dynamic behaviour of 316L stainless steel is only slightly lower [12]. Lewandowski and Seifi also describe the mechanical properties of AM material [13]. They argue that if surface defects and residual stresses are controlled, the fatigue properties of the material can be similar to those of conventionally produced material. An interesting fact that Edwards et al. address, is that even though the fatigue performance of coupons is lower, designed parts do not fail as early as one would expect based on that [14]. It can thus be said that in general, the fatigue life of AM parts can be expected to be lower, but a large amount of scatter between different researches exists.

It is thus clear that the behaviour of AM material in fatigue is different, as compared to conventionally produced material. This can be explained by the origin of the production process. In the following subsections, it will be further explained how the different production parameters, post-processing steps but also different sizes of part geometry change the behaviour of the material.

Production related differences

By changing the production parameters, differences in fatigue life can be found for AM material [15]. The build direction of test specimen has an effect on the fatigue performance of these parts. In general, vertically built parts perform worse in terms of yield strength, ultimate strength and fatigue. This is contributed to a rougher surface due to more added layers, other void content and a changed microstructure [11, 16]. The microstructure is shown to be anisotropic for multiple materials, with the grains being elongated in the direction of the printing orientation, i.e. vertically elongated grains in a vertically built part [16–18]. In figure 2.1 the S-N curves of similar specimens of the same material are shown. It can be seen that the vertical (z) direction results in the shortest fatigue life.
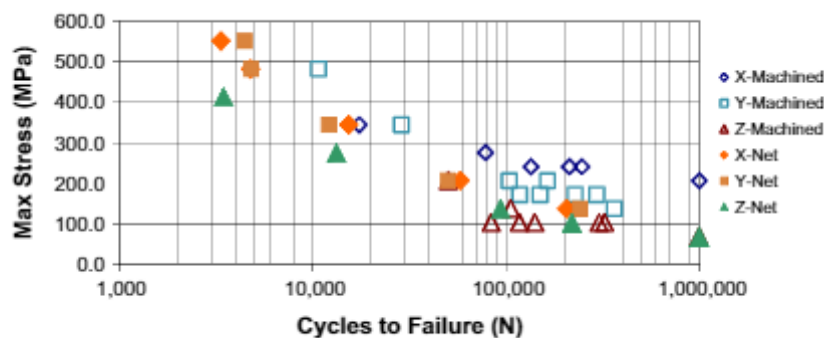
Fig. 6. Fatigue results $R = -0.2$, $Kt = 1.0$.

Figure 2.1: Effect of build direction on fatigue life (from Edwards et al. [11])

Aside from the build direction, the processing time is also of influence. Both Yadollahi et al. and Torries et al. report higher yield and ultimate strength for a longer interval between layer depositions [19, 20]. The longer interval tends to increase the cooling rate, loading to a finer microstructure. In fatigue, both mention better properties for shorter intervals, since less voids are present in these parts due to less extremities in temperature, while the bulk temperature is increased. In figure 2.2, it can be seen that the single built S-N curve is above the double built one, meaning that the shorter interval (since only one part is present) performs better in fatigue.

The effects on the microstructure of the material are material dependent. Most effects, as well as the above ones, are described for titanium alloys. For aluminium alloys, where AlSi10Mg is widely
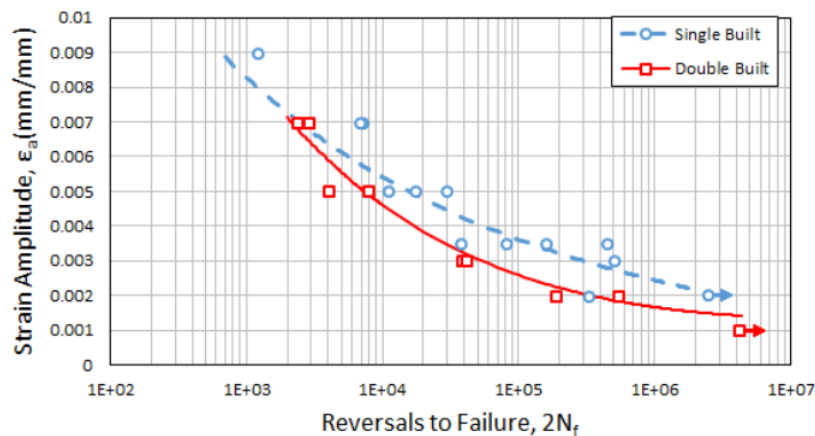
Figure 2.2: Effect of interval time on fatigue performance (from Torries et al. [20])

used, the presence of silicon changes the situation. As Uzan et al. describe, a continuous network of silicon forms a barrier for crack propagation resulting in a higher fatigue resistance for as-built AlSi10Mg material. If the silicon forms separated particles, which happens when heat treatments are applied, the interface with the aluminium matrix can act as an micro-crack initiation site [21]. Because of the finer microstructure, as-built and T6 heat treated samples perform the best in the tests performed by Uzan et al. The same effect of a homogeneous microstructure after T6 heat treatment is shown by Brandl et al. [22]. Brandl et al. name the effect on pores and non-melted powder as success factors for the heat treatment. This is substantiated by Romano et al. and Ch et al. who state that the effect of the microstructure is small compared to defects and pores in the fatigue life [23, 24].

Post-processing

Post-processing steps are often included to improve the performance of AM parts. Hot isostatic press-ing (HIP), heat treatment, chemical etching and surface machining are mentioned in literature [25–28]. Machining and chemical etching are meant to smoothen the surface, relieving stress concentration due to irregularities and thus improving fatigue crack initiation properties. HIP and heat treatments are to improve the microstructure (next to surface improvements obtained for HIP), mainly influencing crack growth. The anisotropy of the grains in the microstructure is shown to be reduced by heat treatment [17]. Persenot et al. show that the fatigue limit of struts in tension-tension fatigue can be increased by 50% by using chemical etching, and that it is increased by 100% if both etching and HIP are used , an effect also found by Van Hooreweder et al. and shown in figure 2.3 [27, 29].

Size effects

For AM produced parts, fatigue size effects exist that are the result of the production parameters and which lower the fatigue performance. Three effects can be distinguished when a different strut diameter is used, which are discussed hereafter. Firstly, the surface finish of larger diameter struts is smoother, which according to Barba et al. stabilises at thicknesses of 1.5 mm and bigger [16]. This effect can be explained by the fact that smaller curvatures are harder to model accurately by small lines that are used during the production.

The second effect is also related to accuracy. The deviation between actual produced cross-sectional size and modelled cross-section is larger for smaller struts, generally making them even smaller [30, 31]. This is different from the first effect, since not only surface roughness is affected and not only the modelling approach plays a role. Because most fatigue cracks initiate at the surface, the rougher surface resulting from these two effects leads to a better fatigue life for larger AM parts [31, 32].

The third effect is related to the microstructure of the struts. The thermal history of the struts has a large effect on the grain size of both titanium and aluminium alloy SLM parts, as shown by Dong et al. and Barba et al. [16, 30]. The bigger struts have a lower cooling rate, resulting in larger grains, which are bigger obstacles for fatigue crack growth. Besides, the bigger struts also have a lower void content due to the thermal history and less unmelted powder, leading to an increased fatigue life [30].
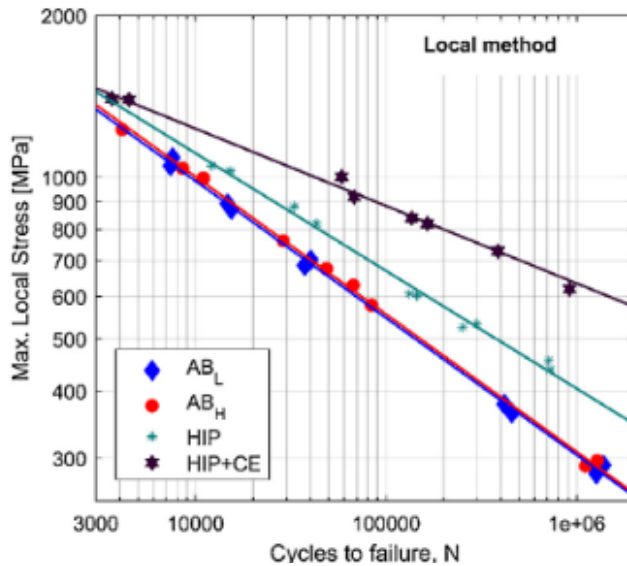
Figure 2.3: Effect of HIP and chemical etching on fatigue performance (from Van Hooreweder et al. [28])

2.2. Design Methods

In the design of products, parts are normally designed with the manufacturing process kept in mind, such that manufacturing problems are avoided and costs can be minimised. This is known as Design for Manufacturing (DFM) [33]. AM processes are different from traditional manufacturing techniques and have more extensive capabilities, like material and shape complexity and multi-scale design. Besides, production, planning, cost and quality control considerations are different [34]. Therefore, new methods and tools are needed and the concept of DFM should be tailored to AM, which is named Design for Additive Manufacturing (DFAM) [33]. The term DFAM is widely used in literature, but many different interpretations exist, depending on the level of detail that it is applicable to.

2.2.1. Design for Additive Manufacturing

Thompson et al. define three levels of abstraction for DFM [34]. The first level is related to tools, techniques and guidelines that are used in the design of a part, which is specific for processes, activities or for the part itself. The second level is the understanding of the relation between the design process and the manufacturing process, needed to improve the use and product specifications. The highest level is about the relationship between the designer and manufacturing, addressing the design process and practice. Thompson et al. mention that these levels of abstraction are also valid for AM and that DFAM has influence at each given level. Definitions given in literature often correspond to these levels.

The first level of abstraction is addressed by Bikas et al., who come up with a design framework that can be used in the design for AM [35]. Its purpose is to transform design processes from iterative to first time right. The framework is focused on AM manufacturing constraints and process parameters that should be taken into account in the design of a part, rather than giving a full process. Topics that are addressed are geometric features such as overhangs and angles, process parameters like build orientation and layer thickness, but also considerations as anisotropic material, surface finish, build time and accuracy. Other considerations at this level are given by Zhu et al., who stress the need for post-processing steps to smoothen the boundary of the part, but also mention the need for shape and sizing optimisation after using topology optimisation [36].

Klahn et al. give four criteria that make a part suitable to manufacture using AM, which can be seen as the second level of abstraction. These criteria are the possibility for integrated design, individualisation, lightweight design and efficient design [37]. These are requirements that must be met to make redesign for AM applicable, thus linking the design process to the manufacturing.

Vayre et al. propose a four step methodology to design for AM [38] and stress that it is needed to identify and respect manufacturing capabilities and constraints. The first step is to analyse the part

specification by defining the functional surfaces, design space and the specific behaviour. Then a single or multiple initial shapes are found, of which the method can vary. Automated procedures as topology optimisation as well as expert and guideline-based design are mentioned. The third step is to choose a set of parameters that are used in the fourth step, which is parametric optimisation, mostly done to minimise volume. The four step methodology can be seen as DFAM at the highest level of abstraction, with the other levels addressed within the steps that are given.

Another way to subdivide the field of DFAM is to look at the motivation for the redesign of parts and the technique used to design, which can be related to the second level of abstraction. Kamal and Rizza give three main techniques that are used in DFAM, which are topology optimisation (TO), part consolidation and part integration [39]. TO is the process to find an optimal structural configuration within a given space, which is optimised for a certain objective, load case, boundary conditions and constraints [36]. Part consolidation is the shift to producing one part that had to be made out of multiple parts with conventional manufacturing processes. Part integration is the addition of material on top of another part. It can be used to join multiple parts in a way comparable to welding, or it can be used in the repair of parts.

Gao et al. divide the existing design approaches for AM in two categories, which are the bottom-up and top-down approaches [7]. The bottom-up approaches are formed of uniform truss or unit cells, which are repeated to get the final shape of the product, also known as lattice structures. Lattice structures are spatial arrays of unit cells which have an open structure [8]. Both 3D and 2D patterns exist and these structures are supposed to have superior properties, such as high specific strength and stiffness. The top-down processes are based on topology optimisation, where an unique shape is determined. Examples for this are shown in figures 2.6, 2.7 and 2.9.

Based on these approaches, the field of DFAM can be subdivided as shown in figure 2.4. The top-down and bottom-up methods can be further subdivided, since different methods can be used to arrive at optimised shape. Different TO algorithms exist and also parametric optimisation is an option. Furthermore, other motivations exist to use AM, such as cost reduction [26]. However, in these cases the part is not specifically designed for AM.
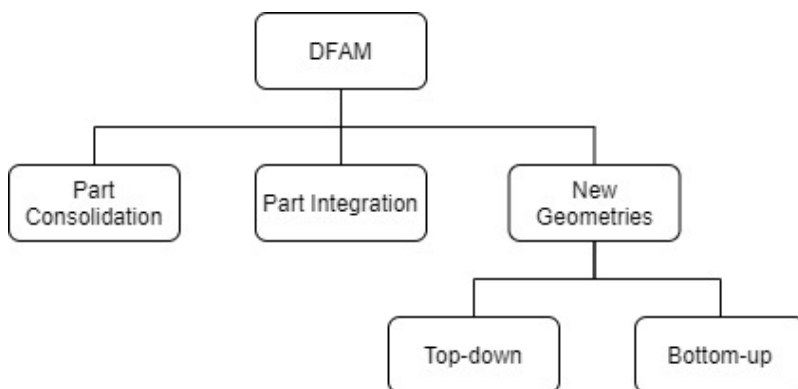
Figure 2.4: Structure of DFAM based on techniques and motivation

2.2.2. Currently Applied Design Methods

The described subdivision of DFAM is used here to show examples of current applications. Part consolidation and part integration are seen in real life applications and will be discussed first. Such a part integration application used for repair is shown by Optomec [40]. Large cost savings can be obtained if integrally bladed rotor parts, which are expensive to produce, can be repaired rather than replaced. A LENS process is used to add material directly to the part to be repaired. After adding the material, the part is heat treated and machined to finish it.

Part consolidation is seen in a jet engine fuel nozzle produced by GE for the CFM LEAP engine [41]. Instead of welding 20 different pieces together, AM is used to produce one single part at once. Earlier attempts to use traditional casting for this part failed due to the complexity of the part. Both cost and weight could be decreased using AM. Magerramova et al. describe a similar consideration in the design of an internally cooled turbine blade [42]. A design based on thermal and strength analysis is too hard to produce by casting, for which reason is switched to SLM.

Not only the motivations described in figure 2.4 are used to use AM, other motivations exist to switch to additive manufacturing. An example where the design of the part is unaltered, is described by Dehoff et al. [26]. A titanium bleed air leak detect bracket which was formerly produced by machining is now produced using AM, resulting in a cost reduction of 50 percent due to less material scrap. Mechanical testing showed that the properties of this part, classified as tertiary structure, is not less than before if a HIP heat treatment and surface finishing are done.

From the three subsections of DFAM, the new geometries are most often described in literature. Cheng et al. describe a bottom-up approach where a bracket is designed and optimised using a lattice structure [43]. A conventional bracket is taken and subjected to a TO density analysis. In that case all elements throughout the part are kept, but the optimised density is used to determine the thickness of the struts of the cubical cell elements. This results in a full lattice structure, but with varying strut thicknesses. At the locations where the highest density is present, the material is fully solid, as can be seen in figure 2.5.

Topology optimisation
The top-down approaches are a synonym for topology optimisation, where a completely new shape is found. TO applications are various in literature. EOS shows the design of an satellite antenna bracket [44]. The design process starts with the testing of an initial structure after which the material selection, process definition and initial material tests are done. The tested initial structure, which has a traditional design, is used as basis for the TO. The objective of the TO is to obtain optimum stress with rigidity and stability requirements. The resulting geometry is typical for TO models and consists of a bionic or organic shaped structure, as can be seen in figure 2.6.
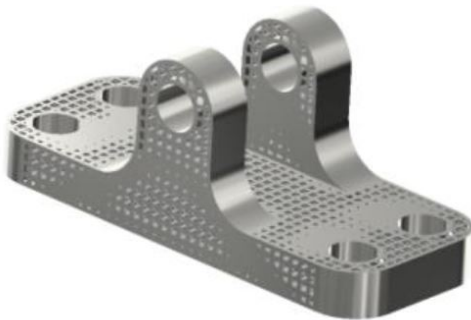
Figure 2.5: Bracket with optimised lattice structure (from Cheng et al. [43])

Figure 2.6: Satellite antenna bracket designed using TO (from EOS [44])

From this application, the structure of a TO process becomes clear. In general, the same steps can be identified in different TO examples. It starts with the definition of a load case and the space that is available to be filled with material, called the design space. This design space is discretised for a finite element model used during the optimisation. A set of parameters describing the elements in the design space is set up, of which some parameters get restrictions following from the requirements. Usually one parameter is chosen to optimise for, which is usually a parameter linked to the stiffness of the part, for example part stiffness or compliance. This is the objective of the TO. An algorithm is used to optimise for this parameter, after which non-critical material can be removed from the design space.

Walton and Moztarzadeh demonstrate TO for an EBM process with the example of a suspension bracket for a Formula Student racing car [45], following the structure as described above. A TO AM part, shown in figure 2.7, is seen as a lightweight alternative for a part designed for machining. Pre-processing of the original part for optimisation marks the start of the design process, followed by definition of the design space, boundary conditions and loading on the part. The optimisation is set up with shape controls, being maximum and minimum member thicknesses to prevent process defects affecting the component. The optimisation is then done with minimised weighted compliance as objective, with limitations on total mass and maximum stress, based on the fatigue limit of the material. The optimisation is carried out using a solid isotropic material with penalty (SIMP) method. SIMP is a TO procedure where the design space gets assigned densities that are updated in an iteration scheme.

These densities are usually found by optimising a parameter like the stiffness of the design space under a certain load condition [36]. The low density elements are filtered out, leading to an optimised shape. In this case, the threshold for this filtering was lowered during the design process, because connectivity problems were present. The lower loaded elements were thus still needed to create a continuous single part. The model of the optimised shape was transferred to CAD, to do modifications, such as rounding of the edges.

In the case described above, a SIMP method was used. Density based approaches such as SIMP are often described in literature. Another approach is the use of so-called evolutionary schemes, that gradually remove material based on a predefined criterion, which is analysed after doing random mutations in one iteration [36]. Both this and density approaches are prone to numerical inaccuracies. For this reason, a correction step is often included in the design process following the TO. In the case of Walton and Moztarzadeh the rounding of the edges in CAD is an example of this. Also the cases hereafter show modifications done after the TO.

The redesign of a helicopter gear box bracket is shown by Süß et al. [46]. Targets included weight saving, but also the consolidation of multiple parts. The TO is done for maximum stiffness. After the TO, the model is recreated in CAD to remove sharp edges, smooth the surface and to remove notches. Also, sharp features and surfaces that are impossible to manufacture are removed. The model before these post-processing steps is shown in figure 2.8.
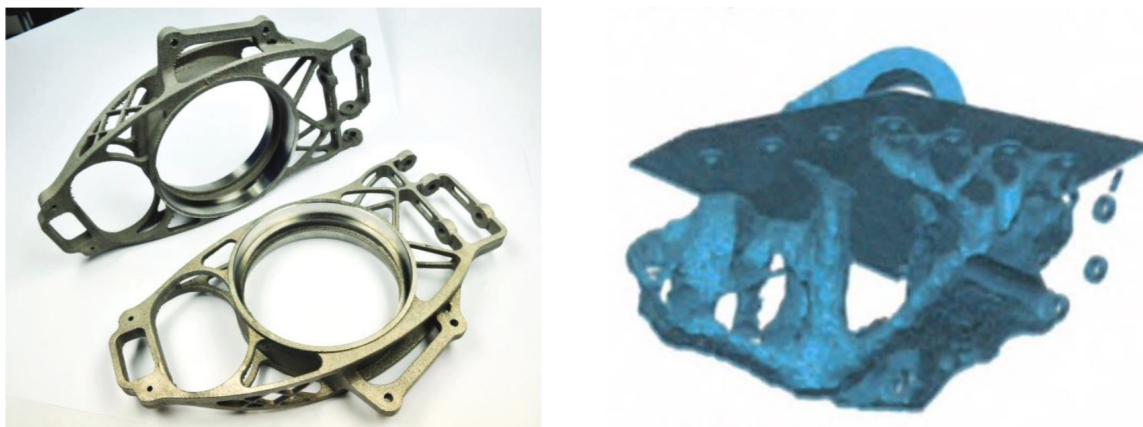
Figure 2.7: Suspension bracket (from Walton and Moztarzadeh [45])

Figure 2.8: Helicopter gear box bracket before surface smoothing (from Süß et al. [46])

Tomlin and Meyer show the redesign of an A320 nacelle hinge bracket, which had large stress concentrations and used a lot of material [47]. A weight saving of 64 % could be obtained even though the part was designed with stresses below the fatigue limit. Two design cycles including TO were needed, since the first results did not give the desired properties. One of the three rows of fasteners was not supported because the TO scheme converged towards a solution with low stiffness in that area. Therefore, a second iteration was done with a changed loading case. After this, the model was interpreted in CAD to shape and size optimise the part. In this case, an intervention is thus done both in-between and after the TO. The final shape compared to the original bracket can be seen in figure 2.9.

From the above cases it becomes clear that a designer interference step is needed in most of the cases, since the TO leaves a shape that is not ready-to-use. This interference step is to adjust parameters for the optimisation or to create a smoother surface. In some cases, major modifications are needed and the TO shape only serves as a first conceptual model. Another observation is that the described cases are redesigns of earlier existing parts. In these cases it is used to show the effectiveness of the new part, but it also shows the early stage that DFAM is in.

Generative design

A design process with more feedback to the designer is presented by Nagy et al. who describe the design of an AM cabin partition [48]. The overall shape of the structure is determined using generative design (GD). In this case, a model with a given amount of fixed connection points and beams connecting all points is set up. Then, using a genetic algorithm, connections are taken away until a given weight

(a)   (b)
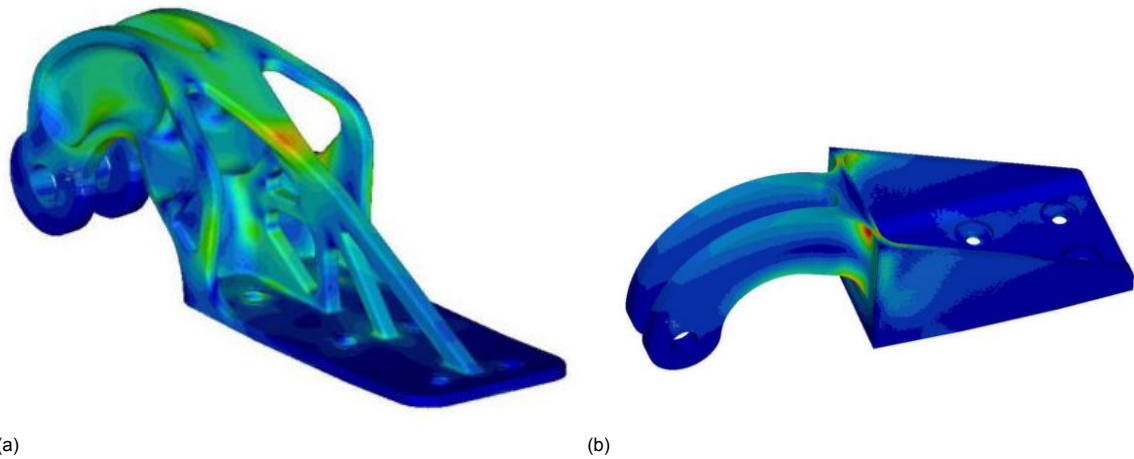
Figure 2.9: Nacelle hinge bracket: (a) AM bracket and (b) original bracket (from Tomlin and Meyer [47])

objective is reached, while adhering to strength requirements. Instead of finding one solution, the generative design gives multiple solutions back to the designer who can choose one design or restart the process with adjusted parameters. The possible models are subjected to FEM analysis to check the performance thereafter. Based on minimum weight and displacement, combined with a stress and material distribution constraint, a final design was chosen.

The chosen design formed the structural layout at the first level. The beams of which this design consist, are themselves subjected to a second optimisation. The beams are replaced by lattice structures of which the diameter of the ligaments is determined based on the local stress distribution. The design of an AM structure is thus not limited to one optimisation step, but can be done as a multilevel process, as described in the next subsection.
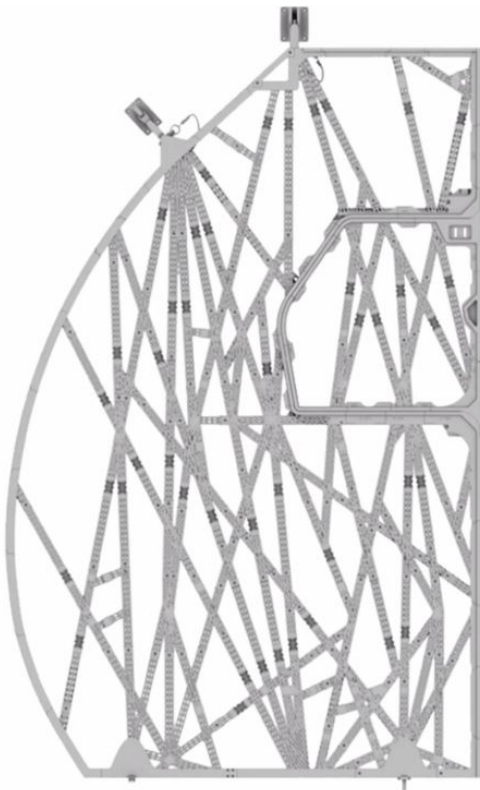
Figure 2.10: AM cabin partition (from Nagy et al. [48])

Multilevel design

Brandt et al. describe the multilevel design of an aerospace bracket [25]. A TO scheme is used to make a conceptual design for the bracket, after which this shape is recreated in CAD. Several new features are included based on design experience and are used to prevent local buckling, increase compressive strength and allow for manufacturing. These features are shown in figure 2.11. The geometry that is recreated is suitable for parametric optimisation, which means that the shape is fixed, but the dimensions such as strut diameter are optimised. In this design, two levels of optimisation are thus used, with a designer interference step in between.

A combination of TO and the use of cellular material is shown by Materialise[2]. The aerospace bracket that is designed using TO resulted in a part with small ligaments which can be seen as a typical TO shape. After this, solid parts and areas between ligaments are replaced by lattice structure that is then given a strut size according to the stress and stiffness distribution. The reason to do so is that it is claimed that lattice structures have similar stiffness while having less weight. This design is another example of a combined approach, in this case as a multilevel design with both top-down and bottom-up approached. The part is shown in figure 2.12.

Figure 2.11: Multilevel designed bracket (from Brandt et al. [25])

Figure 2.12: Topology optimised bracket with lattice structure (from Materialise[2])

Truss optimisation

Instead of interpreting a TO shape as a truss structure as done by Brandt et al. [25], it is also possible to start using trusses from the first stage of designing. He et al. improved the truss optimisation algorithm proposed by Dorn et al., where a domain with nodes and all possible links between those nodes is subjected to an optimisation scheme that removes links [49, 50]. Even though this is an relatively old algorithm, it has not been used often since the resulting geometries are rather complex [49]. The use of AM makes it however possible to produce these geometries. The idea of determining all possible members and than removing some of them is similar to the approach followed by Nagy et al., however the members are removed in another way. In figure 2.13, the method is explained.

He et al. improved the original algorithm by introducing the so-called 'member adding' [49]. By starting the process with only a reduced set of members instead of the full set, computational effort is saved. In an iterative scheme, a maximum virtual strain constraint for all members is checked and members are automatically added until this constraint is satisfied.

This new algorithm is further developed by He et al. in order to make it applicable to AM structures [51]. Constraints are added to solve the problem of limited member orientation due to the building direction of the part and to make sure all material is within the design space. Two methods are described to solve the build direction problem: the members with an inclination angle that can not be produced can be simply removed from the initial set of members before the start of the optimisation, or a cost

---
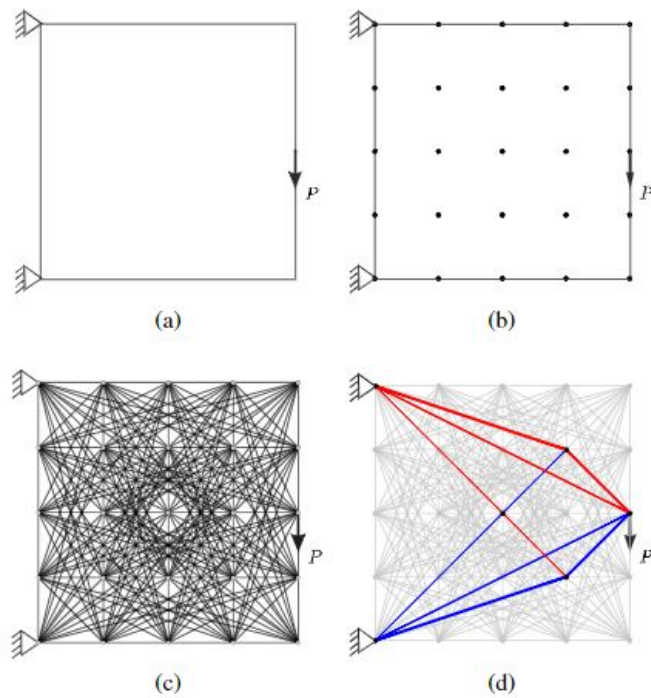
Figure 2.13: Steps in the optimisation method: (a) Design domain specification (b) Node discretisation (c) Add all possible members (d) Optimisation to find optimised structure (from He et al. [49])

penalty can be included for these members, since producing them with supports is possible but these supports need to be removed after production. The trusses are forced to fit in the design space by using linear constraints in case of concave design domains and by taking into account the strut radius in the optimisation scheme. An interactive step is included where a designer can intervene in the design process. Requirements that can not be mathematically expressed can also be included in that way. After this step in which members can be added or removed, the algorithm will restore the equilibrium.

The addition of constraints to a truss optimisation scheme is also mentioned by Fairclough et al. [52]. Mixed integer linear programming (MILP) is used to add constraints with the objective of creating less costly and easier to build parts. The suggested constraints can be on the number, length and cross-section of members and the layout at the nodes. The results from this method are comparable to those from topology optimisation tools such as SIMP. In figure 2.14 a structure designed with the model from He et al. is compared to the results of multiple SIMP models. It can be seen that the structures have a similar geometry. Interesting is the amount of CPU cost that is saved with this algorithm. In figure 2.15 an example is given of a structure that is designed with the truss optimisation tool, in this case a satellite antenna mounting bracket.

From the cases described here it becomes clear that there is no unique approach to design for AM. Combinations and multilevel approaches are possible and although different tools are present to design for new geometries, designers are needed to finalise the part in either TO or GD. As addition to these processes, truss optimisations seem promising, since they are less computationally extensive and make use of standard elements (struts) of which the properties can be better controlled.

2.3. Damage Tolerant Design of AM Structures

To be able to use AM manufactured parts for more critical applications in aircraft, a way must be found to include DT in the methods used in DFAM. Moreover, optimising structures leads to higher loaded and more critically loaded material. It is furthermore observed that DT does not play a major role in the design process of most AM designed parts with the current processes. In this section, the current state of DT in DFAM is analysed and methods are proposed to improve the DT of AM structures, after an introduction to the principle of damage tolerance is given.

	Layout optimization	SIMP (OC)	SIMP (MMA)	SIMP (MMA: tightened bounds)
Case	I	II	III	IV
Compliance	Diff = 0%	Diff = 0.655%	Diff = 7.14%	Diff = 3.56%
Nodal grid	16 × 16	151 × 166	151 × 166	151 × 166
No. variables	40534 (all potential)	50132	50132	50132
Max iterations	6 (LO) + 14 (GO)	200	198	181
CPU cost	1.2s (LO) + 2.4s (GO)	32.9s (FEM) + 187.3s (OC)	26.5s (FEM) + 38.7s (MMA)	24.8s (FEM) + 29.4s (MMA)

LO - layout optimization; GO - geometry optimization; FEM - finite elemet solver; OC - optimality criteria method; MMA - the method of moving asymptotes

Figure 2.14: Comparison of the truss optimisation scheme compared to conventional TO tools (from He et al. [51])

Figure 2.15: A satellite antenna bracket designed with the truss optimisation tool (from He et al. [51])

2.3.1. Damage Tolerance Principle

Throughout the entire lifespan of an aircraft, the structural integrity of it must be ensured. This means that at no point in time, aircraft parts should fail in such a way that catastrophic failure of the aircraft occurs. Ideally, no failure in any part at all would be the best case scenario. However, designing a structure with that property and which is also suitable for flight seems impossible. The low load constraints would lead to heavy parts and environmental or external effects can not be avoided. Therefore, it is assumed that the structure will experience some damage originating from fatigue, corrosion, manufacturing defects or accidental damage during its operational use. However, this damage should not lead to immediate catastrophic failure of the aircraft. Instead, the aircraft must be operated safely until the damage can be detected and repaired [53, 54]. This concept is known as damage tolerance. Over the years, this concept has evolved from other design philosophies for ensuring safety and nowadays it can be seen as an important design approach for designing aerospace structures [55]. Besides, it is included in the certification procedures for aircraft.

The concept of damage tolerance is extensive. Whereas it historically started with safe-life design criteria only, fatigue and corrosion issues became important considerations, maintenance and inspection gained relevance and the models used to describe and predict damage became more elaborate [56–58]. When designing in a damage tolerant context, all of these aspects, and combinations of them, can be considered to improve the design.

Reddick states that in damage tolerance *"the structure is designed to retain adequate residual strength until damage is detected and corrective actions taken"* [59]. From the definition of damage tolerance, together with Reddick's statement that in designing for damage tolerance both residual strength

and damage must be addressed, four main aspects that can be designed for can be identified. In damage tolerance, one can design for:

- Detectability;

- Repairability;

- Predictable damage and

- Residual strength.

Although detectability and repairability are important considerations for AM, the fields of predictable damage and residual strength are most often addressed when it comes to design for DT. Fatigue failure is responsible for more than half of the aircraft in-service part failures [60] and is thus the most important failure mode. Designing for damage tolerance is therefore often done by designing against fatigue.

In designing against fatigue, one can design for slow crack initiation, or slow crack growth, which are two separate phases of fatigue failure with different underlying mechanisms [58]. The crack initiation is related to material surface properties, whereas crack growth is depending on both material effects and the stress intensity at the tip of the crack. The crack initiation is accelerated because of the free surface, stress concentrations at the surface due to the geometry of the part, surface roughness and effects like corrosion that create surface inhomogeneities. Material effects influencing the growth include the bulk material properties, but also heat treatments and the microstructure of the material are of influence.

Fatigue damage, like all kinds of damage, ultimately leads to the failure of a part. The design for residual strength aims for the safe operation of partially damaged structures. The use of a fail-safe mechanism is often mentioned as a way to do so [55, 57, 59]. Both multiple load path structures and crack arresting mechanisms can be used as fail-safe feature. The idea behind the application of multiple load path structures is that if a part of the structure fails, the remaining structure can make up for the failure until the damage is detected and repaired. Not all multiple load path structures are fail-safe as they can behave as single load paths when not designed properly [57]. Designs with this property and design susceptible to multiple site damage must therefore be avoided. Crack arresting mechanisms are structural features that are able to stop a propagating crack [57].

2.3.2. Assessment of Damage Tolerance in Current Design

In the currently applied design methods for AM, little cases are known where the objective of the design is to increase a DT parameter. However, several aspects that can be related to DT are mentioned multiple times in the described cases. In this section, current DT features and potential additions of DT in DFAM are described.

The first observation when analysing the design methods is that in the optimisation step, parameters are manipulated to account for problems related to DT. In the suspension bracket described by Walton and Moztarzadeh as well as in the helicopter gear box bracket described by Süß at al. minimum thicknesses are introduced for the created part members [45, 46]. Walton and Moztarzadeh mention the effect that initial flaws can have on the part as reason to introduce a minimum size. In these both cases, as well as in the A320 nacelle hinge bracket described by Tomlin and Meyer [47], a maximum stress constraint is imposed, based on the fatigue limit of the material. This means that the stresses are kept low enough to avoid any fatigue problems. This means a safe-life approach is applied.

Multiple load path features can be seen in many AM parts, due to the open structures created by optimisation schemes, which often are truss-like structures. This is even more visible in the lattice structures used in the bracket shown by Cheng et al., the partition shown by Nagy et al. and the truss-optimised bracket by He et al. [43, 48, 51]. The many individual trusses can be seen as a fail-safe mechanism that can maintain the loads if one truss fails. This is however questionable when all parts are highly loaded. The failure of one truss could lead to the overload of all other load paths.

Often seen procedures in AM are post-processing steps. Süß et al. and Walton and Moztarzadeh mention surface smoothing when interpreting the TO shape in CAD, which is done by slightly adjusting the shape by for example rounding the edges [45, 46]. Stress concentrations at sharp notches are avoided, leading to less crack initiation sites. Furthermore, in the helicopter gear box bracket case described by Süß et al. post-processing of the part after manufacturing is also mentioned. Applying a surface finish for obtaining a more smooth surface which is less susceptible to crack initiation and corrosion is shown by Dehoff et al. and Brandt et al. [25, 26]. To remove porosity and to get a more

homogeneous material, HIP is used in these both cases as well. These pores could serve as crack initiation sites and are therefore not desired.

The inspectability of AM parts is more difficult than for conventional parts. Instead of having straight and simple surfaces, the AM parts are characterised by more complex shapes. Moreover, Brandt et al. show that their bracket uses hollow elements with an internal stiffened structure [25]. These features can not be inspected by visual inspection and more advanced techniques will be needed. Advanced techniques are used by Walton and Moztarzadeh and EOS, who use CT-scanning to check the produced parts [44, 45]. These cases describe single parts and use a relatively new process, but CT-scanning for large scale production is rather expensive.

2.3.3. Addition of Damage Tolerance to DFAM

The used steps to increase the damage tolerance of AM parts might not be sufficient when the criticality and loading on these parts increase. As mentioned by Gorelik and shown in section 2.3.2, large design margins are applied to stay away from the fatigue limit [3]. Besides, post-treatments are used to improve material parameters. However, large scale changes in the geometrical design are not considered yet as way to improve the DT. To take DT into account in the full design of a part, constraints with respect to DT should be included earlier in the design process.

In early stage design, the geometrical design can be influenced, which has an effect on the multiple aspects of DT as described in section 2.3.1. Of these aspects, designing against fatigue and for progressive failure seem to be the most important ones. Fatigue is responsible for a large portion of all aircraft failures [60]. Moreover, designing for progressive failure can be done by geometrical design, for which the high flexibility offered by AM can be used. Material and environmental factors cannot be influenced on the same large scale. Detectability and repairability are important aspects that should also be taken into account, but designing specifically for these is not a common approach. As described earlier, designers are still involved since the tools used in current designs result in shapes that are not ready-to-use. Because of the complexity and non-mathematical description of DT, this step done by designers qualifies as a suitable point to include additional DT considerations at an early stage of design.

Multiple load path structures

Designing against fatigue and for gradual failure can be done by changing the geometry, through the introduction of multiple load path structures. The use of fail-safe mechanisms with crack arresting capability slow down cracks and provide enough strength until the part can be repaired. The use of AM allows for the production of redundant structures on a smaller scale and is therefore an effective way to increase the DT. Important in this case is that multiple site damage (MSD) must be avoided. Redundant AM structures are however different from other structures that are susceptible to MSD because the amount of parallel load paths can be increased extensively instead of having only a few, cracks can not link up like in a sheet if the material is not continuous at some locations and structures can be designed that are non-homogeneous such that the multiple load paths are not equally loaded. Furthermore, it is interesting to assess if based on this and the new production processes, lattices and redundant structures can indeed be made more damage tolerant.

The use of multiple load path structures to increase the damage tolerance, or fatigue life, of AM parts can be applied in various ways. Redundancy can be included in TO schemes, as shown by Jansen et al. [61]. Based on a model that takes away 'damaged' patches of design space, the algorithm finds a robust shape with redundant struts. The outcome is however strongly dependent on the input damage size and is computationally demanding. Zhou and Fleury proposed an improved TO scheme based on this [62]. They propose a solution capable of doing 3D optimisation with an improved damage model and with the need for less computational power. Both models strongly depend on the damage model and propose a fail-safe solution. Multiple site damage problems are not mentioned in these papers and the structures provide only a few alternative load paths.

Lattice structures as multiple load paths

Lattice structures are multiple load path structures by definition. Seen the high levels of redundancy that can be reached, they seem suitable DT alternatives for aerospace applications. However, the fatigue and failure characteristics compared to conventional materials seem to limit this. Huynh et al. performed uniaxial fatigue tests in tension on lattice structured specimens [63]. They reported lower

(a)   (b)
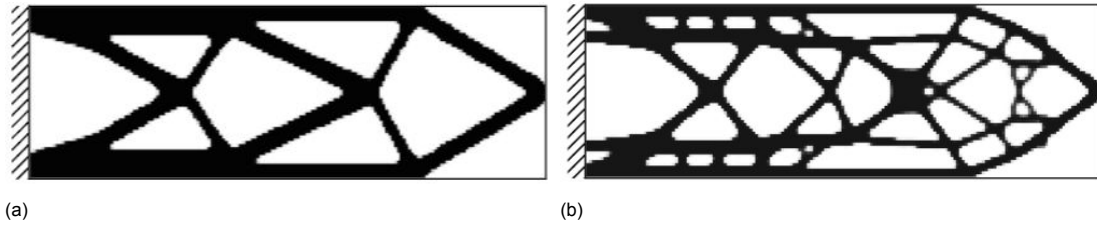
Figure 2.16: Redundant TO structure: (a) Original without redundancy and (b) one of the proposed redundant structures (from Jansen et al. [61])

tensile and fatigue strength compared to dog-bone specimen of the same material, both manufactured with traditional processes as with AM, as shown in figure 2.17. This can be explained by the higher stress concentrations in the lattice structure. An interesting observation is the damage propagation. It is stated by Huynh et al. that the lattice failed with one ligament at a time, after which strain accumulation occurs in the remaining ligaments. This quickly accelerated the failure of the remaining ligaments.

The failure of lattice structures in both static loading and fatigue seem to follow a standard pattern in which the failure plane is inclined at 45 degrees [64–66]. Most of the structures that are used are bending-dominated lattices, where the individual struts are subjected to bending upon loading the structure. On the contrary, the struts of stretch-dominated lattices are subjected to axial loading. Köhnen at al. describe a comparison between f2cc,z and spherical unit cells where the mechanical behaviour is stretch and bending-dominated respectively [67]. The nature of the mechanical response is thus different, resulting in different properties per cell. As Wu et al. show, the failure of a triangulated lattice that is stretch-dominated does not follow the 45-degree pattern anymore and is more catastrophic. The rapid failure of lattices after failure of the first ligament is a well-known effect described in literature [63, 66, 68]. Due to this fast catastrophic failure, the use of uniform lattices does thus not increase the damage tolerance.

(a)   (b)
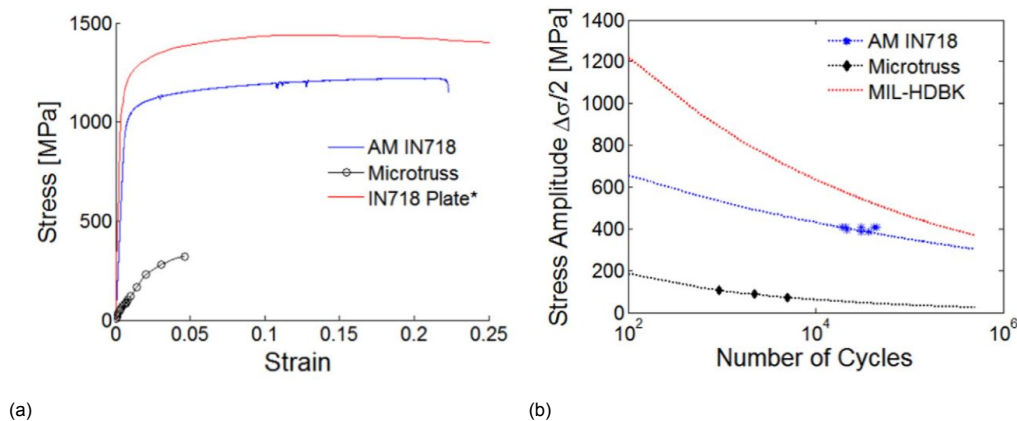
Figure 2.17: Lattice structure (micro-truss) compared to a dog-bone sample of AM produced material and conventional material:(a) Stress-strain plot (b) S-N curve (from Huynh et al. [63])

Non-homogeneous lattices
Although the fatigue strength of lattice structures is generally lower than that of conventional specimens, the combination of multiple unit cell topologies or multiple densities inside one specimen seem to be able to increase the mechanical properties [69]. Heterogeneity is introduced by Li et al. to influence the properties of the lattice in a way similar to the use of functionally graded materials (FGM), in which the micro-structure and composition of the material that is used in a product can be be changed gradually. This makes it possible to optimise through the material instead of the geometry [7].

Li et al. state that graded cellular structures have superior mechanical properties compared to uniform meshes [69]. This is demonstrated through the design and test of graded mesh structures with two different densities within the part and structures with two different unit cells. The dual density structure, which has a bar of higher density elements in the centre of the structure, showed a standard 45 degree

failure behaviour. The low density elements however failed earlier than the high density elements in compression. This difference in failure can be used as a way to control the failure of a structure. The dual unit cell structures showed higher strength and energy absorbing capability compared to uniform structures, because a high-strength high ductility combination can be obtained.

The fatigue properties in compression of graded cellular materials are further investigated by Zhao et al. [70]. Again a structure with two different unit cells (figure 2.19) and a structure with a graded density (figure 2.18) are produced. The graded meshes fail from highest to lowest strength in fatigue. Cracks initiate and propagate in the different meshes in this specific order. Because the stiffness decreases upon crack propagation, the stresses redistribute over the different constituents and retard the crack propagation in the damaged regions. This mechanism is shown for both varying density as for varying unit cells. Due to this mechanism, the fatigue life of the graded structure is better than expected based on a rule of mixtures, which is able to predict other mechanical properties. From Wang et al. it is known that the described effects are only present under iso-strain conditions [71].
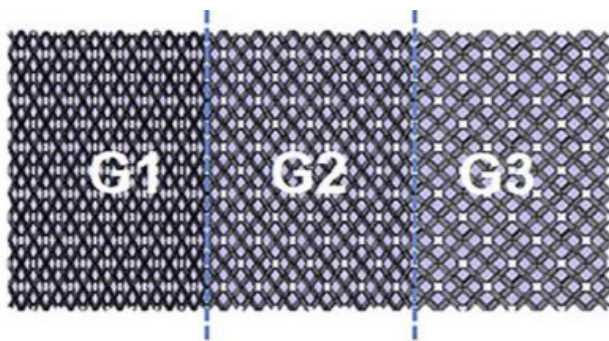
Figure 2.18: Graded lattice structure with loading in vertical direction (from Zhao et al. [70])
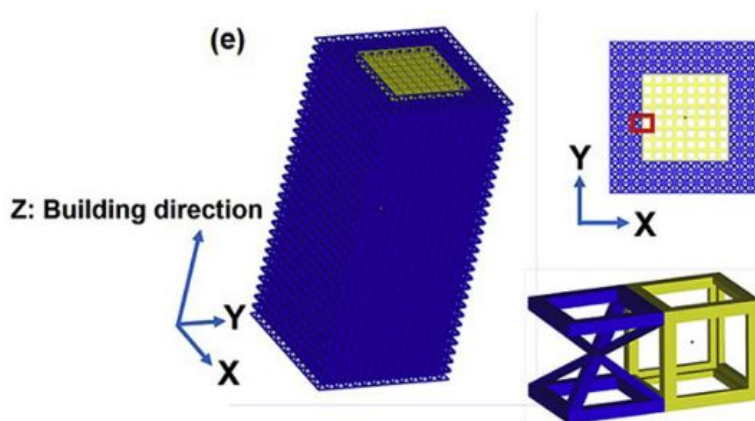
Figure 2.19: Structure with varying unit cells, different cells in the centre beam (from Zhao et al. [70])

Another way of creating a non-homogeneous lattice structure is by mimicking the micro-structure of crystalline materials, as shown by Pham et al. [72]. Locally, the lattice was disoriented to create grain boundaries, lattice parameters were changed to create precipitates and multi-phase materials were created by using multiple cell topologies. The quasi-static mechanical properties were improved by this method and possibly it could be used to create more damage tolerant lattices. The difficulty to create these lattices could however limit its potential.

Failure of multiple load path structures
Zargarian et al. modelled the fatigue behaviour of lattice structures numerically and described the S-N curves of these lattices with a power law function, of which the exponent is influenced by the specific fatigue behaviour of the struts, originating from for example irregularities, whereas the coefficient is influenced by all possible parameters [68, 73]. These parameters include cell topology and relative density of the lattice. Failure happens on inclined planes, where struts fail quickly after each other.

The 45-degree orientation of the fracture plane can be explained by shear stresses. The prediction of the S-N curve, failure pattern and failure propagation shows that the underlying mechanisms are understood.
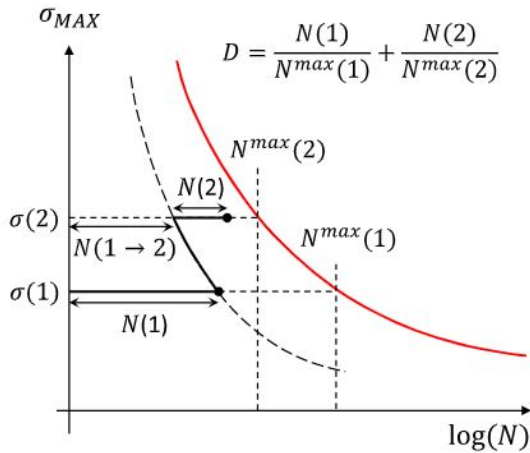
Figure 2.20: S-N curve for a cascading damage model with two elements (from Burr et al. [74])

 The failure of lattices is also described by Burr et al. [74], who set up a damage model for redundant lattices. Due to statistical differences and the complex geometry of unit cells, it is expected that not all cells or struts fail at the same time, which is accounted for in this model by taking into account the redistribution of loads upon failure of one strut. Two sources of variability are introduced, which are different radii of struts and scattered S-N curves. For every strut a different S-N curve can be used, which is the result of the usual statistical scatter. The failure of the individual struts is predicted with the Miner's rule, according to figure 2.20, where one load redistribution step after a given number of cycles is shown on a S-N curve for an individual strut. In contrast to earlier findings on the quick failure of lattices [63, 67, 68], Burr et al. describe that the period between the first failed strut and final failure of the part can be as large as 33% of the overall fatigue life.

 This relative gradual failure is furthermore described by Kotzem et al. [31]. A specimen consisting out of six identical tensile bars was created using AM and subjected to a fatigue test. The reason for the use of parallel struts is that in order to predict the damage behaviour of complex structures, such as lattice structures, the behaviour of damage in a individual strut should be known. One of the findings of Kotzem et al. is that after failure of the first strut, the remaining struts could maintain an even increased load for many cycles. This suggest that multiple parallel struts, and potentially lattices, are more damage tolerant than a single strut, since the partly damaged part could maintain the load for a period of time. In figure 2.21, the gradual failure can be seen from the change in electrical resistance graph. As can be seen, the stress amplitude was changed during the test, making it harder to interpret the quantification of the gradual failure.

 It is thus shown that the fatigue life and the failure pattern of multiple load path structures and lattices can be modelled and are at least partly understood. The findings on how quick these structures fail range from almost immediate to 33% of the overall fatigue life as shown by Burr et al. [74]. Also, the amount of redundancy that is needed to obtain these effects is not known. In order to apply multiple load path structures as damage tolerant alternatives in the design of additive manufactured structures, the failure mechanism in reality and its dependency on redundancy should be better known.
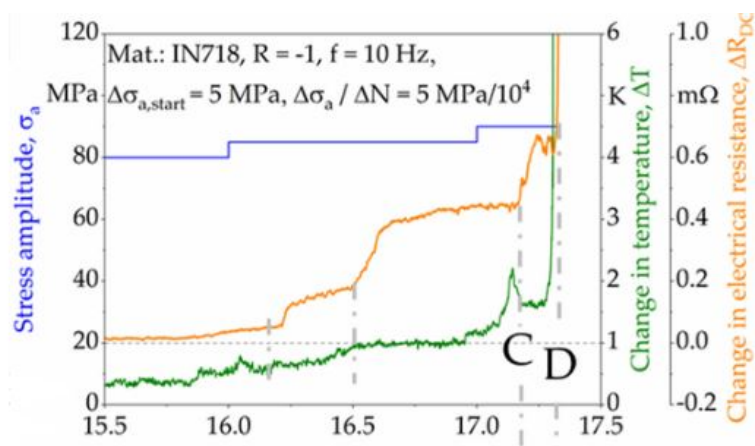
Figure 2.21: Gradual failure of a redundant structure (from Kotzem et al. [31])

3

Research Definition

It follows from the literature review that the geometrical possibilities offered by AM are not widely explored yet in terms of damage tolerance, while a potential shift to more critical aerospace parts in the future is expected, as described in the introduction [3]. This raises the question whether geometrical features that are now producible using AM can be used for increased damage tolerance. Multiple load path and lattice structures are common structures that are mentioned when it comes to new geometries. From Kotzem et al. and Burr et al. it is known that not all elements of a redundant structure fail at the same time and that a reasonable life is left after the first failure [31, 74]. This gradual failure could be used to improve the damage tolerance of AM structures.

The envisioned relevance of this concept for the design of additive manufactured parts is that redundant structures or lattices can be applied to create structures with improved damage tolerance. In that case, lattice structures or optimised trusses as described by He et al. and Fairclough et al. can be used in parts that are required to be damage tolerant [51, 52]. The cross-sections of single ligaments are in that case split into multiple thinner elements. The switch to redundant structures can be made through applying a design constraint, or by splitting the cross-section during a designer interference step. Moreover, in secondary optimisations in the design process this switch can also be made, as shown by the part designed by Nagy et al. [48]. Based on the questions that arise on the gradual failure and fatigue life of these multiple load path structures, the research objective and sub-goals are set up, as will be described in this chapter.

3.1. Research Objective

Although it was shown before that a step-wise failure pattern is present in multiple load path structures, it is not known how this type of structure compares to single load path counterparts and whether they can be used for improving damage tolerance. Also, the dependency on the amount of redundancy, i.e. number of struts, is unknown. Therefore, the objective of this thesis is formulated as follows:

> The objective of this thesis is to assess the damage tolerance of additive manufactured multiple load path structures by analysing the fatigue life and damage propagation of specimens with increasing redundancy.

To be able achieve the stated objective, the following sub-goals need to be addressed. Firstly, it should be investigated how the fatigue life of the multiple load path structures compares to that of single load paths. The effect of using differently sized elements for the analysed structures should be found, in order to make a fair comparison. The damage behaviour and pattern in the redundant structure also needs to be investigated. The reason for this is that the damage propagation and pattern will differ from conventional crack initiation and growth, due to the multiple load paths that are present. It is the question how the individual failure events of the elements relate to each other, if a specific mechanism for the damage propagation can be found and if specific patterns are visible. Another sub-goal is to find a way to predict the damage behaviour, since in that way, assumed mechanisms can be put to test. Finally, the damage tolerance should be assessed on the basis of the findings of the study.Based on the described objective for this research, the main research question is defined here and is as follows.

What is the effect of redundancy on the fatigue life and damage behaviour of additive manufactured structures?

The sub-questions of the central research question follow from the defined sub-goals and are listed below.

- How does the fatigue performance of multiple load path structures compare to that of single load paths?

- What are the effects of using differently sized elements throughout different multiple load path structures?

- Which damage propagation mechanism can be identified in the multiple load path structures?

- How can the damage in redundant structures be predicted?

- In which way are additive manufactured multiple load path structures more damage tolerant?

3.2. Hypothesis

Concerning the outcome of the research, the following is hypothesised. An increase in the total fatigue life of the multiple load path specimens is expected compared to single load path counterparts, since failure of the weakest link of the structure will not immediately lead to overall failure. When multiple load paths are present, the remaining will take over the loads when one fails, whereas a single load path only has one element that can fail. A more gradual failure will thus be present when multiple load paths are used.

Concerning the damage, two extreme cases can be thought of in case of redundancy. In the first case, damage in all elements initiates independently of each other at the same time, corresponding to the S-N curve data of a single element. All elements will then fail at the same time. In the other scenario, a crack initiates in one element, grows and causes local failure. After this, this "crack" propagates and it needs to initiate again before it can grow. In this sense, the growth through a solid part is replaced by re-initiating and growing through the redundant structure.

In reality a situation in between these extremes will occur, as described by Burr et al. [74]. Because of statistical scatter, the fatigue life of the individual elements in the structure will be different. Cracks will initiate independently throughout the structure, but as a result of scatter, this will not happen at the same time. The weakest link will fail first, after which the remaining parts take over the (increased) load. Because the other elements were already loaded for a number of cycles, crack initiation will be faster in these. Based on this, a gradual failure of the structure will occur. The geometrical pattern of this failure is random in the ideal case, as it is the result of the scatter between the elements. If a certain pattern will be visible, either boundary conditions are not sufficiently satisfied, or a so far unknown effect is present. Because of the mentioned statistical scatter, combining multiple elements is likely to decrease the scatter of the combined properties and thus to increase the predictability of the fatigue life of the multiple load path structures.

Prediction of the damage propagation can be done as described in section 2.3.3. It is expected that the cascading damage model as described by Burr et al. and fitted for these experiments will result in the most accurate prediction [74]. The addition of the growth life to this model, will result in a more accurate prediction, even though only a small effect of the growth life is expected, compared to the total fatigue life.

4
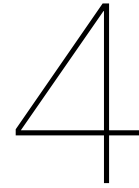
Experimental Methodology

The primary objective of this thesis is to investigate the potential for increasing redundancy through multiple load paths in AM structures, by analysing their fatigue and damage tolerance behaviour. Providing a fair basis of comparison for structural configurations with varying degrees of redundancy is not straightforward. To make such a comparison within this study, the following constraints were imposed:

- **Only axially loaded structures and structural elements were considered.** This eliminated the challenge of including bending and differences in local and global bending stiffness in the basis of comparison. Stretch-dominated structures generally have a higher relative stiffness and fatigue strength, making these more suitable for aerospace applications. Moreover, in the case of replacing a single strut by multiple struts in a truss environment, an axial loading case is also foreseen.

- **A constant cross-sectional area was used between the structures** to ensure that the nominal tensile stress in the structures is the same in the undamaged state for the same applied load.

- **A constant surface area for the structures was maintained** to eliminate the statistical size effect in fatigue. It is well established that crack initiation is highly dependent on the quality of surface and sub-surface regions of a part and thus a larger surface area increases the likelihood of initiation of fatigue cracks. Maintaining the same surface area of the parts minimises this effect.

Based on these constraints, a set of uniaxial fatigue test specimens was designed with 1, 9, and 81 load paths as shown in figure 4.1. The parallel configuration of the struts arises from the axial loading constraint, while the decreasing diameter and length of the struts in 9 and 81 strut configurations are done to maintain the overall cross-sectional and surface areas of the specimens. These specimen configurations were used to evaluate the fatigue performance in both an undamaged and pre-damaged state. To obtain insight into the damage progression during the fatigue tests, the direct current potential drop (DCPD) method was used to measure the change in electrical potential along the specimen associated with the cracking and failure of individual struts. The remainder of this chapter details the specifics of the experimental program, including the design and production of the individual test specimens.

4.1. Test Specimens

The design and production of the test specimens is described in this section. The basic strut geometry is presented first, from which the multiple load path specimens with 1, 9 and 81 struts are designed. A selection of these specimens is furthermore used as pre-damaged specimen. Finally, a set of single strut specimens is designed and produced, as addition to the multiple load path samples.

4.1.1. Geometries

The multiple load path specimens consist out of 1, 9 or 81 struts which have the same basic geometry. This geometry is shown in figure 4.2. The specific drawings per specimen type are included in appendix

Figure 4.1: Overview of multiple load path specimens

B. Although the specific dimensions vary per specimen type, the overall shape is kept similar. In table 4.1, the dimensions per specimen type are given. The strut diameters are based on the smallest usable diameter for the 81-struts (81-1mmØ) specimens. A minimum diameter of $d = 1$ mm was chosen, since this size proved to be reasonably producible for earlier produced parts. Besides, at this size the overall specimen dimensions were kept small enough to fit all specimens in one build job.

The test section length L of the specimens was determined by the height of the build job during production and the constant surface area condition, meant to eliminate the statistical size effect in fatigue. Because of this condition, the 1-9mmØ specimens have a 9 times longer test section than the smallest samples, which makes the 1-9mmØ specimens the longest. An optimum was found for producible length for the largest specimens, while the smallest also had reasonable length. Taking into account the used grips for load introduction, test section lengths of 10, 30 and 90 mm were chosen for the 81-1mmØ, 9-3mmØ and 1-9mmØ types respectively.

The horizontal spacing in between the struts was kept to a minimum, such that the total grip width and depth was kept small. Due to this, the designed grips are as small as possible, saving material and ensuring proper load introduction in the test section with the required boundary conditions. To ensure that the maximum stresses are located in the test section, a cross-section ratio of 4 is used, according to ASTM E466 [4]. As a result, the top part of the strut has a width of $2d$, meaning that the spacing between the struts is equal to the diameter, as shown in figure 4.2.

Elliptical fillets are used to introduce the loads from the solid grip into the cylindrical test section. The cylindrical struts follow these elliptical shapes through changing their diameter. Ellipses are preferred over circular radii, since the stress concentration factor will be kept lower [58]. The size of the semi-minor axis r_a is based on the spacing between the struts, such that the full ellipse would fit between the struts. The semi-major axis r_b follows from a standard ratio of 5 which leads to a similar stress concentration factor independent of the strut diameter. This also means that the transition region increases in length for specimens with a larger diameter. The ellipses are cut off at an angle of 45°, because

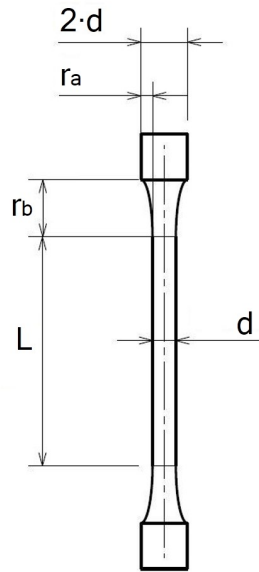Figure 4.2: Basic strut geometry used for multiple load path specimens

Table 4.1: Dimensions of multiple load path specimen struts

Specimen	81-1mmØ	9-3mmØ	1-9mmØ
Number of struts	81	9	1
d [mm]	1	3	9
L [mm]	10	30	90
r_a [mm]	0.5	1.5	4.5
r_b [mm]	2.5	7.5	22.5

this is the maximum angle at which can be manufactured without supports. A flange with this angle is continued until the intersection with the next strut base is reached.

The test benches that were used required the specimens to be clamped between two clamps with given dimensions. To transfer the tensile load, a grip had to be added to the specimens. Because no standardised test is available for the kind of structures tested here, a new grip design was done. The resulting geometry is shown in figure 4.1 and a technical drawing is present in appendix B. For the 9-3mmØ and 81-1mmØ samples, the grip is the connection between a flat clamped piece and the rectangular cross-section, comparable to grips found in other researches [63, 75]. A slightly different approach was chosen for the 1-9mmØ specimens, since the rectangular cross-section is not needed. At the base of the elliptical transition, the specimen remains cylindrical, making it a cylindrical dog-bone shape. This cylinder can be clamped in another clamping piece that has a circular cut-out. With this approach, the length of this specimen is reduced, reducing the height of the build job.

The clamp thickness was designed based on the available clamping mechanism, the length corresponds to 80% of this clamp length. This was the minimum required part of the clamping that needed to be filled with material in order to avoid rotation of the clamps, which would result in an unevenly distributed shear application. The radii of curvature in the grips are designed to have a maximum stress concentration factor of 1.013, resulting in a lower stress than the nominal stress in the struts. The maximum inclination of the edge is designed at 30° to ensure production is possible and to keep the displacements as uniform as possible.

Aside from load transfer, an equal displacement constraint is provided by the grips, such that all struts are loaded equally. To obtain this, the displacement on the top of the grip needed to be equal over the entire cross-section. Therefore, 10 mm of solid material was attached on top of the grips to ensure this equal displacement. The size of the solid material was determined based on the displacements found with a FEM analysis of the grips. The FEM analysis, as shown in appendix A, is furthermore used to verify the specimen design.

4.1.2. Pre-damaged Specimens
In order to test the hypothesised damage propagation in the redundant structure, extra specimens were produced and tested with an initial damage. The reasoning behind testing with initial damages is as follows. If a crack initiates after the previous strut has failed, introducing an initial damage would drastically lower the fatigue life. On the other hand, when all initiate at the same time, taking one strut away would only slightly increase the load and have less effect on the fatigue life. Furthermore, with these initial damage tests the damage tolerance in terms of sensitivity to damages could be determined.

For the initial damage tests, the 81-1mmØ and 9-3mmØ specimen types were used. Three samples per type were prepared. These samples were given a notch that was created with a bandsaw. The notches have a 0.5 mm radius and are machined halfway through the strut. A notch was preferred over a completely through crack since the cracking is then included in the test, making it possible to analyse the influence of the crack and failure itself rather than doing a test at a higher load and with less struts. As a result of the production, two 81-1mmØ were already damaged as will be described in section 5.2. As a consequence, only one specimen of this type was prepared with a notch. In section 5.2, an example is shown of a notched specimen and of two other pre-damaged 81-1mmØ specimens.

4.1.3. Additional Specimens

To test the effect of using different diameter struts, an additional set of single specimens was designed from the used standard samples for fatigue testing. The test section length was increased to match the size of the struts of the 9-3mmØ samples. The specimens are shown in figure 4.3a. To rule out effects of producing these specimens in another batch, one 9-3mmØ sample was cut into 9 single struts, as shown in figure 4.3b. This was done to compare these to the new standard specimens and to increase the number of tested single struts. With a large number, a more reliable statistical distribution can be created, for which these samples are also used.

(a)   (b)
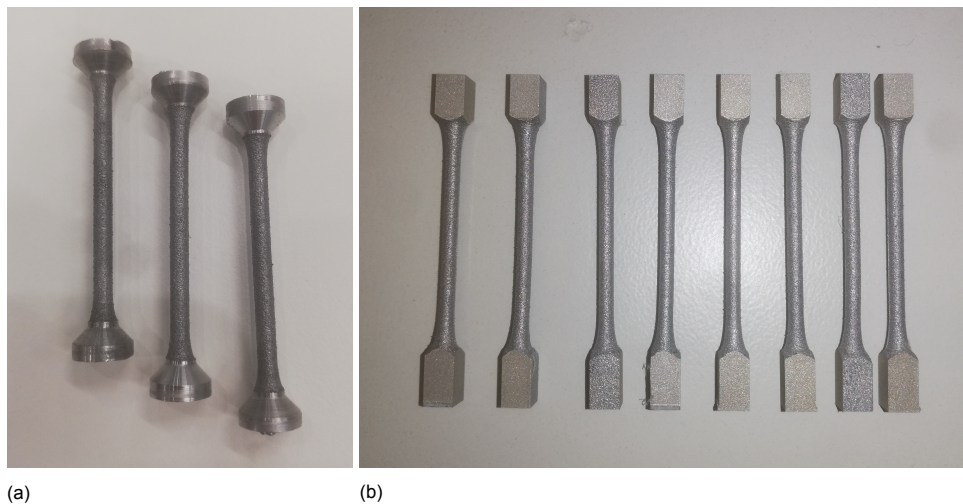
Figure 4.3: Single strut specimens: (a). New produced 3 mm specimens (1-3mmØ) (b). 3 mm specimens from 9-3mmØ sample (1(9)-3mmØ)

4.1.4. Material and Production

The material that is used for all specimens is AlSi10Mg. The reason for using this material is the availability at the moment of production, and the potential applicability for aerospace parts. The specimens were produced by laser powder bed fusion (L-PBF). A SLM280 HL machine manufactured by SLM Solutions GmbH was used for this. The specimens were produced in two batches. The first batch contained 40 specimens with the standard geometry, the second batch only contained the additional single strut specimens of the type 1-3mmØ. In both batches, the exact same production parameters were used. The specimens in the first build job are shown in figure 4.4.

A vertical build direction was used for the production of the specimens. It is known from literature that a build direction effect exists which results in lower mechanical and fatigue properties for the vertical build direction [11, 16]. However, if a horizontal orientation was used, support structures would be needed on the entire part, including the test section with the parallel struts. Besides the surface irregularities that would be the result of removing these supports, it would be almost impossible to remove the internal supports in the case of many parallel struts.

A stress relief heat treatment was applied after manufacturing. This was a 2 hours cycle at 300 °C. With this heat cycle, internal residual stresses resulting from the non-homogeneous thermal history and the solidification are removed. After the heat treatment, the specimens were removed from the build plate with a bandsaw.
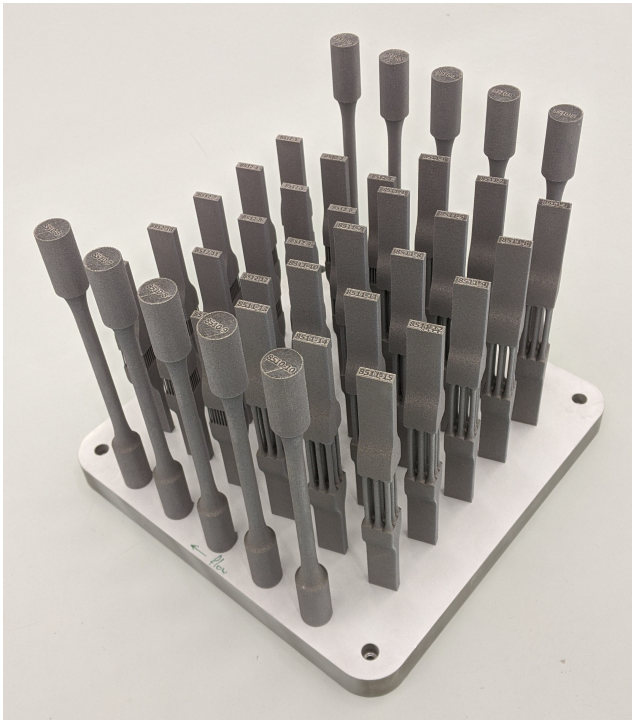
Figure 4.4: Multiple load path samples on build plate

4.2. Test Setup

After designing and producing in total 64 specimens, these were subjected to tension-tension fatigue testing at different stress levels. Besides, a set of 9 specimens was tested statically for validation of the part geometry. In this section, the setup of the experimental fatigue tests and static tests is described. The equipment that was used and the method to determine the stress levels is presented here.

4.2.1. Fatigue Test Setup

The fatigue testing of the multiple load path specimens, both with and without initial damage, was performed in a Schenck Hydropuls test bench with a 100 kN load cell. For the 9-3mmØ and 81-1mmØ samples, clamps with a flat surface were used that were pressed against the bottom section of the designed grips. Since the 1-9mmØ specimens have a cylindrical grip, clamps with a cylindrical cut-out with matching diameter were used. Bending in the specimens is ruled out by aligning the test bench on beforehand and carefully clamp the specimens in the test bench.

For the additional single strut tests, the clamps were replaced by a system in which the wider grip section of the specimens is locked. This system is shown in figure 4.5. The new 1-3mmØ specimens were designed for these clamps, the other ones (1(9)-3mmØ) fitted as well. A 10 kN load cell is used for more accurately controlling the loading during the test.

The specimens are tested at multiple stress levels. A goal was set to reach ideally two stress levels with given numbers of cycles that have one order of magnitude in between. This is done for the completeness of testing at multiple levels, while keeping the test duration within reasonable range of a few weeks in total. Because the fatigue behaviour of the used material was not known before testing, three or four stress levels were needed to arrive at the desired number of cycles for the 9-3mmØ and 81-1mmØ specimens. The strategy to determine the value of the stress levels at which was tested is as described in the following. From static testing, the yield strength of this material was known before. Based on literature values of the yield strength and corresponding S-N curves from Tang et al., Brandl et al. and Uzan et al., an estimate was done for the stresses at the desired number of cycles [21, 22, 76]. Testing at the calculated stress level could be done, after which the stress was adjusted. The 9-3mmØ specimens were used for the initial testing, since extra specimens of these were manufactured. It was also assumed to be the in-between case, most representative for all specimen types. Aside from that, the presence of multiple struts could give an early insight in the behaviour of the redundant structures.

The value for the remaining stress levels was determined by fitting an exponential curve through the already available data points and extrapolating to the desired number of cycles. This strategy was repeated for the 81-1mmØ samples and the 1-9mmØ samples. The stress levels for each specimen type are given in the test matrix at the end of this chapter.

The other test parameters are as followed. To keep the specimens in tension during testing, a load ratio of $R = 0.1$ is used. The test frequency is 25 Hz. All fatigue test described here were performed at room temperature.
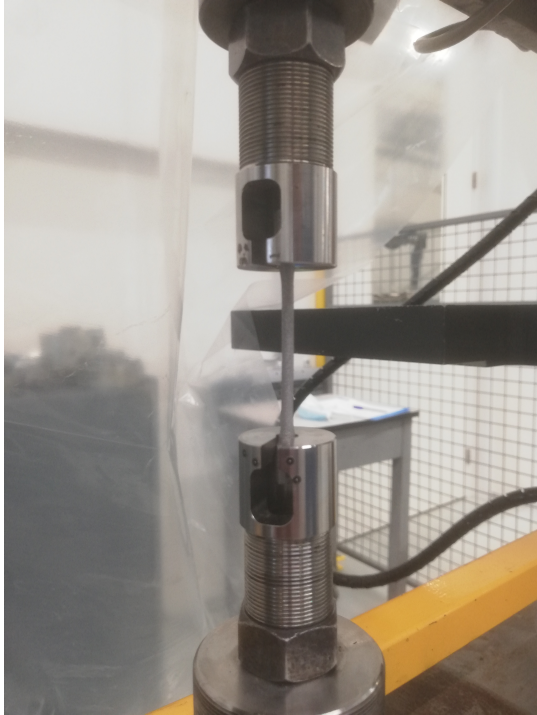
Figure 4.5: Clamping system used for the 3 mm single strut specimens

The individual failure events could be captured by a direct current potential drop system (DCPD). This system was used for the multiple load path samples and the 1-9mmØ samples and will be described in section 4.3.2. Two connections that were needed for applying the current were chosen at the top and bottom of the specimens, leading to a maximum possible homogeneously distributed current in the test section. Two other points were needed to measure the potential. Because the location of the cracking could influence the response if applied to only one side of the specimens used here, the potential was measured on two sides.

The potential measurement points needed to be placed far enough from the test section to capture equal responses for damage in the middle and at the side of the test section. Small holes with a diameter of 1 mm were needed to connect the wires at the measurement points. Therefore, the points are located 10 mm from the test section in the grip, since at this location the stresses are low enough to be subjected to the stress concentration factor originating from the holes. Since no flat area is present for the 1-9mmØ specimens, the holes were made in the grip section. In appendix B the locations of the holes are shown.

The specimens were insulated at the bottom side clamps by adding 1 mm thick glass fibre tabs between the clamps and the specimens. Due to the relatively low shear stresses and the surface roughness of the specimens, the tabs could simply be clamped in between without using adhesives. The flat glass fibre tabs were not suitable for the cylindrical specimens. Besides, these samples were designed to match the test bench grips, leaving no space for glass-fibre insulation. Therefore, these samples were tested without insulation.

4.2.2. Static Test Setup

Three specimens of both the 9-3mmØ and 81-1mmØ type were loaded quasi-statically up to a stress below the fatigue test stress in an Instron 5989 600 kN test bench. The strain was determined from a optical extensometer which measures the displacement between two stickers that were added to the specimens. For three 1-9mmØ specimens, the static test up to the same load was done in the Schenck Hydropuls test bench, as used the fatigue tests. Digital image correlation (DIC) was used in this case instead. The reason for this difference is the absence of a flat visible surface to attach the stickers for the cylindrical specimens and the too small diameter for the 9-3mmØ and 81-1mmØ which makes DIC impossible. The environmental conditions of the test were equal to those of the fatigue testing.

4.3. Data Collection

From the fatigue and static testing, relevant data is required to analyse the behaviour of the specimens. Which data is collected and how this is done, is described in the following. The methods to manipulate the output of the tests to usable variables are given. This is done for the specimen state analysis, potential drop system and fractography.

4.3.1. Specimen State

The produced specimens were verified to check how the as-built properties compare to the as-designed properties. This was needed to apply the correct force to the specimens, corresponding to a given stress, and to avoid wrong conclusions based on this. The verification included a general characterisation of the specimens with the measurements of the struts. Also, a non-destructive tensile test was done for the multiple load path structures, to find differences in cross-sectional area through comparing the spring stiffnesses of the parts.

Caliper measurements

The diameters of the struts were measured with a digital caliper. Because of accessibility, only the outer struts could be measured. The actual cross-sectional area of the total of the struts was extrapolated from this. For the 1-9mmØ specimens, 5 points were measured at different height and orientation per specimen. All specimens were measured, which was the same for the 9-3mmØ specimens. There, only one point per strut was measured, although the points were taken at different heights in the struts. For the 81-1mmØ specimens, the struts of 5 specimens were measured to reduce the amount of measurements to be done. The specimens that were measured are taken from different positions on the build plate, to avoid having an effect of build plate position in the results.

Surface characterisation

The surface of the specimens is interesting, since it was found in literature that the properties change due to a size effect. Also, printing deficiencies could lead to different surface conditions. Seen the additional tests that were done with single struts to test for size effects, the surface characterisation was limited to the analysis of close-up photographs. This provided a general impression of the conditions and the dependency on the strut diameter. Extensive surface roughness testing is outside the scope of this research.

Tensile test

The strut diameters of the specimens were verified with a non-destructive tensile test. This was needed since only the outer struts could be measured with the digital caliper. A standard error could be present if the inner struts would have a different size due to their position. Moreover, the surface roughness led to less accurate measurements. The goal of this verification test was to show that the struts were loaded with the correct stress in the performed fatigue tests.

   The concept is as follows. The strain on the specimens as a result of a known constant force is determined during the tensile test. The force F, stress S, cross-sectional area A, stiffness E and the strain ε relate to each other as shown in equation 4.1.

$$F = S \cdot A = E \cdot \varepsilon \cdot A \qquad (4.1)$$

   It was assumed that the diameter of the largest specimen, with the 9 mm single strut, could be accurately measured to determine the cross-sectional area. Also, it was assumed that the stiffness of

the material that was used does not change for the different specimens. With a known cross-sectional area, the material stiffness could be determined. With all other parameters known, the cross-sectional area of the 9-3mmØ and 81-1mmØ specimens could be estimated, as shown in equation 4.2.

$$\Rightarrow A_{est} = \frac{F}{E\varepsilon} \tag{4.2}$$

Another consideration is that not only the test section, but also the elliptical region and a small part of the solid block were included in the strain measurement of the 9-3mmØ and 81-1mmØ samples. This was needed since the stickers for optical measurement could not be attached to the cylindrical geometry. Since these stiffer regions were included, the actual strain in the test section was underestimated and thus the cross-sectional area was overestimated. To compensate for this, the measured strain was adjusted for this cross-sectional change.

The tested region is divided into the solid rectangular section, ellipse and cylindrical test section. The 45-degree slope at which the ellipse is ended is neglected here for simplicity, for which reason the solid region is slightly larger in this estimation. Together with the fact that the actual stiffness in the smaller parts is less than in the 1-9mmØ specimens, due to AM related size effects, the value found with this estimation provides the lower bound of the area estimation.

The area of the lower bound was calculated as follows. From measurements, the length L of the solid section that was included in the strain was known, as well as the length of the designed ellipse and cylindrical section. From the total strain and total length, the total displacement was known. This total displacement ΔL is due the displacement of the individual sections, as shown below. Since the cross-sectional areas of these regions could be estimated, the measured strain could be linked to the area of the cylindrical test section for n struts following equations 4.3-4.5.

$$\Delta L = \varepsilon_{tot} \cdot L_{tot} = \int_0^{L_{tot}} \frac{F dx}{E A(x)} \tag{4.3}$$

$$\Delta L = \frac{F}{En} \left(\frac{L_{solid}}{A_{solid}} + 2 \int_0^{L_{ellipse}} \frac{dx}{A_{ellipse}(x)} + \frac{L_{cyl}}{A_{cyl}} \right) \tag{4.4}$$

$$A_{cyl} = \frac{L_{cyl}}{\frac{En\Delta L}{F} - \frac{L_{solid}}{A_{solid}} - 2 \int_0^{L_{ellipse}} \frac{dx}{A_{ellipse}(x)}} \tag{4.5}$$

The solid area is rectangular with width and length two times the diameter. Since the sizes of the ellipse are known, the area could be found through the equation of the ellipse, which provides the diameter of the cylindrical strut at that position. The shown integral could be solved numerically. As such, the corrected strain in the cylinder was found, and thus value of the cross-sectional area based on this.

4.3.2. Fatigue Tests

Measured variables

For the fatigue tests, the number of cycles until failure is used as output variable. From repeated experiments with the same conditions at the same load, the variation of the results was analysed as standard deviation over the log-average result. Also the grace ratio (GR) was analysed. This parameter was introduced by Burr et al., who introduced two new parameters: the GR and the grace period (GP) [74]. The GP is the time between the first failure and the final failure of the structure. The GR is the ratio of this period compared to the total fatigue life. The GR can be calculated from dividing the GP by the total fatigue life N, as shown in equation 4.6. The DCPD output was used to identify the individual failures of the struts and thus the GP and GR.

$$GR = \frac{GP}{N} \cdot 100\% \tag{4.6}$$

Potential drop measurements

The measured electrical resistance increases when less material is available throughout the cross-section, so when cracks are growing and struts are failing. This resistance was measured through the voltage in the tested specimen and a reference specimen. The wires were connected such that the two sides were in parallel, which gave an averaged output from both sides. In figure 4.6, the electrical diagram for the DCPD set-up is shown.
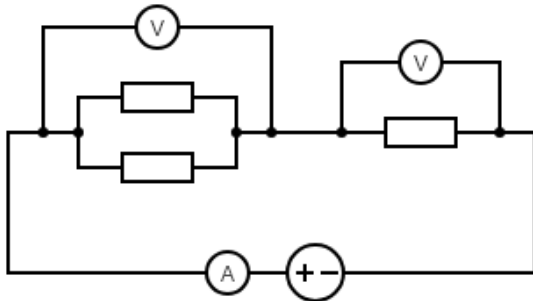

Figure 4.6: Electrical diagram of the potential drop system set-up

The output of the DCPD system is the ratio between the measured voltages of the tested specimen and the reference specimen. From this voltage ratio, the parameter of interest, namely the reduced cross-sectional area of the tested specimen was determined. The resistance R is related to the area A and the voltage V in a simplified way, as shown in equations 4.7 and 4.8.

$$R = \rho \frac{L}{A} \tag{4.7}$$

$$V = I \cdot R = I\rho \frac{L}{A} \tag{4.8}$$

From this, the failed area over the initial area was determined from the output ratio r of the DCPD system in equation 4.9 and 4.10. The ratio was corrected for an offset at the start of the test, since the resistances of the specimens did not perfectly match.

$$r\frac{V_{test}}{V_{ref}} = \frac{A_{ref}}{A_{test}} = r_0 \cdot \frac{A_0}{A_0 - A_{failed}} \tag{4.9}$$

$$\frac{A_{failed}}{A_0} = \left(1 - \frac{1}{r/r_0}\right) \tag{4.10}$$

It should be noted that this is only valid for the test section, whereas in the actual specimens there is also an influence of the solid blocks. However, because of the size of these blocks the influence was assumed small. Besides, a crack will not reduce the cross-section over the entire length, but in the 9-3mmØ and 81-1mmØ case a failed strut does lead to complete ineffectiveness of this strut in conduction. This means the above equations are usable to analyse the failed struts, but not the area of the growing crack. Because the output is thus not equal to the failed surface in the crack growth region, the damage parameter as used in the numerical model described in chapter 6 is introduced here, as well in equation 4.11. This parameter is a measure of the ratio of struts that have failed, with complete failure if $D = 1$. Finally, this can be related to the number of failed struts, n_{failed}, as shown in equation 4.12.

$$D = \frac{A_{failed}}{A_0} = \left(1 - \frac{1}{r/r_0}\right) \tag{4.11}$$

$$n_{failed} = n_{tot} \cdot D = n_{tot}\left(1 - \frac{1}{r/r_0}\right) \tag{4.12}$$

4.3.3. Fractography

After the fatigue tests, all tested samples were analysed with a standard optical microscope. This was done to get a general overview of the fracture surfaces. From this analysis a selection was made of specimens that were analysed in the scanning electron microscope (SEM). For the SEM analysis, a FEG-SEM of the brand FEI was used. In this microscope, ten samples were analysed to create figures of the fracture surface, find the initiation spots and determine the sizes of these spots. Two samples per type were chosen for the multiple load path specimens and the single strut specimens.

4.4. Test Matrix

In tables 4.2 and 4.3, the test matrices are shown. The fatigue test matrix shows the normalised stress at which the specimens are tested and the number of samples tested at that condition. The stresses are normalised to a known in-house value of the yield tensile strength (YTS) of the used material, which is kept constant for all geometries. The specimen type name is based on the number of struts and the diameter of one of those struts. To indicate specific individual samples, the specimen ID is used. In the table it is shown which specimen is used for which test.

Table 4.2: Fatigue test matrix

	Specimen	Description	S/YTS [-]	Number	ID
	1-9mmØ	1 Strut 9 mm	0.88	5	01, 02, 04, 05, 07
			0.63	5	03, 06, 08, 09, 10
	9-3mmØ	9 Struts multiple load path	0.89	5	03, 04, 12, 13, 14
			0.69	1	15
			0.56	5	01, 02, 06, 08, 11
	81-1mmØ	81 Struts multiple load path	0.88	2	01, 02
			0.63	5	03, 04, 05, 07, 12
			0.47	4	09, 10, 11, 15
			0.41	1	08
	9-3mmØ-D	9 Multiple load paths, pre-damaged	0.88	3	05, 09, 10
	81-3mmØ-D	81 Multiple load paths, pre-damaged	0.63	3	06, 13, 14
	1(9)-3mmØ	1 Strut machined from 9-3mmØ	0.89	9	01-09
	1-3mmØ	1 Strut 3 mm new	0.88	16	01-16

Table 4.3: Static test matrix

	Specimen	Description	Number	ID
	1-9mmØ	1 Strut 9 mm	3	03, 06, 09
	9-3mmØ	9 Struts multiple load path	3	04, 06, 08
	81-1mmØ	81 Struts multiple load path	3	12, 13, 14

5

Experimental Results

5.1. Data Presentation

The experimental data presented in this chapter and throughout the remaining part of this thesis is normalised for confidentiality reasons. For cross-sectional properties of the specimens, average dimensions are used to normalise the results of the specimen state analysis and the initiation spots in the fractography. Which variable is used for normalisation, is indicated in the figures.

For the stresses and number of cycles in the experiments, the following strategy is chosen. A constant yield tensile strength (YTS) is chosen to normalise the stresses. This value is representative for the material that is used and is based on a known value from earlier static testing. Although the YTS may vary for different geometries, the same value is used for normalisation. The number of cycles is normalised to a random scale, which scales linearly with the original scale. This means that the zero cycles coincide.

The fatigue test results are presented in S-N curves. In contrast to what is conventional in literature, the number of cycles is plotted on the y-axis and the stress level on the x-axis. This is because in the tests performed here, the stress is the independent variable, whereas in literature the S-N plot is used as a design curve. Normally, one designs for a given number of cycles, for which a matching stress level is found.

In the S-N plots, either the experimental data points and/or a best-fit curve are shown. This best fit is based on a power law curve, fitted with linear regression. For the modelled S-N curves, the shown graph shows the average results. When averages are shown throughout all data, the error bars show plus and minus one times the standard deviation of the presented variable, unless explicitly stated otherwise.

5.2. Specimen Production and Specimen State

After successfully producing the specimens, the diameters were measured and the surface was analysed. The measured diameters, diameter deviations and cross-sectional deviations from the as-designed geometry are shown in table 5.1. The table shows averages, with the standard deviation indicated for the measured values. The diameters that were measured were all smaller than intended, with larger deviations for the smaller struts.

Table 5.1: Average cross-sectional deviations with standard deviation, from the as-designed geometry based on measurements of all specimens

	1-9mmØ	9-3mmØ	81-1mmØ	1-3mmØ
Intended d [mm]	9	3	1	3
Measured d [mm]	8.95±0.01	2.80±0.03	0.94±0.03	2.90±0.03
Average deviation d [%]	-0.57	-0.55	-5.9	-3.3
Average deviation A [%]	-1.1	-1.1	-11.5	-6.4

The surface conditions were analysed using close-up photographs, which are shown in figure 5.1. The roughness of the surface that is the result of the layer-wise production process is clearly visible. Although the irregularities have a relative larger influence on the smaller struts, the conditions do not seem to differ much between the specimen types. For the 1-9mmØ specimens, the influence of the modelling of a cylinder with straight lines, was visible as vertical lines on the specimen. One further observation is that the surface is rougher at the root of the ellipses at the top of the struts, in contrast to the same root at the bottom of the struts. The rougher surface corresponds with geometry that was built in an overhang. Moreover, some excess material is present around the struts at this location. This is the case for the 9-3mmØ and 81-1mmØ specimens, whereas the 1-9mmØ specimens were created smoothly.

(a)   (b)   (c)
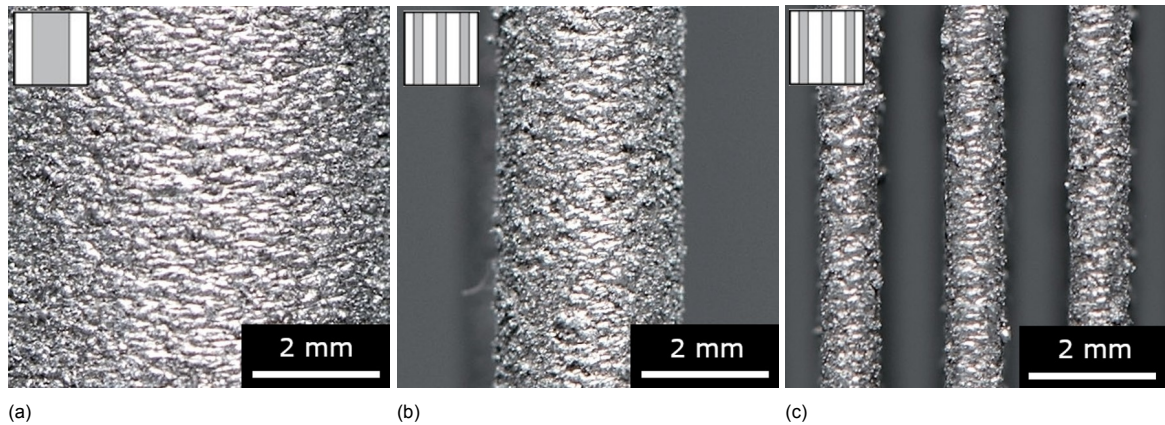
Figure 5.1: Close up view of multiple load path specimen surfaces: (a). 1-9mmØ (b). 9-3mmØ (c). 81-1mmØ sample

From the created (undamaged) specimens, the ones that are tested with and initial damage were prepared. A small notch is machined in one strut of the specimens. For the 81-1mmØ samples, two specimens were already damaged during the production, with one having two bent struts at the sides and one having a test section that underwent a shear deformation. These were tested as well, since the damages correspond to situations that could occur in real life applications. Because of this, only one sample with a notch was prepared. In figure 5.2, three of the four types of initial damage specimens are shown.

(a)   (b)   (c)
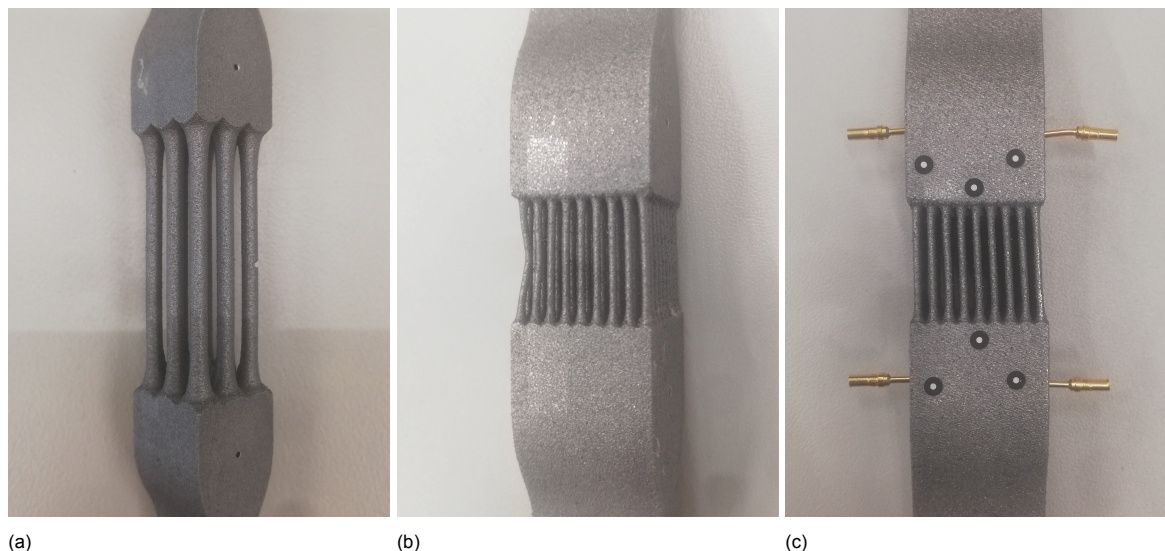
Figure 5.2: Initial damage specimens: (a). 9-3mmØ-04 sample with notch (b). 81-1mmØ-06 with bent struts (c). 81-1mmØ-13 with shear deformed test section

5.3. Static Tests

The results of the tensile tests of the 9-3mmØ and 81-1mmØ specimens are shown in figure 5.3. Table 5.2 provides the results from the DIC of the 1-9mmØ specimens, of which the average value over the entire part was given as output only. In figure 5.4 the estimated cross-sectional areas are shown, based on the calculations shown in section 4.3.1. The error bars indicate the standard deviation. The area of the 81-1mmØ specimens is determined with only 2 out of 3 specimens, since one had a test section which had undergone a shear deformation during production. Upon applying a tensile load and stretching the specimen, this shear was removed, leading to a 40% higher value of the strain. In figure 5.3, this outlier can clearly be seen as the sample with the largest tensile strain at the maximum stress.
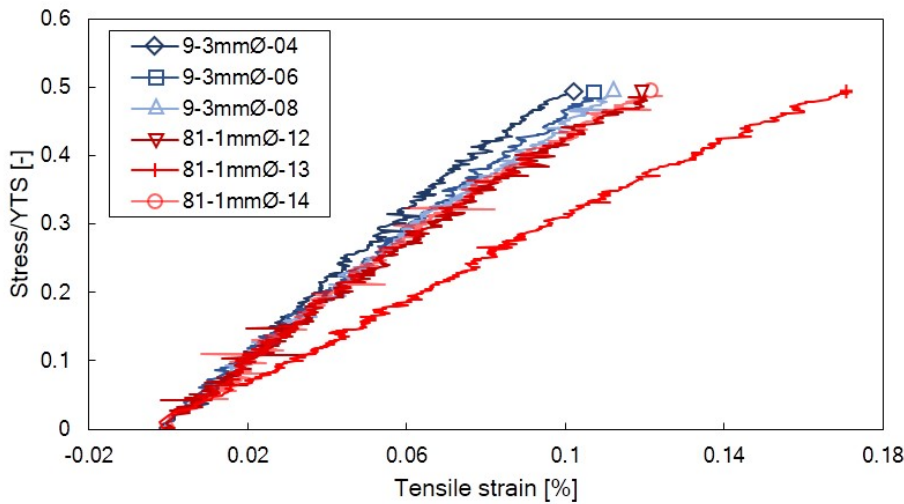
Figure 5.3: Static test results of 9-3mmØ and 81-1mmØ specimens

Table 5.2: Strain measurement of 1-9mmØ specimens

Specimen	Measured average strain DIC [-]
1-9mmØ-03	0.113
1-9mmØ-06	0.117
1-9mmØ-09	0.107
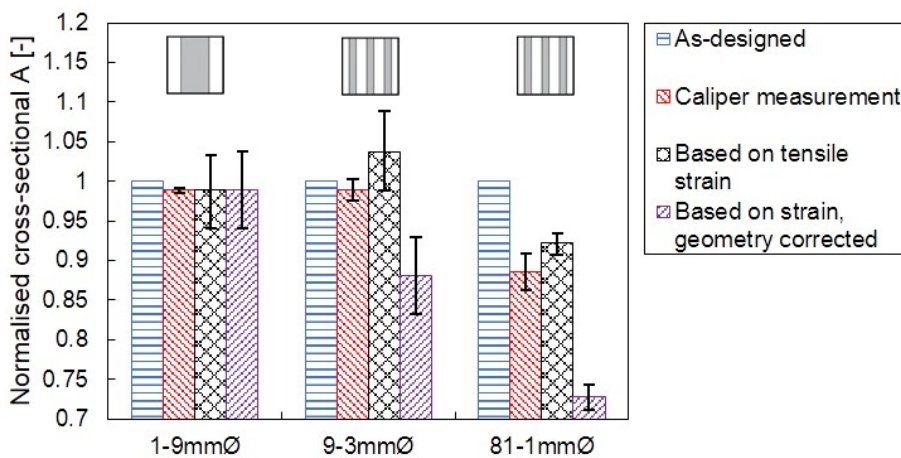
Figure 5.4: Cross-sectional area estimations based on tensile test, normalised to as-designed area

5.4. Fatigue Life and Potential Drop

Undamaged specimens

In figure 5.5, the S-N plot is shown for the multiple load path specimens. The individual data points can be found in appendix C. Clear trends are visible for each of the three specimen types. The power law fit shows that the exponent, corresponding to the slope in this plot, is similar. The total fatigue life decreases with increasing redundancy here. It should be noted that the 9-3mmØ specimens are tested at a slightly higher stress than intended at the highest stress level, as shown in the plot.
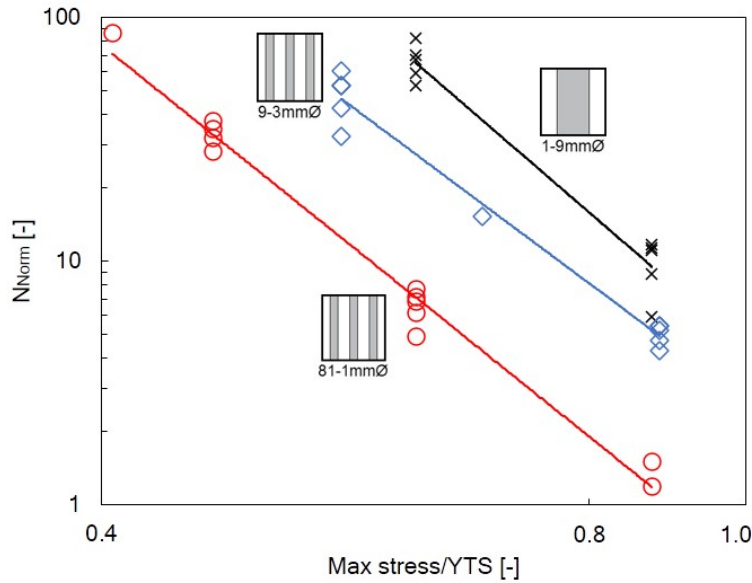
Figure 5.5: S-N curve of multiple load path specimens fatigue test

The scatter of the tests is analysed by looking at the standard deviation over the log-average of the fatigue life per stress level. The results are shown in figure 5.6. The stress levels at which only one or two tests are performed, are excluded from the figure. The results show overlap between different specimens at different stresses, however the value is lower for the 9-3mmØ samples than all single strut specimens at the same load.
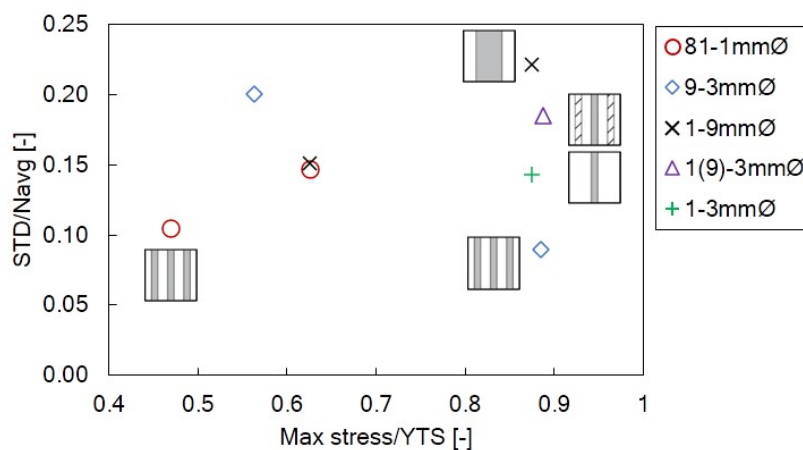
Figure 5.6: Standard deviation over log-average number of cycles for all specimens at all stress levels

For the redundant samples clear steps can be seen in the DCPD output where the signal rapidly increases. An example potential drop curve is shown in figure 5.7, where the calculated number of

failed struts is plotted against the number of cycles for the 9-3mmØ specimens at the 0.56 YTS stress level. From this output, the GR is determined by taking the first step in the response as first strut failure. The GR of the 9-3mmØ and 81-1mmØ specimens are analysed in figure 5.8, where the GR per stress level is shown. As shown, the GR increases with the number of struts that are present. Also, a dependency on the load seems present where lowering the load increases the GR.
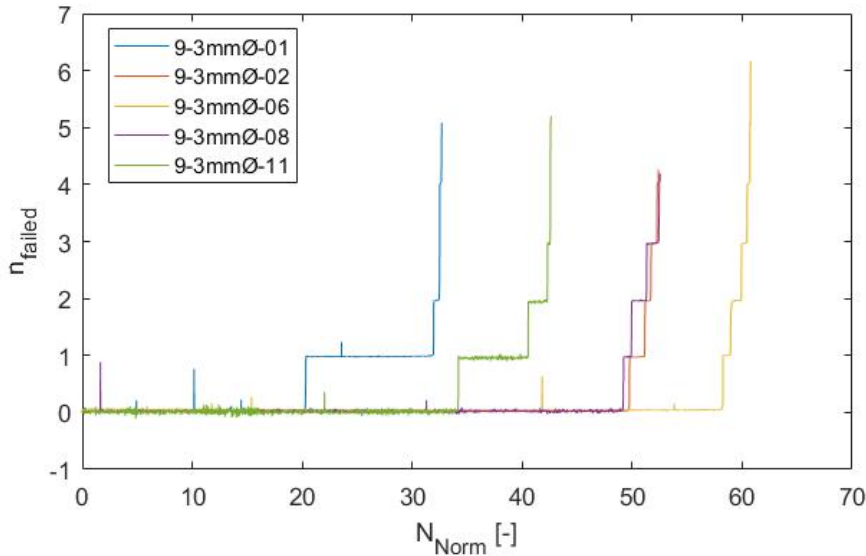
Figure 5.7: DCPD output of the 9-3mmØ specimens at the low stress level
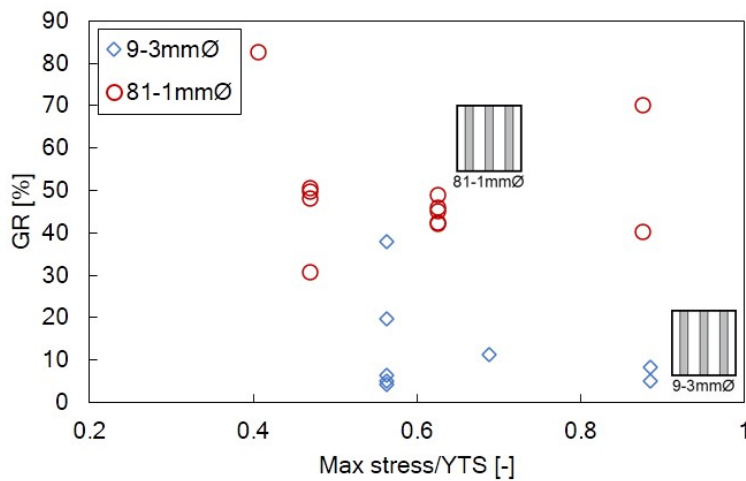
Figure 5.8: Experimental GR per stress level and specimen type

To further illustrate the gradual failure of the specimens, figure 5.10 shows the last 16 seconds of the test of sample 9-3mmØ-D10. The damage increases from left to right with initially two struts damaged. On the second picture, a crack grows in the fourth struts from the left, which fails in the third figure. Then the failure rate is increased and the right and left most struts fail in the last two figures. The damage occurs in a random sequence here, and not from one side to the other for example. Also, the height at which the struts fail, seems to be random. This pattern is observed in all multiple load path samples that were tested. In figure 5.10, another 9-3mmØ sample and an 81-1mmØ sample are shown in which this random height pattern is present. The space in between the fracture surfaces is different per strut, since the struts that failed at the end of the test have experienced more plastic deformation than the ones failed in fatigue at a lower load.
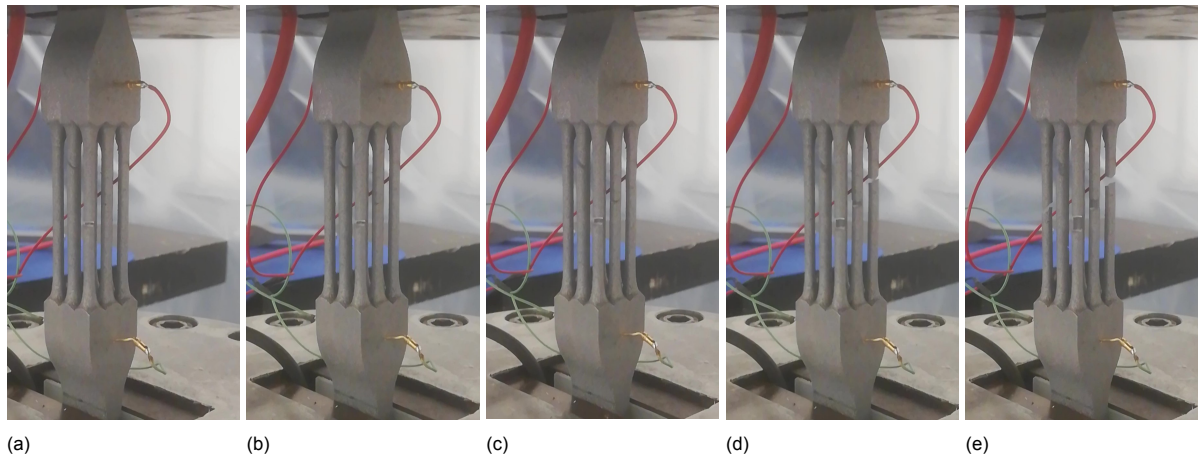
Figure 5.9: Crack initiation in struts of specimen 9-3mmØ-D10: (a). 16, (b). 12, (c). 2 and (d). 0.3 seconds before failure and (e). failed state
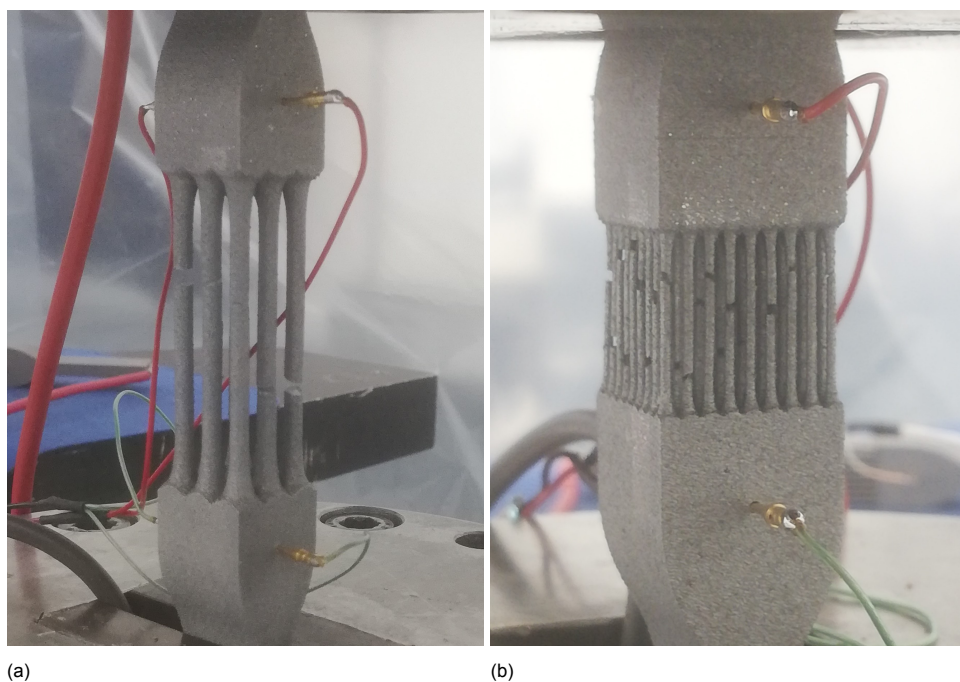
Figure 5.10: Random failure pattern in (a). sample 9-3mmØ-03 and (b). sample 81-1mmØ-08

Pre-damaged specimens

The initial damage results are presented here by showing both the the the S-N curve and the strut failures that are reconstructed from the DCPD. The differences with the pristine, or undamaged, specimens are shown, which helps in the analysis of the effect of including an initial damage. From figure 5.11 it becomes clear that the influence of an initial damage is different for the 9-3mmØ and 81-1mmØ samples. The red filled circles that represent the pre-damaged 81-1mmØ samples, fit within the scatter band of the results of the undamaged specimens at the same load. For the 9-3mmØ specimens shown by the blue diamonds, the fatigue life is significantly shorter.

In figure 5.12, the strut failures are calculated from the DCPD output. The first strut failure is clearly earlier for the damaged specimens, but the time between the second and final failure does not differ much between the damaged and undamaged specimens. In figure 5.13a, where the first, second and final failure are analysed from the DCPD output, the early first strut failure is clearly visible for the 9-3mmØ-D samples. All three pre-damaged specimens had their first failure around the same point and it was observed during the test that this failure was indeed in the notch area. Looking at the grace period,
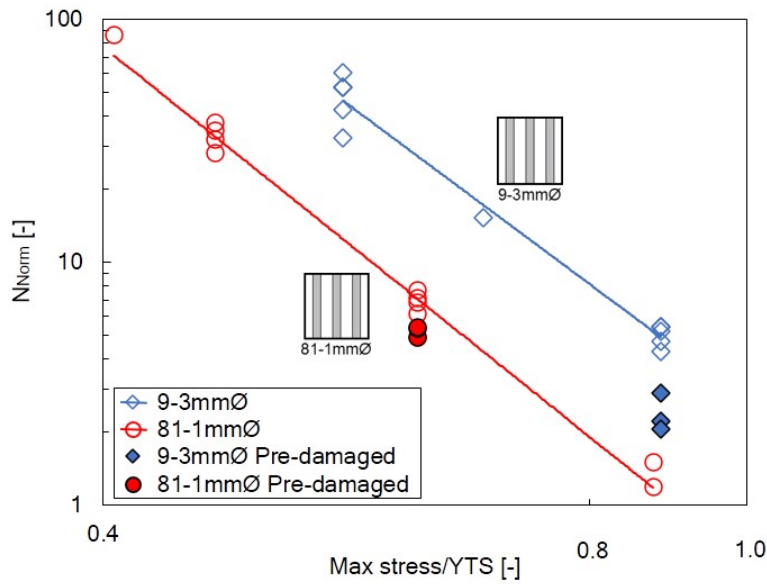
Figure 5.11: S-N curve with initial damage specimens included

indicated by the line in the figure, a large increase can be seen for the initial damage specimens. The final failure is also earlier, however the decrease in number of cycles until this moment is not as large as for the first failure. The second failure lies close to the final failure for all specimens.
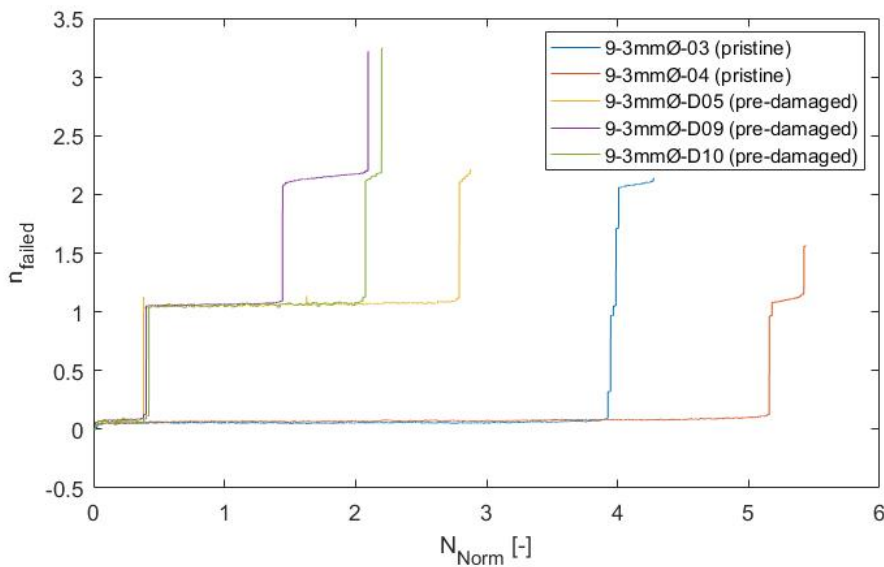
Figure 5.12: Number of failed struts as function of cycles analysed from DCPD data for 9-3mmØ specimens

For the 81-1mmØ specimens, the difference in fatigue life is less clear, as shown in figure 5.13b. Although the initial damaged specimens have a slightly shorter fatigue life, the earliest overall failure is of an undamaged specimen. Also, only one of the initial damaged specimens shows a significantly earlier failure, which is the sample with the shear deformed test section. The notched specimen did not fail as supposed at an early number of cycles. At its first strut failure after more than six times the number of cycles at which the notched 9-3mmØ-D specimens failed, no clear crack was visible in the notch area. This means that another strut failed earlier. Although the grace ratio of the initial damaged 81-1mmØ-D is still higher, the grace ratio between the second and final failure is unchanged.
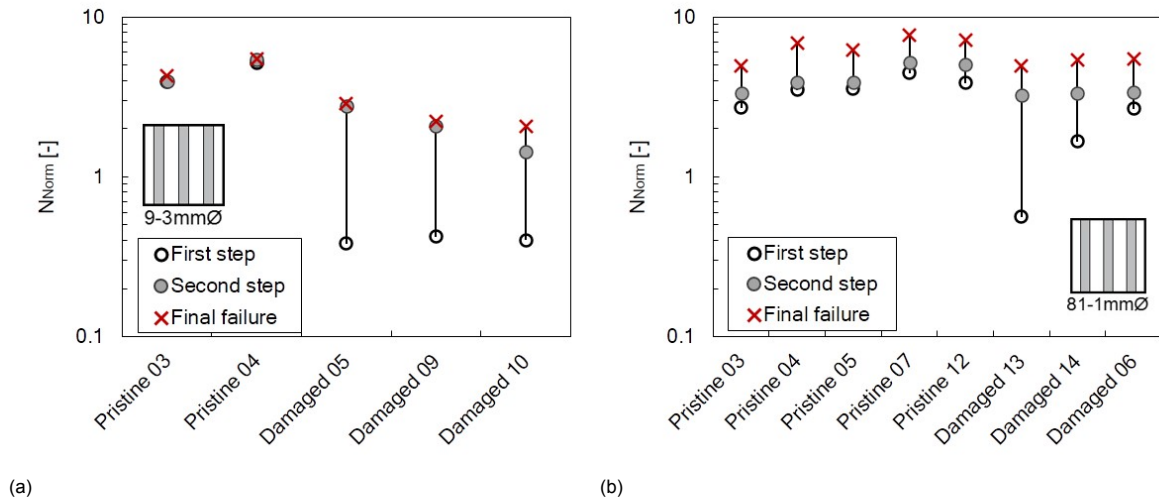
Figure 5.13: First, second and final strut failure of (a). 9-3mmØ and (b). 81-1mmØ with and without initial damage

5.5. Additional Single Strut Tests

For the additional 3 mm single strut fatigue tests, the results are presented in figure 5.14. The results of the 1(9)-3mmØ samples and the new 1-3mmØ are kept separate. The reason for this are the expected differences as a result of the production processes. As shown, differences are indeed present. The new 1-3mmØ specimens have a longer fatigue life than the 1(9)-3mmØ samples. The fatigue life fits within the scatter band of the 1-9mmØ samples, although the average is less. For the 1(9)-3mmØ samples, both the average fatigue life and the scatter are larger than those of the 9-3mmØ samples itself. The lowest fatigue life of these single struts furthermore corresponds to the first strut failure of one of the undamaged 9-3mmØ samples (pristine 1) shown in figure 5.13a.
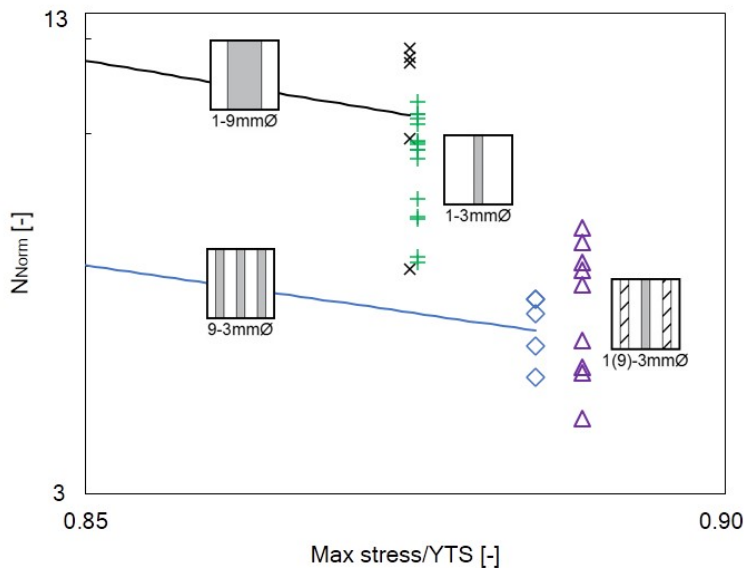
Figure 5.14: Single strut specimen test results, including partial 9-3mmØ results

5.6. Fractography

The findings of the optical microscope analysis per specimen type are described in section 5.6.1. From this analysis a selection was made of specimens that are analysed in the scanning electron microscope (SEM), of which the results are presented in section 5.6.2.

5.6.1. Optical Microscope

In general, fatigue cracks and final static failures can be distinguished, when looking at the fracture surfaces. The surface that failed in fatigue is larger at lower applied loads, as expected. The number of visible initiation sites, can however not immediately be explained by the applied load, since a relatively high number is present in all samples. Initiation sites are also visible in struts that have not failed before the final failure, indicating that cracks start to initiate and grow independently. It was also observed that in some 3 mm and 9 mm struts, large cracks were present at different heights than the fracture surface. Initiation happens almost always at the surface or subsurface and the cracks tend to follow semi-circular shapes. Moreover, in all specimen types porosity is visible.

For the 81-1mmØ samples, the fracture surface is very small because of the size of the cylinders, leaving relatively rough fracture surfaces. This makes is harder to distinguish the areas that have failed in fatigue and statically. Many struts are present, making it almost impossible to find the order in which the struts failed. The pattern is random in most specimens, but for the sheared initial damage sample specifically, it is visible that the part failed from the one side to the other one.

The fracture surface looks cleaner for the 9-3mmØ specimens. The geometrical pattern of failure is random for the struts, seen the locations of the fatigue crack surfaces with decreasing size. The smaller the fatigue crack area, the higher the load was upon failure, thus the later the strut has failed during the fatigue test. Almost all visible surfaces show at least one initiation site. Different situations between equally loaded samples are seen: sometimes multiple smaller crack areas are visible, sometimes bigger ones with more statically failed struts are visible. This does not immediately relate to the fatigue test results, since both specimens with large and small fatigue lifes and grace ratios have this effect. For the multiple load path specimens, it is furthermore observed that some of the struts failed almost completely in fatigue. For these specimens the remaining part of the cross-section which had failed statically only takes up a small portion.

The 1-3mmØ specimens show comparable fracture surfaces with the 1-9mmØ and 9-3mmØ specimens. For a few samples multiple initiation sites are present. Also, cracks at different heights are visible, which was also observed for the 1-9mmØ specimens. The effects shown in the new produced 1-3mmØ specimens correspond to what is seen in the 1(9)-mmØ samples that were machined from a 9-struts sample and tested individually.

5.6.2. Scanning Electron Microscope

From the analysis, the trends observed with the optical microscope were confirmed. The cracks follow a semi-circular shape as shown in figure 5.15. As shown in figure 5.16, multiple initiation sites are present for the 1-9mmØ and 9-3mmØ specimens, which are located at the surface of the struts. This surface initiation is observed for all specimens analysed in the SEM.
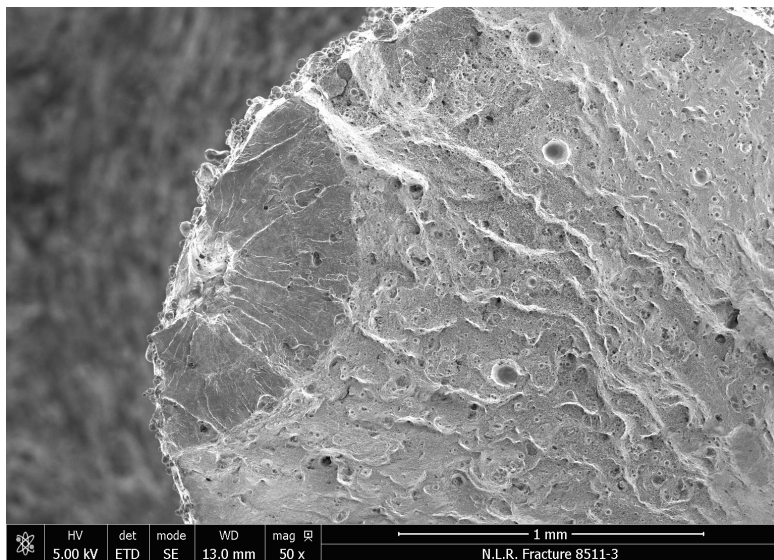
Figure 5.15: Semi-circular crack front in sample 9-3mmØ-03
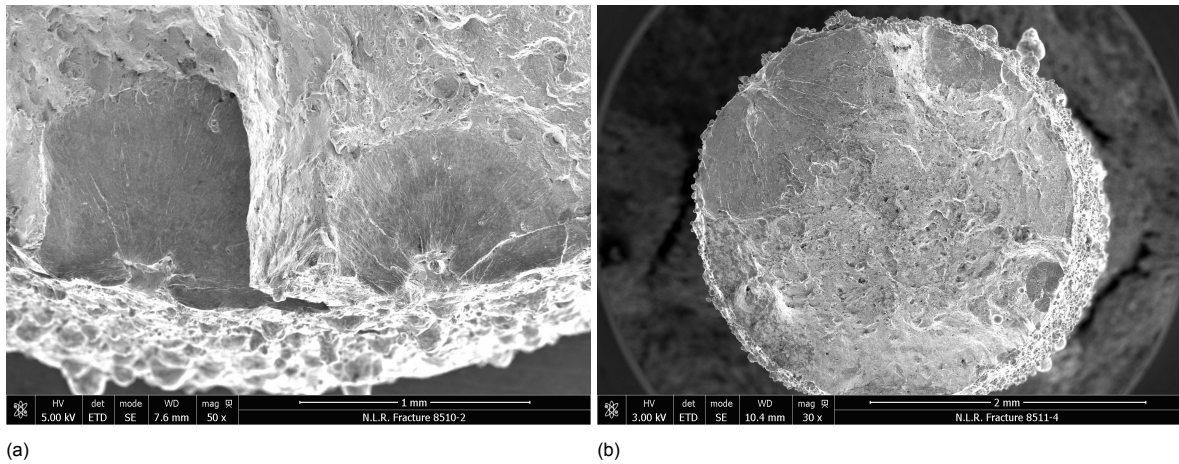
Figure 5.16: Multiple initiation sites in (a). a 1-9mmØ-02 single strut and (b). a strut from sample 9-3mmØ-04

   The size of the initiation spots is determined as well for the analysed specimens. The average width and depth of these spots are presented in figure 5.17. The absolute size of these spots does not differ much between the specimen types. The relative size is however bigger, when a smaller diameter is used. As an example, a crack initiation site in a 81-1mmØ strut is highlighted in figure 5.18.
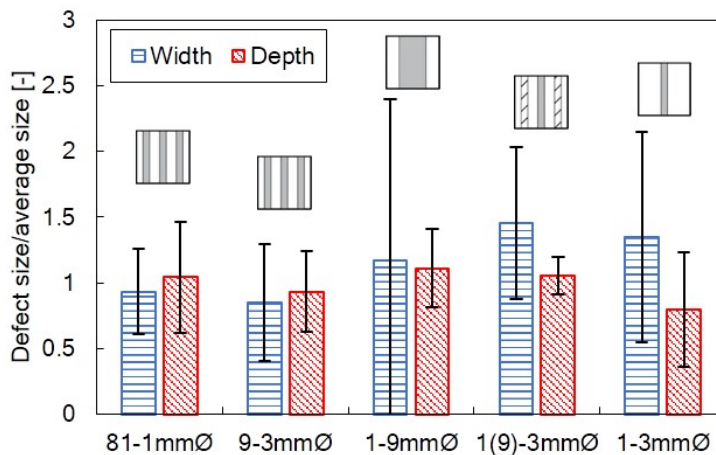
Figure 5.17: Average sizes of analysed crack initiation spots, normalised over the total average

   As observed with the optical microscope, several struts of the 81-1mmØ and 9-3mmØ multiple load path samples showed fatigue crack growth over large portions of the fracture surface. This is shown in figure 5.19. These fatigue fracture surface areas are relatively larger than the largest fatigue fracture surface area observed in single struts of various diameters. In figure 5.20, a 1(9)-3mmØ specimen is shown. As can be seen, the fatigue fracture surface area is smaller than for the 9-3mmØ sample in figure 5.19, even though the samples were tested at the same load. Finally, porosity was observed throughout all specimens. However, no quantification of this was done and no clear differences could be found for the different specimen types.
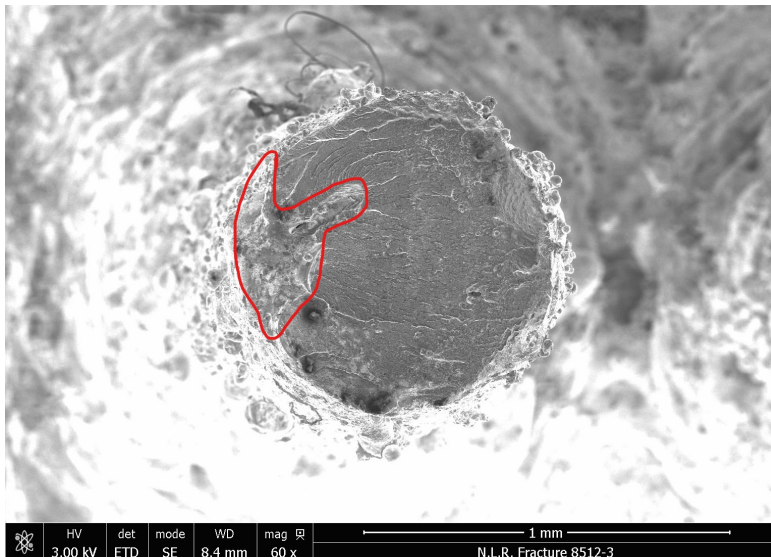
Figure 5.18: Initiation spot in a 1 mm strut of sample 81-1mmØ-03

(a)   (b)
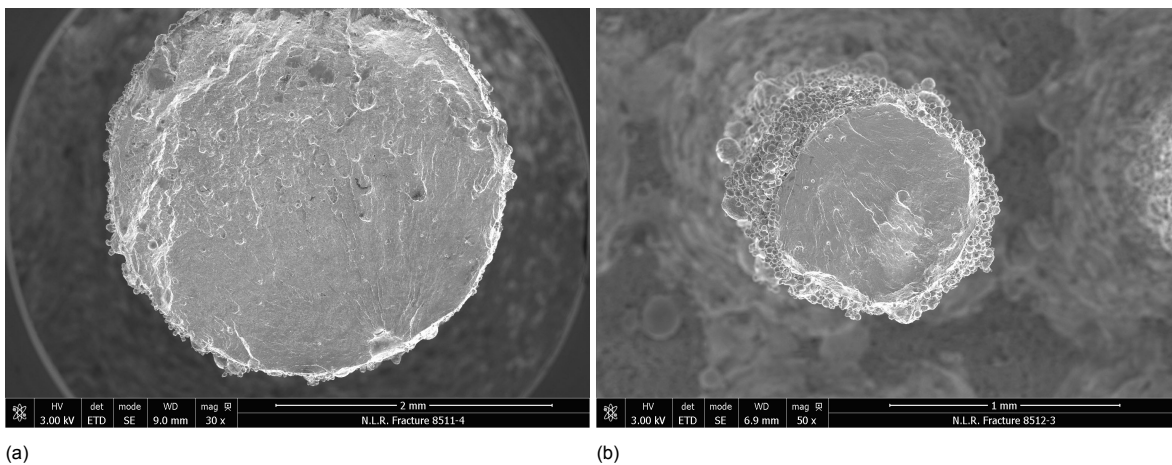
Figure 5.19: Large fatigue fracture surface areas on (a). sample 9-3mmØ-04 and (b). sample 81-1mmØ-03
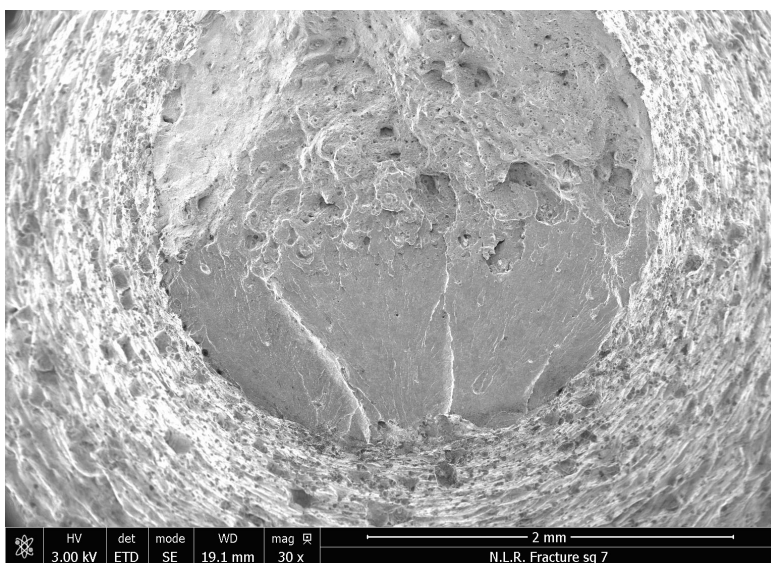
Figure 5.20: Fatigue fracture surface area on sample 1(9)-3mmØ-07

6
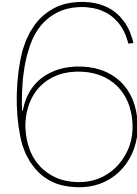
Failure Modelling Methodology

The effects of redundancy that are expected can be predicted by modelling the hypothesised gradual failure. In this section, such a model is created to compare with the test data, to analyse which effects are present and to analyse the sensitivities of the test. In chapter 3, it was hypothesised that gradual failure would occur in the multiple load path structures. This is based on the individual initiation of the cracks throughout the structure. Because this initiation is scattered, struts will fail at different times and thus have an individual fatigue life. After failure of the first strut, the load is taken over by the remaining ones at an increased stress level. This mechanism is recreated in the model that is described in this chapter. The model that is described here is called the 'cascading damage' model. This model is further extended to include the equal surface case, which is applied during the experimental testing in this report. Also, the crack growth life is analysed, since differences in growth life occur when using different diameter struts. This model is used to investigate the theoretical sensitivity of multiple load path structures, but also to test the damage propagation that occurs in the experiments. Therefore, the model is used in combination with the experimental results, as will be shown in this chapter.

6.1. Cascading Damage Model Set-up

The cascading damage model that is created is strongly based on similar models found in literature. Zargarian et al. created a fatigue failure model for lattices that determines the individual fatigue life for struts with a random thickness distribution at a given applied stress value [68]. Due to the statistical distribution of the radii, different struts have a different fatigue life. When the number of cycles for the strut with the shortest life is reached, this one is taken away and the load is increased. The remaining lifes of the other struts are updated by summing the number of cycles at a certain level over the maximum number at that level, according to Miner's rule. For this sum, the damage parameter D is introduced. When it reaches the value of $D = 1$, a strut fails following Miner's rule. Burr et al. describe a similar model that also includes differently loaded struts for certain lattice unit cell topologies and radius distributions for the struts [74]. Different statistical radius distributions are tested and verification of the model is done with experiments.

The model used here differs from the above-mentioned ones in the following way. Parallel struts are used instead of a unit cell, which means only pure tension is present and the load is equally distributed over the struts. Also, all reasons for differences between the struts are simply captured in having one statistical distribution for the fatigue life of the struts. The parameters of this distribution come from fitting it to given data points. These data sets can either come from the literature or from the experiments done here. With the data from single struts specimens, predictions can be done for the redundant samples. As such, the correct material parameters are used and the effect of including redundancy can be shown and can be compared to the situation in reality.

The model, which is coded in MATLAB, works as follows. The full code is provided in appendix E. As described above, the input data originates from experimental values. Two stress levels are needed to construct a Basquin power law, used to scale the fatigue life with all stress levels occurring throughout the simulation. From the mean of the data points at the input levels, the exponent of the Basquin's relation, shown as b in equation 6.1, is determined analytically [77].

$$S \cdot N^b = c \tag{6.1}$$

The coefficient in the above equation can be found by using a single data point when the exponent is known. Either one of the data sets used for the exponent can be used, or a new one. The latter is the case when simulating with the experimental values in this report. Tests at multiple load levels are only done for the multiple load path and 1-9mmØ samples, whereas a good estimate of the behaviour of a single strut with 3 mm diameter is given by the additional single strut tests performed at only one load. Moreover, the number of repeated tests for these single struts is higher, making it possible to create a more reliable distribution. For the above-mentioned reason, the statistical distribution that is needed is fitted to the input data set for the coefficient. The model allows for the fitting of various types of distributions, depending on which one describes the data best. For the current analysis, both log-normal distributions and Weibull distributions are considered applicable, because of the ease of use and the use in fatigue analyses throughout literature respectively.

With the power law relation, the fatigue life distribution is scaled to the stress level at which the simulation starts. From this distribution, random values are taken to recreate the scatter in fatigue life between the struts at the tested level. A vector with the length equal to the number of struts present and with statistically distributed fatigue lifes is thus created.

Since all struts have the same diameter and thus the same cross-sectional area, the encountered load levels that occur upon increasing number of failed struts are independent of the failure pattern. These load levels can thus be determined beforehand. Because the load levels are known, the fatigue life vector can be extended to a matrix with the random variables, of which each one is scaled with the power law to every possible stress level. Negative values for the fatigue life, which can occur when using a normal distribution, are corrected to zero.

With all possible load levels and the corresponding fatigue lifes per strut known, the damage accumulation can be modelled. A loop is entered where for every repetition one strut fails. The strut to fail is found from the constructed matrix by taking the minimum value of the calculated remaining life at the correct stress value. The remaining fatigue life for strut j at level k is determined as follows. The value for the damage parameter is known from the previous repetition of the loop, or is equal to zero for the first strut failure. Since a value of one would mean failure of the strut, the remaining life at level k is related to the damage as shown in equation 6.2.

$$D_j(k-1) = \sum_{i=1}^{k-1} \frac{N(i)}{N_{max,j}(i)} = 1 - \frac{N_{rem,j}(k)}{N_{max,j}(k)} \tag{6.2}$$

Rewriting this results in equation 6.3. Since the maximum number of cycles for strut j at level k is known from the earlier constructed matrix, and the damage parameter is known, the remaining life of all struts can be found.

$$N_{rem,j}(k) = N_{max,j}(k) \cdot \left(1 - D_j(k-1)\right) \tag{6.3}$$

The strut with the minimum remaining life is then removed from the model by deleting its row in the fatigue life matrix and the damage vector. The number of cycles corresponding to this remaining life is added to the total of cycles that have passed. After that, the load level is increased one step and the damage parameters are updated according equation 6.4.

$$D(k) = D(k-1) + \frac{N(k)}{N_{max}(k)} \tag{6.4}$$

This loop is repeated until the input ultimate tensile strength (UTS) is reached. Based on the input UTS, the number of struts at which this happens is calculated. At this number of remaining struts, the programme is stopped.

Because a random set of fatigue life values for the individual struts is determined for each run of this model, running the same code another time would yield different results. To avoid misinterpreting the results due to random variation, the model is run M times. The outputs of the model are again statistically distributed as shown in figure 6.1. For the distribution fits, normal and log-normal distributions are used in this figure. Input data from Persenot et al. is used, similar as in the work performed by Burr et al., and is analysed at 200 MPa [74, 78]. The material used by Persenot et al. is Ti6Al4V. By

taking the mean value for M outputs, a more reliable output is created for each parameter. Moreover, the standard deviation for each output variable can be used, which is a parameter for the accuracy of the results. From running the model for multiple values for M, it was found that for $M = 100$ and higher the average output values stay within a range of 5%.

(a)   (b)   (c)
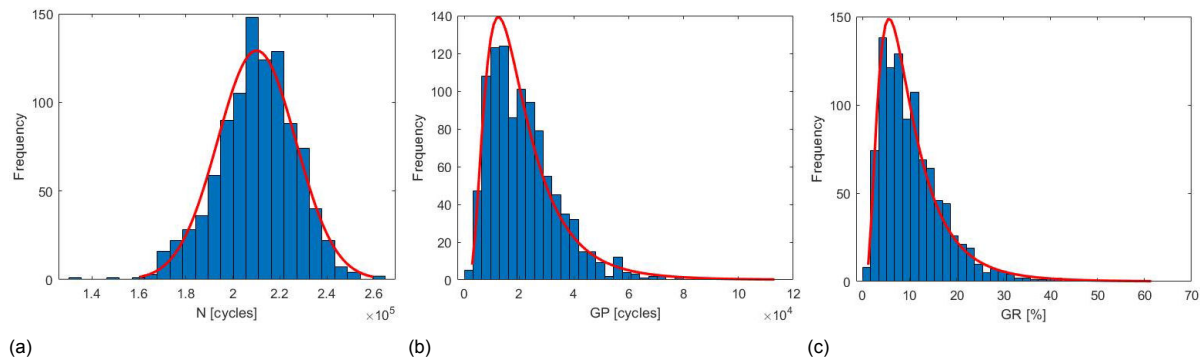
Figure 6.1: Statistical distribution and histogram of (a) The total fatigue life, (b) the GP and (c) the GR for M = 1000 samples, 9 struts and the input data from Persenot et al. [78]

6.1.1. Length Correction
In the model presented here, the number of random variables taken from the statistical distribution is equal to the number of struts. As a result, more struts have a shorter total fatigue life in the model. This is attributed to the fact that more draws from the distribution, so more struts, have more spread. Since the onset of the cascading damage is determined by the weakest strut, the total fatigue life decreases. This can be seen as the fatigue size effect. However, in the experimental tests performed in this thesis, it has been tried to rule out this effect by keeping the surface area of the specimens equal. In case of the single struts for example, the same surface is present in a single bar, so in series instead of parallel. The weakest point in this structure is responsible for the overall failure and should comply with the same weak point if the surface is divided over multiple struts following the hypothesis. Therefore, the cascading damage model is corrected for this size effect.

The correction of the model is applied as follows. Instead of taking the same number of random variables from the distribution as the number of struts, 81 draws (or more if applicable) are taken independent of the number of struts. In the case of 1 or 9 struts, it is assumed that the 'weakest' elements determine the fatigue life of a strut. The matrix containing all fatigue lifes is for this corrected model created for the number of draws that are defined. A larger matrix is thus initially created. Depending on how many struts are present, the matrix is sectioned in this amount. For example, the 9-strut case would have 9 sections of 9 draws, equalling up to 81 draws in total. The lowest fatigue life per section is the critical one. For every section, the higher values are removed, such that a matrix appears that has the correct number of struts again, containing the weakest link per strut.

6.1.2. Crack Growth
In the model presented in this chapter as well as in S-N curves, the effect of fatigue crack growth is assumed negligible. However, as seen in the results from Kotzem et al. and from analytical analyses with data from Di Giovanni et al., it appears to be worthwhile to include the effect of crack growth, since the values of the crack growth life are reasonable large [31, 79]. Moreover, the crack growth life is dependent on the diameter of a strut, leading to differences in growth life between the specimen types used in this report.

A simple analytical model is created to estimate the fatigue crack growth in a cylindrical strut. Using the Paris law, the crack growth rate is determined and numerically integrated in MATLAB, of which the code is included in appendix E. The Paris relation and the stress intensity factor are given by equations 6.5 and 6.6 [58]. It should be noted that for the crack growth, a stress range is required instead of a maximum stress. Since a stress ratio of $R = 0.1$ is applied in this report, this is also done for the crack growth model.

$$\frac{da}{dN} = C\Delta K^m \tag{6.5}$$

$$K = \beta S\sqrt{\pi \cdot a} \tag{6.6}$$

The geometry correction factor β for a thumbnail crack in a solid cylinder with diameter d is given by equation 6.7, taken from Forman and Shivakumar [80]. This geometry factor complies with the crack shape observed during the analysis of the fracture surface described in chapter 5.

$$\beta = \left(0.92\left(\frac{2}{\pi}\right)\sec\left(\frac{\pi a}{2d}\right)\sqrt{\frac{\tan\left(\frac{\pi a}{2d}\right)}{\frac{\pi a}{2d}}}\right) \cdot \left(0.752 + 1.286\frac{\pi a}{2d} + 0.37\left(1 - \sin\left(\frac{\pi a}{2d}\right)\right)^3\right) \tag{6.7}$$

The crack growth life is found from numerically integrating the Paris equation from an initial crack length to a defined final crack length, while counting the number of cycles. The initial crack length can be taken as small as 0.005 inches or 0.13 mm for aluminium alloys according to Schijve [58]. The final crack length is taken as the full diameter of the analysed strut, since the growth rate rapidly increases at larger crack lengths. Therefore, the influence of integrating to the full diameter on the total growth life is small.

To create a better view on the effect of growth on the output of the cascading damage model, the crack growth life is added to this model. Since the crack growth depends on the current stress level and because the initiation of cracks in other struts continues while a crack is growing, this addition should be done inside the cascading damage loop. This is done by calculating the growth life and adding it to the number of cycles that have passed in the current iteration. The addition occurs after identifying the minimum remaining life, such that the fatigue life matrix is not changed, and before updating the damage parameters, such that the cycles during which the crack grows, do count for the initiation in the other struts. Since the input data for the entire model already includes the crack growth life, the input should be corrected when doing a prediction with the growth life included. This can be done by subtracting the growth life at the input points, which can be found using the same crack growth model.

6.2. Sensitivity Studies

Sensitivity studies are done for different parts of the model. The crack growth life model is analysed, as well as the effect of including it in the cascading damage model. Also, the effect of including the length correction is analysed. Finally, the sensitivity of the pure cascading damage model is described. With this information, trends observed in the model can be connected to real life cases, such that the experimental results in this report can be placed in perspective.

6.2.1. Growth Life Sensitivity

The analytical growth life model is analysed for different initial flaw sizes, diameter struts, stress levels and different materials. Based on the chosen inputs, the growth life can reach values that are of influence on the situation in reality, and therefore it should be known how sensitive the model is. A table is set up with the growth life at different inputs, for two materials. The constants for the Paris equation for are taken from Di Giovanni et al. [79]. In this paper, crack growth rate experiments are done for additive manufactured AlSi10Mg. Constants for Ti6Al4V are taken from Wang et al. [81].

6.2.2. Effect of Including Growth and Length Correction

To analyse the effect of including growth and length correction, the total fatigue life, but also the first strut failure is analysed. With this information, the grace period can also be shown, and thus the effect on this parameter. For the analysis, a stress of 200 MPa is used. An initial crack length of $a_0 = 0.5mm$ was chosen and $M = 1000$ samples were taken. Use is made of Ti6Al4V data provided by Persenot et al. [78].

6.2.3. Cascading Damage Sensitivity

For the cascading damage model without growth, sensitivity studies are performed. The inputs that are changed for this study are the stress level, number of struts and scatter of the individual strut behaviour. The analysed outputs are the mean fatigue life, standard deviation of this fatigue life and grace period and ratio. For all analyses, the model is run $M = 1000$ times. The input data for these sensitivity studies is provided by Persenot et al. [78].

The first sensitivity analysis is done for increasing stress level. All other parameters are kept equal and a situation with 9 struts is chosen, since this number is also present in the test and assumed to be in a reasonable range when designing redundant structures. The analysis is done both with and without length correction for 81 draws. The second analysis is on the number of struts. Since the experimental tests are only limited to a given set of specimens, the effect of redundancy to a larger extent is analysed with a sensitivity study on the number of struts. A maximum number of struts of 225 is chosen.

To model a change in scatter, the input data was fitted by a normal distribution and manipulated to have a different amount of scatter. The found standard deviation was multiplied with a given constant, as shown in figure 7.4. A change in input scatter can in reality be the caused by using more stable manufacturing processes, different materials and other variations in the structure. For these reasons, the scatter analysis is thus included.

6.3. Test Data Modelling

In this section, the model is run with the experimental results shown in chapter 5. These results will be used to support the discussion in chapter 8 and to show the applicability of the model. In this section is described which inputs are taken, and which outputs are required. The 9-3mmØ case will be analysed, because information on the fatigue life of the 3 mm single struts with the same material properties is available.

6.3.1. Inputs for Test Data Modelling

As input data for the coefficient of the power law and the statistical distribution, the fatigue results from the 1(9)-3mmØ specimens are used. This is done because these struts have the exact same material properties as the struts used in the 9-3mmØ case, whereas the 1-9mmØ samples and new produced 1-3mmØ struts appear to have different material properties. Since these specimens are only tested at one load level, the power law exponent input is provided by the 1-9mmØ specimen results. With this input, the model should thus be able to predict the behaviour of the 9-3mmØ samples. The distribution that is fitted to the data is the Weibull distribution. This distribution showed the best fit to the results of both sets of 3 mm single strut specimens, as shown in figure 6.2.

(a)   (b)
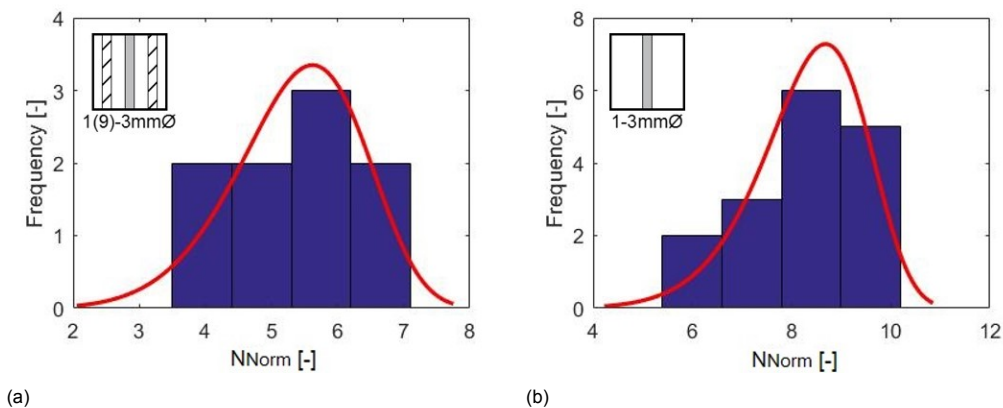
Figure 6.2: Histogram and Weibull distribution fit to 3mm single strut results: (a).1(9)-3mmØ samples (b). New produced 1-3mmØ samples

To be able to simulate with the crack growth model included, the parameters for the crack growth should be known. From the DCPD output, the growth in the tested samples can be analysed. However, due to the complex geometry of the specimens, the exact relation between the crack surface area and the DCPD signal is unknown, as described in section 4.3. This means only the number of cycles in

which crack growth occurs is known. The fitting of a growth model is thus limited to assuming the material parameters and determining the initial crack length based on the DCPD data. For the material parameters used in the Paris law, the values provided by Di Giovanni et al. are used here [79]. The values chosen are applicable to AlSi10Mg for the vertical build direction. The initial crack length is found through determining a suitable value such that the crack growth life of the 1-9mmØ specimen corresponds to the estimated growth life visible in the DCPD output. Furthermore, when the growth model with these parameters is applied to the 9-3mmØ specimens, the growth life of the first failed strut also corresponds to the DCPD signal.

To compare the initial damage results of the 9-3mmØ specimens, the model is modified to have one early failure. Since the first strut failure occurred around the same number of cycles, this number is used as first strut failure in the model as well. The created fatigue life matrix per strut is adjusted to have the first failure at this number of cycles. For this first strut failure the growth will be neglected, since in reality the growth was also not through the entire strut due to the notch. The total fatigue life as well as the damage accumulation curve, similar to the DCPD output of the experiments, will be created for comparison.

6.3.2. Analysed Outputs for Test Data Modelling
The analysed outputs are categorised into three parts, to make a full analysis of the model possible. First, the created output probability density function (PDF) of the model is compared to the experimental values at the same stress. This is done for two stress values. With this, the accuracy of the model can be shown. Then, the S-N curve created by the model is compared to the one from the experiments. Aside from the fatigue life, the GR and standard deviation of the fatigue life are also assessed at the stress levels at which multiple experimental values are present.

Finally, the step-wise failure modelling is analysed to show how it compares to the DCPD outputs from the experiments. The number of cycles between two failures is plotted against the number of failed struts for both the model and experiments. At two stress levels, the log-average of the number of cycles between strut failures is shown per number of failed struts, which is calculated from the DCPD response. For the model, the average of $M = 1000$ iterations is taken for the failure events.

7

Failure Modelling Results

7.1. Sensitivity Studies

The results of the performed sensitivity studies are given in this section. For the growth life model, an analysis is done for different inputs. Also, the effect of including the growth life and length correction on the cascading model is analysed. The effects of changing the inputs of the cascading damage model on the outcome of the model are also described in the following.

7.1.1. Growth Life sensitivity

From analysing the fatigue crack growth life for the alloys for which the Paris constants are provided, the results shown in table 7.1 are obtained. It can be seen that the influence of the initial length on the total growth life is large and even larger than the influence of the total strut diameter and the stress level. Furthermore, the growth life also scales with the stress input, being lower at higher stresses. Seen the values for aluminium and the differences between the largest and smallest diameter, the growth life is likely to have an influence on the experimental results. It should be noted that the results show the growth life through a single strut, instead of growing through multiple struts with changing stress level, as is the case in the cascading damage model.

Table 7.1: Output of the growth life model

a_0 [mm]	d [mm]	S_{max} [MPa]	N_{growth} AlSi10Mg [kcycles]	N_{growth} Ti6Al4V [kcycles]
0.13	1	100	93	64
	3		202	143
	9		251	219
0.5	1	100	0.14	2.9
	3		9.8	42
	9		28	109
0.5	1	150	0.022	1.2
	3		1.4	17
	9		4.0	45

7.1.2. Effect of Including Growth and Length Correction

Including the growth life and length correction, gives the following effect on the outputs. The difference in total fatigue life of the samples and their first strut failures are shown in figure 7.1. As can be seen, the total fatigue life increases when the crack growth is included. Also the first strut failure is at a higher number of cycles, since this failure only occurs after growth. This trend is observed for all three specimen types that are analysed. However, the effect is smaller if a thinner diameter strut is used. The growth life though a larger diameter strut is longer, even when multiple smaller struts are used through which the crack has to grow. It should be noted that the total growth life here is different from
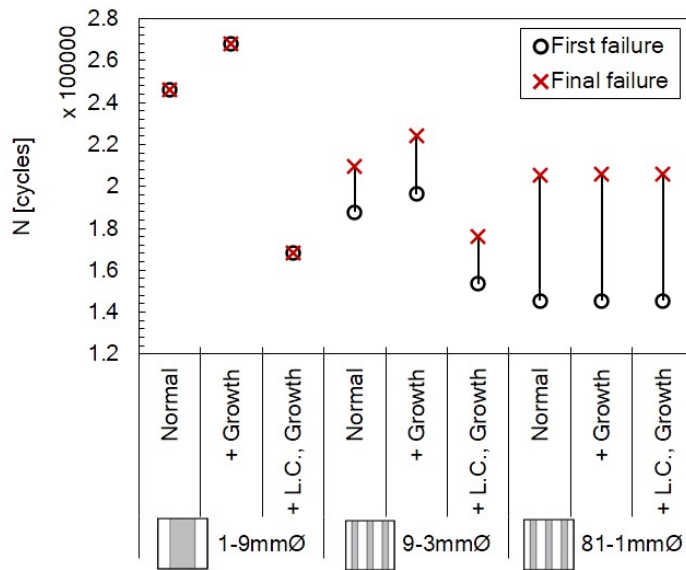
Figure 7.1: Effect of including the length correction (L.C.) and growth on the fatigue life and first failure, averaged for 1000 samples

the number of struts times the individual growth life, since load levels change when struts fail. In the case analysed here, the growth life is still small enough to not affect final conclusions on which number of struts has a longer fatigue life. However, it is large enough to take into account since an increase in fatigue life of 9% is reached for the 1-9mmØ specimens.

By applying the length correction, the first strut failure is earlier for the 1-9mmØ and 9-3mmØ specimens. The effect of the length correction is larger for the 1-9mmØ specimens. By definition, if 81 draws are taken, the 81-1mmØ specimen is unaffected. When the length correction is applied, the first initiation should be at the same number of cycles. Due to the application of crack growth however, the first strut failures of the different specimens do not coincide.

In figure 7.1, the GP is visible as the line between the first and final failure. As can be seen, the increase in GP is limited for the multiple load path specimens with almost no effect on the 81-1mmØ sample. The application of the length correction influences the GP, since not only the first, but also the following failure events are earlier. Since the growth stays the same with and without length correction, the decrease in GP due to the correction is partly counteracted by the growth. For this reason, the GP for the normal and length corrected plus growth case is similar in the figure.

7.1.3. Cascading Damage Sensitivity
The results of changing the input stress level are shown in figure 7.2. It is observed that increasing the load at which is tested, decreases both fatigue life and grace period, since the input fatigue life at the higher level is also shorter. The input point is shifted along the Basquin curve. As a result, the fatigue life mean and standard deviation, as well as the grace period follow an exponential curve similar to the Basquin law. The observed difference between the normal and length corrected graphs, is in accordance with the differences shown in figure 7.1. The difference is explained by the earlier initiation in the length corrected model. The grace ratio appears to be independent of the load and of the length correction. In the model, the entire distribution is scaled with the load. Both the mean values as the scatter undergo the same transformation.

By running the model for an increased number of struts, a trend is visible that the total fatigue life decreases. However, the grace period and ratio increase for the normal situation as shown in figure 7.3. For the length corrected model an increase in fatigue life is visible. Because 225 draws were taken, the curves converge towards this value where both models are equal. It is observed that the total fatigue life stabilises at a certain level of redundancy, but that the grace ratio keeps increasing. Upon increasing number of struts, the standard deviation of the total fatigue life decreases rapidly. This means that upon having more redundancy, the final failure is more predictable. Since the same number of draws is taken in the length corrected model, this curve is less sensitive to this effect.
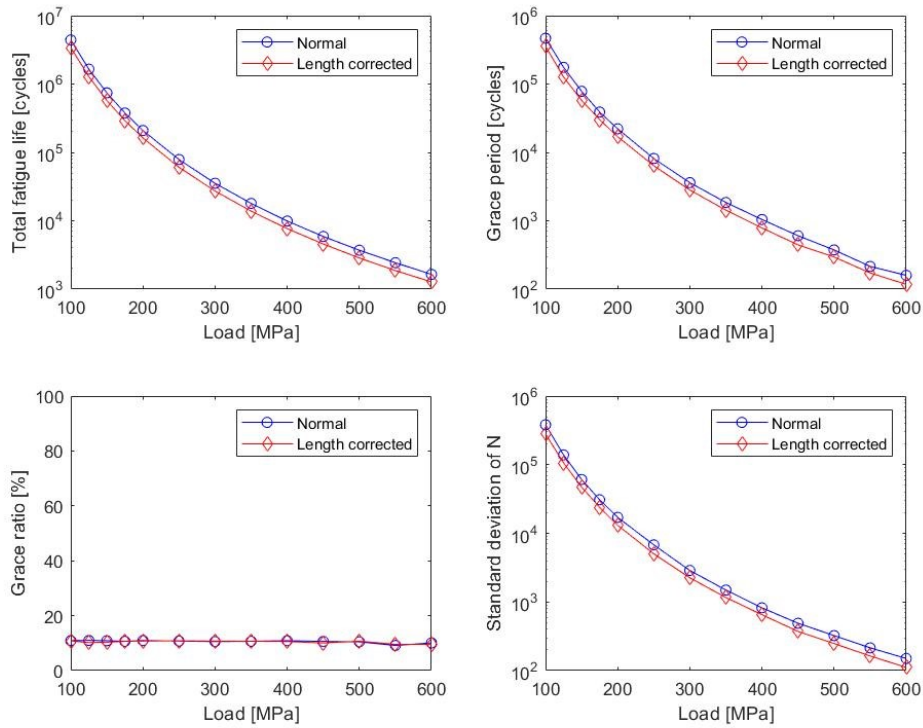
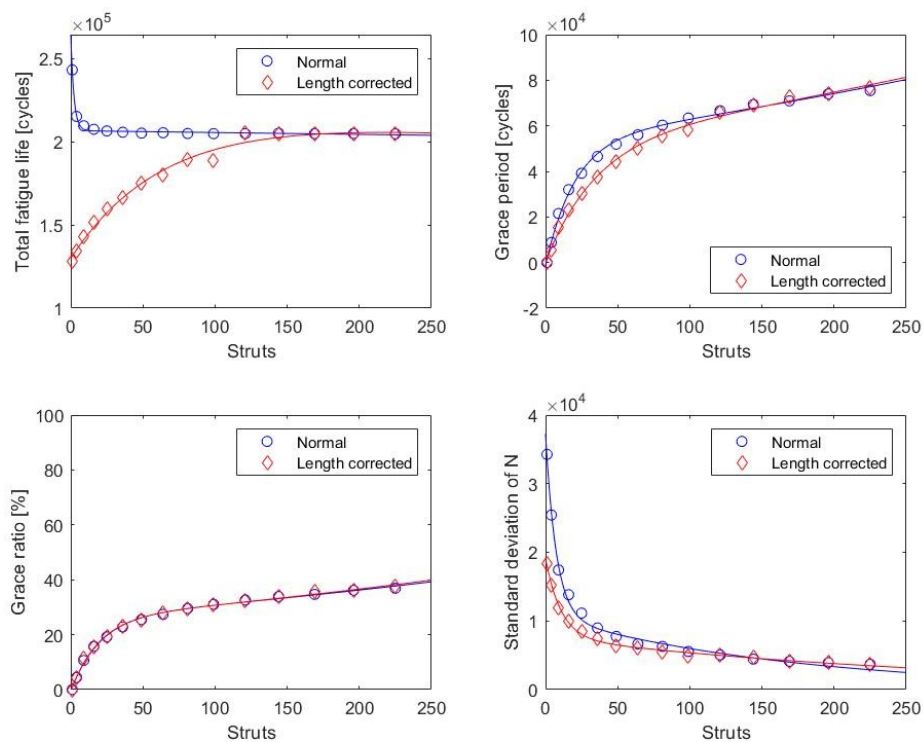Figure 7.2: Trends for increasing load at 9 struts

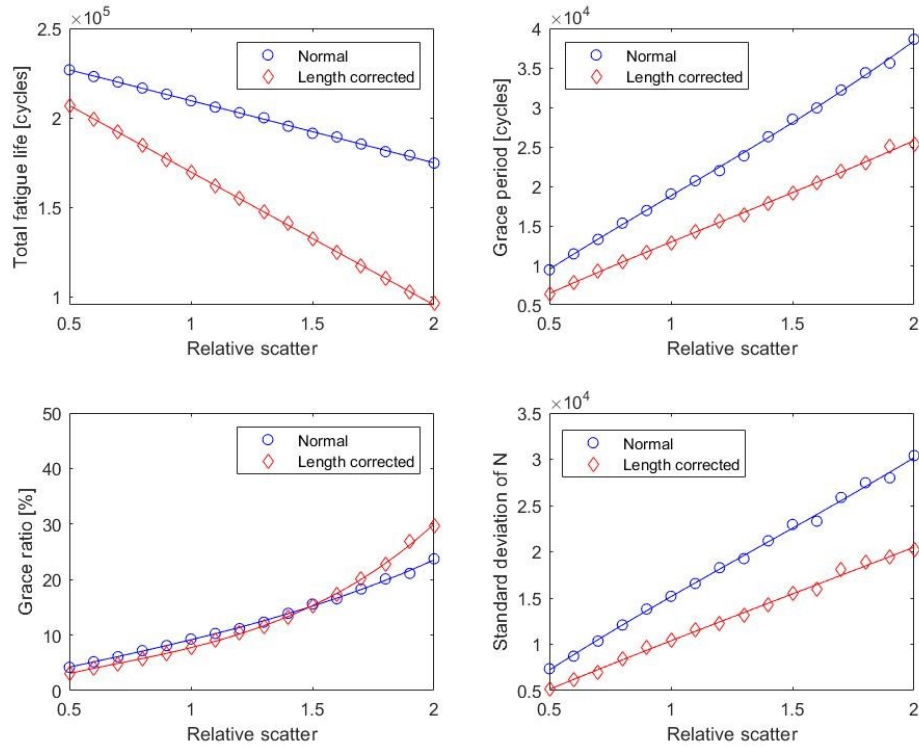Figure 7.3: Trends for increasing amount of struts at 200 MPa

Figure 7.4: Trends for increasing amount scatter at 200 MPa and 9 struts

The scatter of the input data directly influences all output parameters, as it determines the onset of the failure cascade, the time between failures and as such the total fatigue life. The observed effects are as follows and are shown in figure 7.4. The higher the amount of scatter, the lower the total fatigue life, but the higher the grace ratio and period. These variables follow a linear trend. The plots of the grace period and fatigue life standard deviation show similarities.

7.2. Test Data Modelling

In this section, the results from running the model with the inputs obtained with the experiments are shown. The model was run with fatigue growth life, for $M = 1000$ iterations. Since the fatigue test results of the multiple load path specimens showed an opposite trend as compared to the model with length correction, i.e. the struts with a larger diameter show a longer fatigue life rather than shorter, the length correction was not used in the analysis of the test data. This does not mean that the length correction is not applicable at all. However, since an AM related fatigue effect occurs next to the statistical size effect and the relative sizes of these effects are unknown, any size correction was left out to approximate the trends seen in the experiments.

The growth life was included in these simulations. A value for the initial length is found that gives a good estimation for the growth life of all specimens at both stress levels, in combination with the growth life model described in section 6.3. For the 1-9mmØ and 9-3mmØ specimen types, the number of cycles of crack growth are shown together with the DCPD response in figure 7.5.

In figure 7.6, the output of the model, which is a probability density function (PDF) curve, and the experimental values for the fatigue life are shown. The fitted distribution is a Weibull distribution, corresponding to the input distribution. Crack growth is included in this simulation, the length correction is not. The peaks of the PDF correspond to the mean value of the estimation, which is shown in figure 7.7, in which the S-N curve is shown for both the experiments and the simulations. The 81-1mmØ and 1-9mmØ cases are also modelled here.

The prediction for the 9-3mmØ samples lies within the scatter band of the experimental results. At the higher stress level, the fatigue life is correctly predicted. However, the prediction and experi-
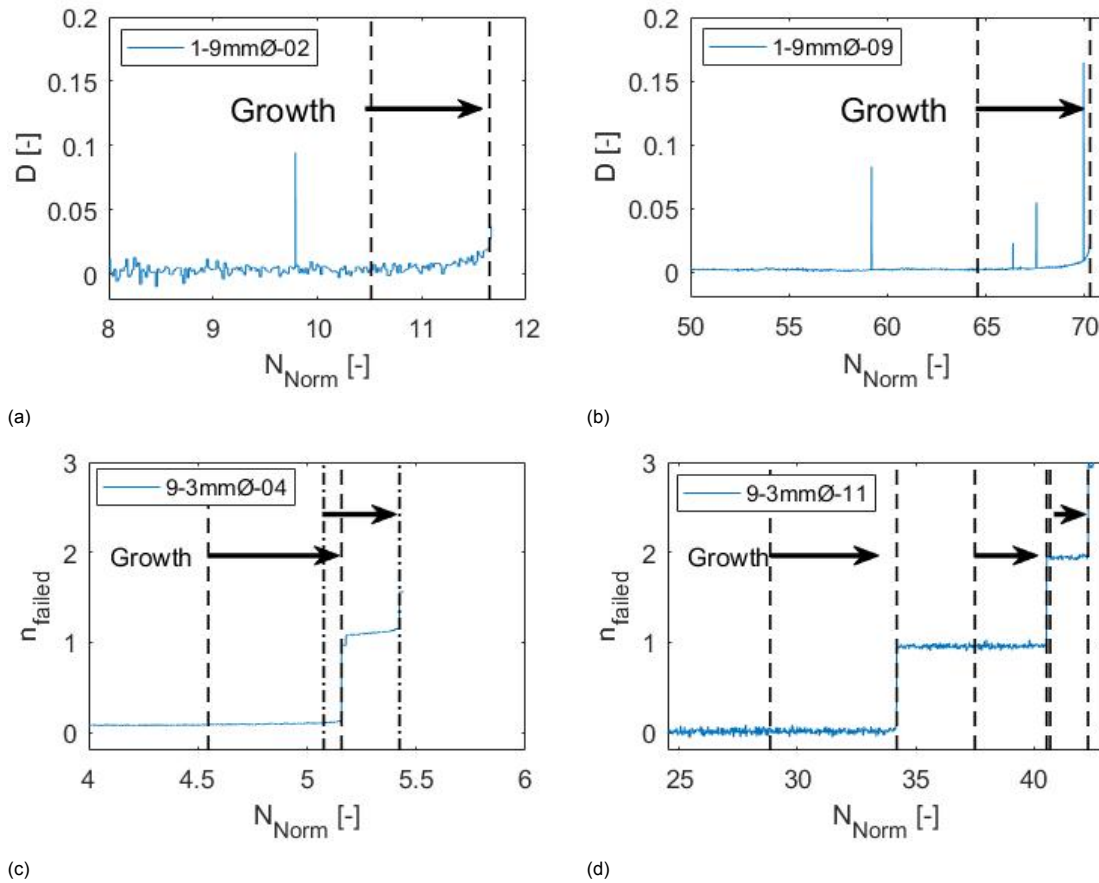
Figure 7.5: Experimental DCPD response and modelled growth cycles for the 1-9mmØ (a,b) and 3-9mmØ (c,d) specimens at two stress levels
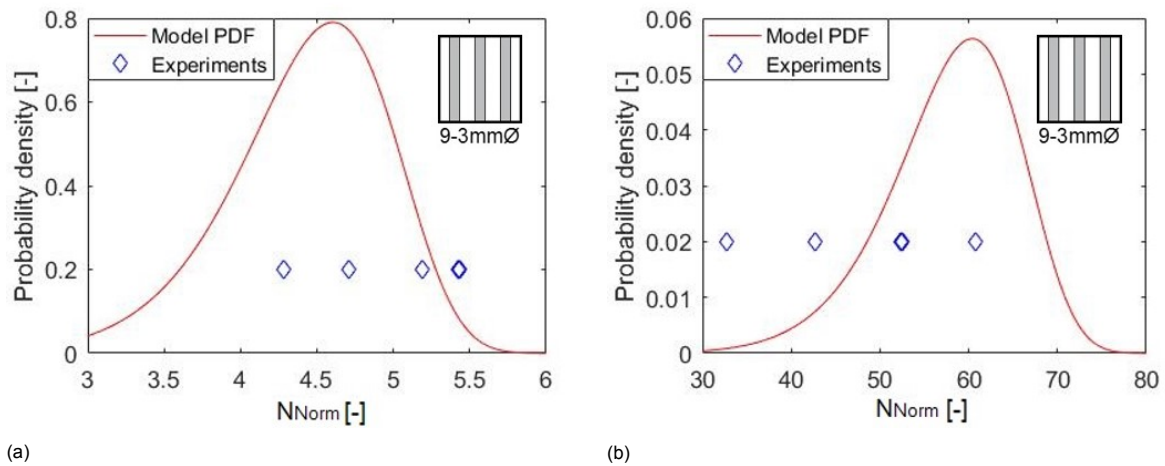
Figure 7.6: Output probability density function of the model and experimental values for (a). 0.88 YTS stress level (b). 0.56 YTS stress level

mental curves diverge towards the lowest stress level since the slope follows the 1-9mmØ power law. Therefore, the number of cycles is overestimated at the high stress level. The 1-9mmØ and 81-1mmØ predictions are above and below the 9-3mmØ curve respectively. This agrees with fatigue test results qualitatively, however, it can be seen that the curves created with the 1(9)-3mmØ input data cannot accurately predict the value of the fatigue life.
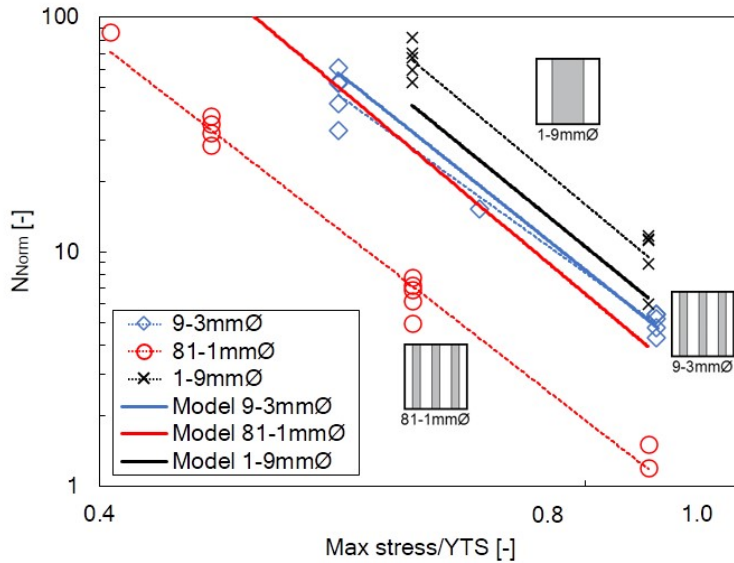
Figure 7.7: S-N curve of simulation and experiments

The obtained GR and standard deviation of the model are shown in figure 7.8a and 7.8b respectively. In these figures, no difference is made for the different applied loads, since the GR and standard deviation over the fatigue life are independent of the stress in the model. It is shown that the GR can be predicted accurately. A slight underestimation is done by the model for the GR of the 81-1mmØ specimens. This is also true for the standard deviation in this case. The standard deviation is predicted close to the average of the standard deviation at multiple stress levels, except for the 81-1mmØ samples.

(a)   (b)
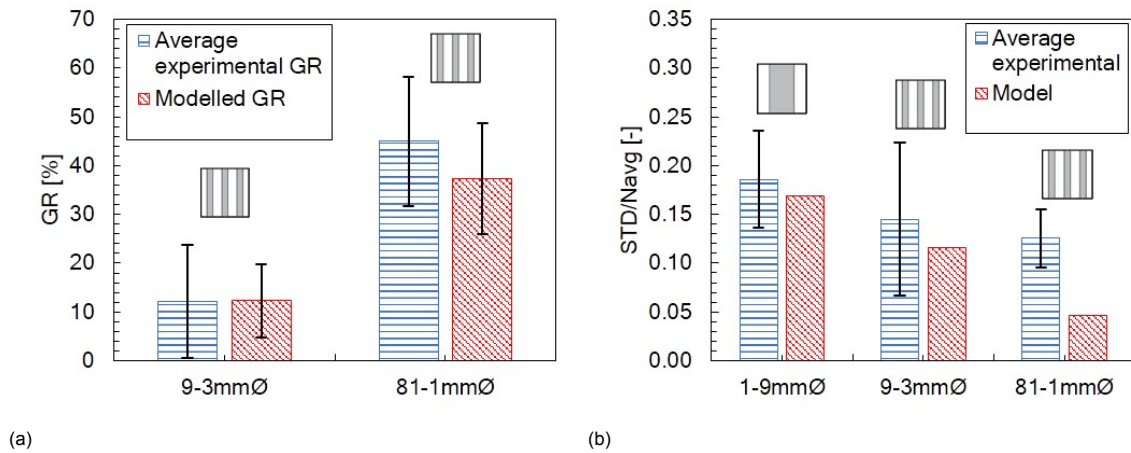
Figure 7.8: (a). GR and (b). Standard deviation over the fatigue life for model and experiments

To assess how the gradual failure is modelled compared to the gradual failure in reality, the number of cycles between the failure events are shown in figure 7.9, for two stress levels. As can be seen, the failures have a decreasing interval for increasing number of failed struts. The model and experimental values for the 0.56 YTS stress level are in good agreement. For the 0.88 YTS stress level, the average is based on only two samples. There, a more scattered result for the experimental values is observed.

The damage accumulation curve of the 9-3mmØ specimens with initial damage and the corresponding modelled curve are shown in figure 7.10. As shown, the first step was manipulated correctly to match the experimental results. The second and third steps lie in between the minimum and maximum experimental results. As such, the predicted curve fits correctly between the experimental ones.
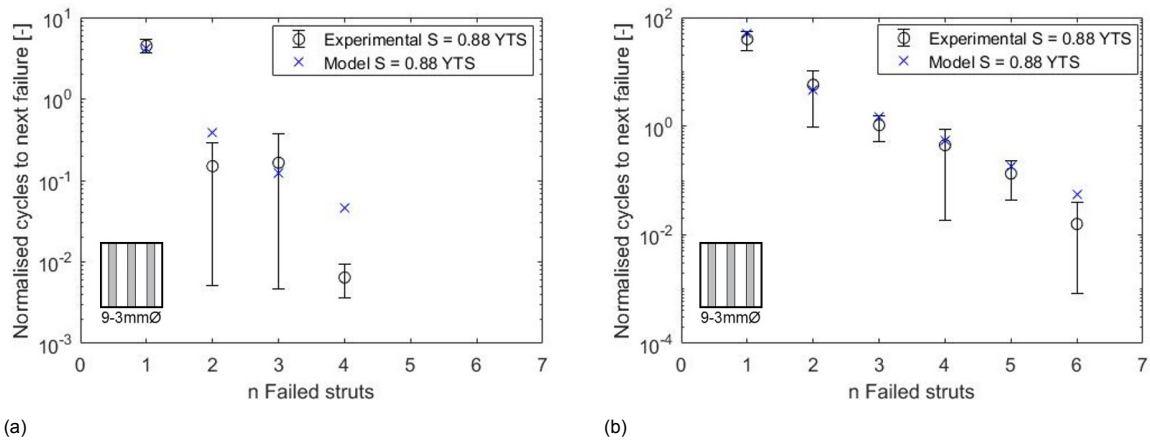
Figure 7.9: Failure interval per number of struts failed of the 9-3mmØ specimens for the (a). 0.88 YTS stress level and (b). 0.56 YTS stress level
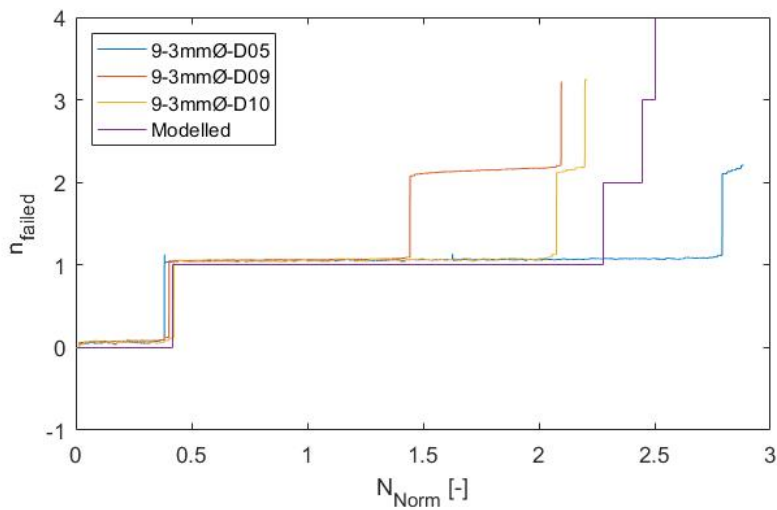
Figure 7.10: Experimental and modelled failure accumulation curves for 9-3mmØ specimens

8
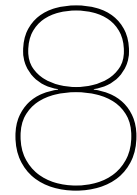
Discussion

With the experiments done in this thesis, the behaviour of specimens with multiple and single load paths and with varying diameter struts is shown, both on the field of fatigue life and damage propagation. It is clear that the fatigue life of the more redundant samples with thinner struts is shorter, but multiple effects that influence this fatigue life can be identified. Firstly, the manufacturing of differently sized struts leads to differences in the fatigue life, from which a shorter fatigue life of thinner struts can be expected. Aside from this, effects of crack growth life and the placement of multiple struts in parallel are also investigated in this chapter. The different effects are analysed and compared to find out their relative influence.

The step-wise failure pattern that is observed in the experiments is compared to the modelled damage propagation, to show that this pattern is well understood. The statistical differences between struts lead to a gradual failure with a higher GR for more redundant structures. This in combination with less sensitivity to damage is the reason for increased damage tolerance of multiple load path structures. At the end of this chapter, the damage tolerance and meaning for the design of AM structures will be further explained. With the analyses presented in this chapter, well substantiated answers to the research questions of this thesis will be provided.

8.1. Manufacturing Related Effects

The material and geometry that is formed during the SLM process is highly dependent on the part itself that is manufactured and the surrounding elements on the build plate. Therefore, differences were expected in the geometry and fatigue behaviour of a single strut when the diameter and distance to other struts change. To investigate the influence of this on the interpretation of the overall fatigue results from this study, the fatigue performance of all single struts that are tested can be compared. These are the 1-9mmØ, 1-3mmØ and 1(9)-3mmØ specimens. For the analysis of the geometry, all specimens that were produced can be analysed, as will be done in the following.

Looking at the geometry, it can be seen that the produced diameters deviate more from the as-designed geometry for the thinner struts. This is best shown by table 8.1, where the diameter deviation is the most extreme for the 81-1mmØ specimens. The same effect of having larger deviations for smaller diameters is also described throughout literature and is related to both the accuracy of the SLM and different thermal histories, leading to shrinkage [16, 30].

Table 8.1: Cross-sectional deviations and standard deviations of measured specimens

	1-9mmØ	9-3mmØ	81-1mmØ	1-3mmØ
Measured d [mm]	8.95±0.01	2.80±0.03	0.94±0.03	2.90±0.03
Average deviation d [%]	-0.57	-0.55	-5.9	-3.3
Average deviation A [%]	-1.1	-1.1	-11.5	-6.4

The static tests are meant to verify the diameter measurements. This was needed because of human errors, the rough surface and the impossibility to measure the inside struts. Due to plasticity

during the final phase of the fatigue tests, the diameters of the inside struts could not be measured after testing. In figure 5.4 the estimated cross-sectional area based on the static test is shown for the multiple load path specimens. The same trend of larger deviation from the as-designed shape is visible for the thinner elements.

In figure 5.4, both an estimation and geometry corrected lower bound value for the cross-sectional area are included, next to the caliper measured and as-designed values. The estimation value is an overestimation of the actual area, since thicker elements throughout the length of the specimen were included in its determination. This leads to less deformation, so a larger estimated area. This is compensated for in the lower bound, which provides an underestimation. This is because the stresses are most-likely not completely equally distributed over the elliptical part and solid rectangular part of the strut. Also, it is known that the stiffness of thinner diameter struts is in general lower [30]. For the lower bound area value this means that in reality the cross-sectional area is larger than this calculated value. For the actual value of the cross-sectional areas of the specimens, the following can be said. The exact value can not be calculated from the static tests, due to the complex geometry, accuracy of the test, and potential stiffness variations. The caliper measurement value is however between two extremes, meaning that the measured value is an reasonably good estimate for the actual size.

The surface roughness is also mentioned in literature to be different for different sizes of AM part features [16]. In figure 5.1 the surfaces of the multiple load path samples were shown. The roughness does not seem to deviate much, however for the thinner struts the influence of a same size irregularity is relatively larger. Although the surface roughness is not quantified in this thesis, the relative influence of irregularities is also shown with the fractography done in section 5.6. The sizes of the crack initiation site are not dependent on the used diameter for the strut. However, since these spots are relatively large for the 1 mm struts, the influence of these irregularities on the fatigue life of the 81-1mmØ specimens is larger due to decreasing effective cross-sectional area. Eventually, a shorter fatigue life can thus explained by this.

The average fatigue lifes of the differently sized single struts are shown in figure 8.1. The error bar shows the maximum and minimum number of cycles for the specimens that were tested. Although the scatter bands of the tests show overlap, the average fatigue lifes are clearly different, with a trend for lower fatigue life for the specimens with smaller diameters.
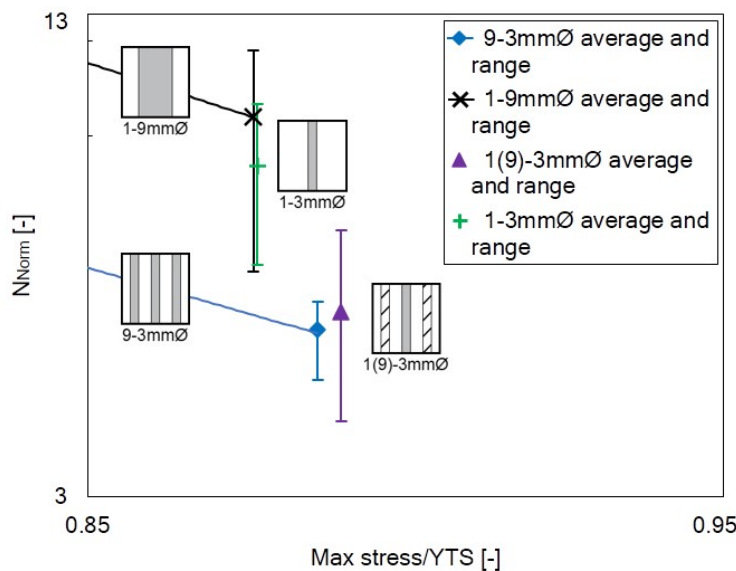
Figure 8.1: Average fatigue results and range of the single strut specimens and the 9-3mmØ samples

Comparing the 3 mm struts to the 1-9mmØ specimens, it becomes clear that the geometry in terms of diameter and length influence the fatigue life. The thicker but longer struts have a longer fatigue life. The effect that explains this, is the size effect for AM. It is well-known that the fatigue life of thinner elements is generally lower for AlSi10Mg [16, 30]. Based on this, it could be thus be expected that the thinner strut elements performed worse. An exact quantification of this AM size effect can however not

be given by the results of this study. Since the 9 mm struts also have a larger length, the statistical size effect plays a role as well in these results. The statistical size effect would lead to a lower fatigue life for larger struts, counteracting the AM size effect. From figure 8.1 it can however be concluded that the AM related effects are stronger than the statistical size effect, since the smaller specimens have a lower fatigue life. This can be further explained by the fact that the statistical size effect is less pronounced for axial loading [82] and that this effect stabilises at a certain specimen size [83]. The observed multiple initiation sites in the cross-section and the cracks at multiple heights in one strut of the same specimen prove this, since the minimum specimen size of having at least one maximum size defect seems to be exceeded.

The results show a relatively large difference between the 1(9)-3mmØ specimens and the new 1-3mmØ ones. The fatigue life of the 1-3mmØ specimens is longer, for which an explanation can be found in the surrounding part geometries during production. The spacing in between parts is larger than that of the 1(9)-3mmØ specimens, which are the specimens without other struts in the close proximity on the build plate. This effect also plays a role when comparing the 9-3mmØ and 1-9mmØ specimens. It should be noted however that a new batch of powder was used for the 1-3mmØ samples and that a shorter layer deposition interval time was present due to the smaller batch size. The latter is shown in other materials to lead to better fatigue properties [19, 20].

The above-mentioned effects influence the results of the multiple load path fatigue tests. Based on the smaller diameters combined with the AM size effect and the relatively larger influence of irregularities, as well as the close proximity of other struts, the specimens with more and thinner struts are expected to perform worse in fatigue. This can not be completely counteracted by the statistical size effect, as shown in the results in figure 8.1.

Because the diameters of the specimens were measured and shown with static testing to be realistic, the correct cross-sectional area could be used to determine the stresses and forces during fatigue testing. In the extreme case of the determined lower bound value of the cross-sectional area, the fatigue curves are closer to each other. However, this value was discussed to be a large underestimation. It can be said that the cross-sectional deviations do not change the trends seen in the results of the fatigue tests.

8.2. Fatigue Life Performance

The fatigue life of the tested specimens decreases with increasing redundancy, meaning that the 81-1mmØ samples have the shortest and the 1-9mmØ samples the longest fatigue life. This is the opposite of what was hypothesised. In chapter 3, it was described that the fatigue life would increase with increasing redundancy, since initiation would be at the same time due to an equal surface area. The step-wise failure of the redundant structures would lead to an increased time between initiation and overall failure, increasing the fatigue life.

The manufacturing related effects and the statistical size effect, as described in section 8.1, contribute to the differences in fatigue life between the 1-9mmØ, 9-3mmØ and 81-1mmØ specimens. The total of these effects namely result in a decreasing fatigue life for the individual struts of decreasing diameter and with increasing redundancy. Aside from the changed single strut behaviour, the combination of multiple struts in one specimen also changes the fatigue characteristics.

In figure 8.1, this combination effect can be seen by comparing the 9-3mmØ and 1(9)-3mmØ specimens. The first observation is that the combination of multiple struts lowers the average fatigue life. This is explained by the fact that in the 9-3mmØ specimens, the remaining struts upon gradual failure are loaded at a higher stress, leading to a shorter remaining fatigue life. Because more struts are present, it is more likely to have an early initiation and thus an early onset of the gradual increase in stress for the struts. This effect is also mentioned by Burr et al. [74] and behaves similar to the statistical size effect in fatigue.

The second observation is that the range of the results is smaller for the 9-3mmØ specimens, i.e. the results show less variation. This difference in spread of the results is explained by the nature of a repeated experiment, which results in a more averaged outcome if repeated more often. This combination effect is also shown in the sensitivity studies done for the cascading damage model in section 7.1. In the results of the model shown in figure 7.3, the exact same strut properties are used and the same stress is applied. Upon increasing the number of struts, the fatigue life and standard deviation of the results both decrease.
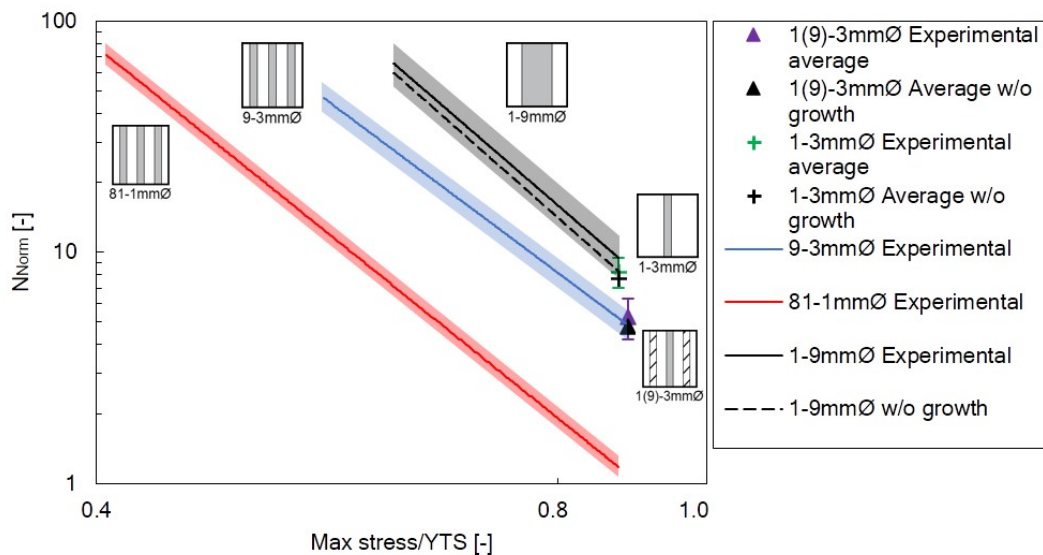
Figure 8.2: Experimental S-N curves and fatigue life after subtraction of theoretical growth life from the experimental S-N curves for the single strut specimens

The crack growth life through the struts has an influence on the total fatigue life in the S-N plot, which changes for different diameter struts. A simple crack growth model was fit to the DCPD data to quantify this growth period. In figure 7.5, it is shown that the modelled number of cycles of the growth life correspond to the observed increase in DCPD signal. This shows that an accurate model is used. Based on this, the experimental S-N curve can be shown with the modelled growth life subtracted, as is done in figure 8.2. Only the growth life of the single struts is subtracted, since initiation and crack growth overlap when multiple struts are used. With the approach chosen here, it can be shown that when the difference in growth life is compensated for, the difference in fatigue life between the differently sized specimens is still present. Moreover, seen the small decrease of the fatigue life of the single struts specimens with different diameters, it is shown here that the growth is also not entirely responsible for the lower fatigue life of thinner single struts.

The growth life of multiple load path structures can be extended due to load shedding. Load shedding is the redistribution of stresses in a multiple load path structure under equal displacement [84, 85]. Due to the decreased stiffness of a strut which contains a crack, it takes up a lower load, leading to slower crack growth. In case of load shedding, a large portion of the fracture surface would contain fatigue fracture surface areas [86]. This is also the case in the experiments done here and shown by the relative large fatigue crack areas in the 9-3mmØ and 81-1mmØ samples, in section 5.6. For the fatigue test results this means that the strut failures of the multiple load path structures are slightly delayed due to the redistribution of loads. The effect of load shedding is however a small influence in determining the total fatigue life. As stated by Zargarian et al., load shedding only plays a minor role compared to strut failure in the failure propagation in lattices [73]. This is attributed to the small change in stiffness due to crack growth in a strut, compared to stiffness changes resulting from strut failures. Furthermore, the continuing crack initiation in the other struts is present. Also, the load in the remaining struts is increased during load shedding, shortening its duration.

The results of the test data modelling presented in section 7.2 show the effect of the combination of multiple struts and the influence of crack growth. In figure 7.7, the prediction of the fatigue life with the 1(9)-3mmØ results as input are shown. The length correction is not included, since the statistical size effect it tries to model, is counteracted by manufacturing related effects. It is shown that for both the undamaged and damaged 9-3mmØ specimens, the fatigue life can be accurately predicted. As can be seen, the combination effect and crack growth as discussed in this section also contribute towards a lower fatigue life for the more redundant structures. This combination effect is furthermore shown in figure 7.8b, where can be seen that the standard deviation of the fatigue life decreases upon using more struts, for both the model and experiments. It is also visible in figure 7.7 that the trends are in reality more extreme compared to the estimation. This is attributed to manufacturing related effects.

8.3. Damage Propagation

It is observed that the failure of multiple load path structures happens in a gradual way, as was hypothesised. As expected, the failure rate increases upon decreasing number of load carrying struts, resulting ultimately in static failure. This failure pattern is shown by the DCPD output, which could be connected to the actual failure through the observation of visible and hearable damage during the fatigue testing and through the manipulation of the DCPD response according to equation 4.12. Figure 8.3 shows the relation between the output ratio r of the DCPD and the observed failed struts compared to this equation. As can be seen, the number of failed struts could accurately be connected to the output data.
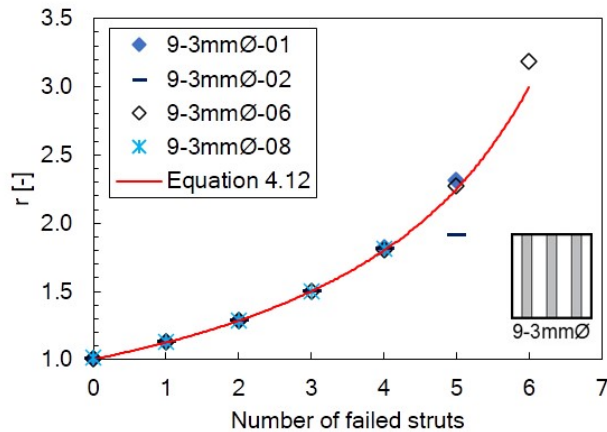
Figure 8.3: Observed and modelled DCPD output ratio per number of failed struts

The understanding of this step-wise behaviour is shown by the results of the model. The 9-3mmØ case is used for the modelling, due to the availability of correct input data. In figure 7.9 the average number of cycles between the individual failure events of struts in a specimen are shown, for both the model and the experiments. These show good agreement. In combination with the damage accumulation curve of the damaged specimens, shown in figure 7.10, it can be said that the individual failure events can be correctly modelled.

As a result of the accurate gradual failure prediction, the output GR of the model is close to the average experimental value for the 9-3mmØ specimens. This is shown in figure 7.8. For the 81-1mmØ specimens, the GR is underestimated. This same trend is observed in the standard deviation of the fatigue life of these specimens. This is because of the variation of properties in the individual struts. This variation is responsible for the scatter in the results, but also for the gradual failure. As an extreme case, zero variation would lead to failure of all struts at the same time, hence a GR of 0%. The sensitivity study in section 7.1 shows this trend of increasing GR with increasing input scatter as well. The underestimation of the GR and standard deviation by the model, is thus because in reality more variation is present in the 81-1mmØ struts.

The GR is increasing with increasing number of struts as shown by both the experiments as the results of the model. One difference between the experiments and model is found in the dependency of the GR on the applied load. In fatigue testing, the amount of scatter increases at lower loads and higher number of cycles [58]. In figure 5.8 the increasing GR for decreasing loads can be seen. However, the model only uses one statistical distribution as input since only at one load a representative set of data was generated. Therefore the same scatter is used at all loads. As a result, the model GR is insensitive to the load.

The initial damage tests show the nature of the gradual failure mechanism as well. An early strut failure, as forced to happen in these tests, led to a lower fatigue life for both the pre-damaged 81-1mmØ and 9-3mmØ specimens. This shorter fatigue life is explained by the higher stress that the remaining struts experience due to this early failure. Because this effect is higher for the 9-3mmØ case, the relatively larger decrease in fatigue life of these specimens could be expected. To show that the load increase is the only reason for a shorter fatigue life, a prediction with the model is done for a damaged 9-3mmØ specimen. As shown in figure 7.10, the outcome of this simulation fits in the results of the experiments.

The time between the second and final failure was not changed for both the 9-3mmØ and 81-1mmØ specimens with initial damages. Figure 5.13 shows this for both specimen types. It can thus be said that no other effects than increased load were present, and that the assumption made for the model, where struts are given an individual fatigue life, is thus valid.

Concerning the geometrical damage pattern, the following can be said. The pattern of the strut failures is random, both in height of the strut failure and throughout the cross-section of the multiple load path structures, as shown with the results of the fractography and as observed during testing. Also, multiple initiation sites are present. This random pattern with multiple initiation sites shows that the initiation of cracks is an individual and independent phenomenon that is not influenced by surrounding cracks or failed struts, aside from the increase in stress level. Moreover, the random pattern shows that the equal strain condition was sufficiently satisfied by the specimen design, even though a different, fictional, material was used for this design, as shown in appendix **??**. This material was stiffer than the AlSi10Mg that is used, but no difference for the equal strain conditions was expected based on simulations with stiffer materials in the design phase.

8.4. Damage Tolerance Evaluation

To answer to the objective of this research, which is to assess the damage tolerance of AM multiple load path structures, the results are reviewed in terms of DT in this section. Also, the meaning of this for the design of AM structures is described.

Concerning damage tolerance, the first advantage of using a multiple load path structure is the increased time between the first visible failure and the overall failure of the part. It is shown that the GR is relatively large and increases with increasing number of struts. For comparison with the 1-9mmØ specimens, the GR was also calculated for this specimen type as being the time between a visible crack and overall failure. As initial length 1.027 mm was chosen and the growth model with the earlier mentioned parameters was used to calculate the growth life. The results are shown in table 8.2, as well as the experimental values for the other specimens. It can be seen that for the 1-9mmØ specimens the equivalent GR is even lower and that thus a large increase in time between visible and final failure can be obtained by introducing redundancy.

Table 8.2: GR for different types of specimens, including calculated equivalent GR for 1-9mmØ specimens

Equivalent GR 1-9mmØ [%]	GR 9-3mmØ [%]	GR 81-1mmØ [%]
0.94 ±0.30	12.2 ±11.5	45.0 ±13.2

Another advantage of the multiple load path structures is found in the lower sensitivity to initial damages. In table 8.3, this sensitivity of the fatigue life and GR is shown. For the 1-9mmØ specimens, the initial damage is a 1.027 mm crack and the shown result is calculated rather than experimentally tested. The fatigue life decrease as a result of an initial damage is less in case more struts are present. Moreover, the effect on the GR is also smaller in case of more redundancy. This is explained by the fact that the load increase that occurs when one strut fails or is damaged, is relatively small in the case of more struts. The smaller change of GR is further explained by the already relatively large values that are found for the GR in case of 81-1mmØ, but is also influenced by the type of initial damages that were used in this research. The 81-1mmØ samples with initial damage did not fail as early as intended, making the number of cycles to failure an overestimation and the GR an underestimation as compared to the case where the first failure would occur earlier.

Table 8.3: Sensitivity of specimens to initial damage

	81-1mmØ		9-3mmØ		1-9mmØ	
	N_{Norm} [-]	GR [%]	N_{Norm} [-]	GR [%]	N_{Norm} [-]	GR [%]
Pristine	6.5 ±1.1	45 ±2.8	5.0 ±0.5	6.6 ±2.3	9.5 ±2.4	0.9 ±0.3
Damaged	5.3 ±0.3	69.6 ±19	2.4 ±0.4	82.7 ±3.5	0.1 ±0	100 ±0
Change [%]	-20	+55	-52	+1146	-99	+9596

Concerning the predictability of the failure, the redundant specimens also show an advantage. Less scatter is present in the results, when more struts are used. This is shown in figure 7.8a and 7.8b for both the model and the experiments. The standard deviation over the mean of the fatigue life shows a decreasing trend for increasing number of struts. From a design standpoint this effect is beneficial, since lower design margins can potentially be applied.

8.4.1. Damage Tolerance and Fatigue Life

Based on the more gradual failure, less sensitivity to initial damage and the increased predictability, AM multiple load path structures are more damage tolerant. It was however shown before that the fatigue life decreases when more and thinner struts are used. In the design for such a structure, a balance between these design objectives should be found, since maximising both is not possible. For a given stress and fatigue life combination, a multiple load path structure could be applied as damage tolerant alternative, but for the single load path a higher design margin could be used while the same amount of material is used.

To show how both damage tolerance and fatigue life relate, figure 8.4 includes the experimental S-N curves as well as their standard deviation as measure of predictability. The sensitivity to initial damage is shown by extrapolating the experimental results of the damaged specimens along the S-N curves of their undamaged counterparts. Finally, the gradual failure is included by showing the average number of cycles of the first strut failure and the distance to the overall failure at the data points where the experiments were done. In the figure, it is shown that for increasing number of struts, the standard deviation decreases, the failure is more gradual and that the damaged results are closer to the undamaged curve, indicating less sensitivity to damage.
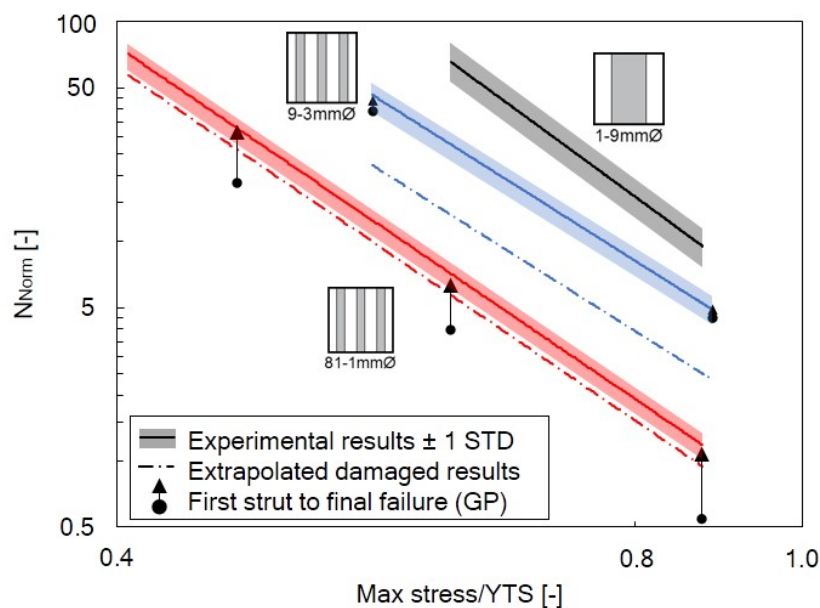
Figure 8.4: Experimental fatigue test results with standard deviation, experimental GP and damaged S-N curve extrapolated from results at one stress level

It should also be mentioned that the trends shown in this report are dependent on the material that is used, the type of post-processing and the specific diameters. If the AM size effect was better controlled, the total fatigue life is expected to be higher for the thinner struts. The situation where the initiation is the same for all specimens tested here, as is the case in the length corrected model in chapter 6 would be approached then. This could also happen when the minimum diameter was chosen larger than 1 mm, since the size effect seems to stabilise at larger diameters, where the properties converge towards the cast AlSi10Mg properties [30]. The fatigue life could also be improved by heat-treatments and surface finishes, although the latter one is not applicable due to the accessibility of the inner struts [25, 27, 28]. Aside from increasing the fatigue life, this could also influence the GR and variation in the results.

9

Conclusion and Recommendations

9.1. Conclusion

With the fatigue testing of multiple load path specimens, a clear trend is shown in this study that the fatigue life decreases when more struts with thinner diameters are used. The parallel placement of multiple struts with the same properties leads to a shorter fatigue life with less variation, as compared to the single strut. Moreover, the crack growth life through thinner struts is also shorter. Both of these effects are however not large enough to explain the observed differences in the experiments that were done.

The difference in fatigue life of the multiple load path specimens is originating from manufacturing related effects that occur when different geometries are produced using SLM. With the fatigue testing of differently sized single struts, it was shown that the fatigue life is smaller for thinner struts. This well-known AM related size effect counteracted the statistical size effect and proved to be more prominent in the results. Also effects from producing struts with other part geometry in the close proximity are identified as potential cause for a changed fatigue life. From fractography, it is known that the irregularities at the surface where the cracks initiate, are constant in size. This means that the influence on smaller diameter struts is relatively larger, lowering the fatigue life in a way similar to the AM size effect. Differences between as-designed and as-built diameter were also found. However, this was compensated for by correcting the force input to the required stress level for the different specimen types.

The failure in the multiple load path structures showed a step-wise pattern. Due to this pattern, a relatively large period between the first visible and final overall failure is obtained. This period is dependent on the number of struts, reaching around 45% of the total fatigue life for the specimens with 81 struts. The created cascading damage model could accurately predict this failure pattern. With this model, it is shown that statistical variation throughout the struts is responsible for the step-wise failure. The model is furthermore able to make accurate predictions for the fatigue life, its standard deviation and grace period, if the correct input material parameters are used. The damage pattern was shown to be random throughout the struts, indicating that the struts are independent entities with an individual fatigue life. This is substantiated with the testing of damaged specimens, in which the fatigue life of the remaining undamaged struts was not changed, seen the unchanged time between second strut failure and final failure.

The application of a multiple load path structure leads to an increased damage tolerance, because of the following reasons. The time between the first failure and overall failure of the part is increased, leading to more controlled failure. The sensitivity to an initial damage is lower in the case of multiple struts present. Large advantages are reached compared to the calculated crack growth period in a single strut. Furthermore, the total fatigue life shows less scatter, meaning that the fatigue life is more predictable. In the design for additive manufactured structures however, the decreased fatigue life should be taken into account as well. Therefore, with the materials and parameters used in this study, the application of multiple load path structures instead of single load paths, is not directly the best design choice. Based on the requirements in design, a choice must be made for either high damage tolerance or long fatigue life.

9.2. Recommendations

Throughout the conduction of the research described in this report, several possible improvements of the work became apparent that could not be included due to limited time and resources of the project. Aside from that, the findings of the research suggest various follow-up projects that can be done to further explore the damage tolerance of multiple load path structures. In the following two sections, the recommendations for the improvement of the current work and for future work are given.

9.2.1. Improvements to Current Research

Determination of the cross-sectional area

The actual cross-section in the as-built condition differs from the as-designed one. The diameters of the struts were measured with a caliper and verification was done with the described tensile test. To increase the accuracy of this tensile test, it would be better to use the same method for determining the strain for all three specimen types, such that errors from the test method are ruled out. This also includes the use of the same test bench. Furthermore, the elliptical parts and solid blocks were also included in the strain determination for the multiple load path specimens, whereas only the cylindrical part of the strut is of interest and should be measured. Finally, the load range was limited in this tensile test. Testing until a higher load would result in more accurate results, due to less measurement errors. Aside from using a caliper, other methods to determine the diameter of the struts can be used. X-ray tomography is for example a method described in literature to reconstruct and measure the 3D shape of the struts [27, 74].

The use of a more accurate growth model

The growth model that is used in this research is limited to using literature constants and an initial crack length that fits best to the fatigue test data. Due to the complex relation between crack size and DCPD output, the parameters could not be determined. Tests should be conducted to determine the correct parameters for the used material. Also, the model can be extended to include static final failure instead of completely-through crack growth.

Manufacturing the new specimens in the same batch

The 3 mm single strut specimens were produced later in a different batch. As such, the powder and interlayer time were not exactly the same, leading to different properties. When produced in the same batch as the multiple load path specimens, this could have been avoided. Any influences of the position on the build plate would still exist however.

Sharper notch of the 81-struts initial damage specimens

One of the 81-1mmØ-D samples with initial damage had a notch, like the 9-3mmØ-D samples. For the 9-3mmØ-D samples, fatigue damage occurred at the notch and around the same number of cycles. The relative curvature of the notch was however too large compared to the thin strut diameter of the 81-1mmØ sample, for which reason the fatigue failure was not as early as in the 9-3mmØ-D samples. A sharper notch would have avoided this.

Scatter data at two load levels for model

Since the larger set of 3 mm single strut specimens was tested at only one load level, a reliable scatter input for the model is only available at one load. The model fatigue life scatter output and GR are therefore independent of the load, whereas the experiments show a slight dependency. By having an input scatter at at least two load levels, the modelling with the scatter could be made more realistic.

Better characterisation of AM size effect

Within the limitations of this project, the AM size effect could be further characterised by quantifying the surface roughness of the different multiple load path specimens and investigate whether this is different. Furthermore, by performing (destructive) tensile testing on some specimens, the changed static properties of the material could have been showed.

9.2.2. Future Research

Quantification of the AM size effect
Several researches are done with respect to the AM size effect, also including fatigue. However, to quantify this effect for the experiments done here and to include it in the created model, fatigue data is needed of the correct material, produced with the same parameters and sizes. Extensive fatigue testing should be done to provide this data.

The effect of materials and post-processing
In this research, the specimens are tested with an as-built surface and with only a stress relief heat cycle. Since post-processing and heat treatments are available that improve the fatigue performance of AM components, the AM size effect that results in a lower fatigue life can possibly be (partly) avoided by applying these. This would result in a smaller drawback in fatigue life for the thinner struts, which in combination with the damage tolerant behaviour of multiple load path structures, makes them more useful in design.

The use of different minimum size elements
In the same way as post-processing can be applied, the AM size effect seems to stabilise at a certain minimum diameter strut [16, 30]. If the same research is conducted with larger diameter struts, the effect of different diameters would be less prominent, giving different results and conclusions.

Studying the effect of parts in the close proximity
One of the potential differences between the 1(9)-3mmØ and 1-3mmØ specimens in this study, is found in the production with other struts in the close proximity, which is the case for the 1(9)-3mmØ samples. This is possibly lowering the fatigue performance of these. Since a fair comparison could not be made, due to the production in different batches of the same-geometry specimens, further research into this phenomenon is needed.

Integration of cascading damage model with truss optimisation
He et al. provide a Python script for designing optimised truss structures [49]. An integration of the cascading damage model created here and this truss optimisation scheme could be created. This can be done such that the damage of an optimised truss can be simulated, or such that a design tool is created that optimises for a given GP or GR. As such, damage tolerant structures can be automatically designed.

Bending-dominated structures
This research is limited to stretch-dominated elements loaded in tension. Because most lattice structures are bending-dominated, it would be interesting to investigate whether the same trends are present in those structures. Bending-dominated structures can be built in a simplified way, such that full lattices are not needed. Struts can be placed on an angle or with a corner in the middle of the test section for example.

Structures with more variability
The gradual failure in the multiple load path structures is caused by a certain variability between the struts, in this case statistical scatter. If longer grace periods and ratios are desired, more variation in the struts can be introduced. Zhao et al. furthermore showed that having different densities of lattice in parallel leads to crack retardation of the early cracks [70]. More variability can be introduced through using different diameter struts throughout the cross-section, corresponding to non-homogeneous unit cell densities, or through placing struts at different angles.

Bibliography

[1] A. Uriondo, M. Esperon-Miguez, and S. Perinpanayagam, "The present and future of additive manufacturing in the aerospace sector: A review of important aspects," *Proceedings of the Institution of Mechanical Engineers, Part G: Journal of Aerospace Engineering*, vol. 229, pp. 2132–2147, 9 2015.

[2] L. Chen, Y. He, Y. Yang, S. Niu, and H. Ren, "The research status and development trend of additive manufacturing technology," *The International Journal of Advanced Manufacturing Technology*, vol. 89, pp. 3651–3660, 2017.

[3] M. Gorelik, "Additive manufacturing in the context of structural integrity," *International Journal of Fatigue*, vol. 94, pp. 168–177, 1 2017.

[4] ASTM International, "F2792-10 Standard Terminology for Additive Manufacturing Technologies," 2010.

[5] I. Gibson, D. Rosen, and B. Stucker, *Additive Manufacturing Technologies*. Springer, 2 ed., 2010.

[6] L. Yang, K. Hsu, B. Baughman, D. Godfrey, F. Medina, M. Menon, and S. Wiener, *Additive Manufacturing of Metals: The Technology, Materials, Design and Production*. 3 2017.

[7] W. Gao, Y. Zhang, D. Ramanujan, K. Ramani, Y. Chen, C. B. Williams, C. C. Wang, Y. C. Shin, S. Zhang, and P. D. Zavattieri, "The status, challenges, and future of additive manufacturing in engineering," *Computer-Aided Design*, vol. 69, pp. 65–89, 12 2015.

[8] W. Tao and M. C. Leu, "Design of lattice structure for additive manufacturing," in *International Symposium on Flexible Automation, ISFA 2016*, pp. 325–332, Institute of Electrical and Electronics Engineers Inc., 12 2016.

[9] J.-Y. Lee, J. An, and C. K. Chua, "Fundamentals and applications of 3D printing for novel materials," *Applied Materials Today*, vol. 7, pp. 120–133, 6 2017.

[10] A. Yadollahi and N. Shamsaei, "Additive manufacturing of fatigue resistant materials: Challenges and opportunities," *International Journal of Fatigue*, vol. 98, pp. 14–31, 5 2017.

[11] P. Edwards and M. Ramulu, "Fatigue performance evaluation of selective laser melted Ti-6Al-4V," *Materials Science and Engineering A*, vol. 598, pp. 327–337, 3 2014.

[12] A. B. Spierings, T. L. Starr, and K. Wegener, "Fatigue performance of additive manufactured metallic parts," *Rapid Prototyping Journal*, vol. 19, no. 2, pp. 88–94, 2013.

[13] J. J. Lewandowski and M. Seifi, "Metal Additive Manufacturing: A Review of Mechanical Properties," *Annual Review of Materials Research*, vol. 46, pp. 151–186, 2016.

[14] P. Edwards, A. O'Conner, and M. Ramulu, "Electron beam additive manufacturing of titanium components: Properties and performance," *Journal of Manufacturing Science and Engineering, Transactions of the ASME*, vol. 135, 12 2013.

[15] E. Beevers, A. D. Brandão, J. Gumpinger, M. Gschweitl, C. Seyfert, P. Hofbauer, T. Rohr, and T. Ghidini, "Fatigue properties and material characteristics of additively manufactured AlSi10Mg – Effect of the contour parameter on the microstructure, density, residual stress, roughness and mechanical properties," *International Journal of Fatigue*, vol. 117, pp. 148–162, 12 2018.

[16] D. Barba, C. Alabort, Y. T. Tang, M. J. Viscasillas, R. C. Reed, and E. Alabort, "On the size and orientation effect in additive manufactured Ti-6Al-4V," *Materials and Design*, vol. 186, p. 108235, 1 2020.

[17] M. D. Sangid, T. A. Book, D. Naragani, J. Rotella, P. Ravi, A. Finch, P. Kenesei, J. S. Park, H. Sharma, J. Almer, and X. Xiao, "Role of heat treatment and build orientation in the microstructure sensitive deformation characteristics of IN718 produced via SLM additive manufacturing," *Additive Manufacturing*, vol. 22, pp. 479–496, 8 2018.

[18] M. Simonelli, Y. Y. Tse, and C. Tuck, "Effect of the build orientation on the mechanical properties and fracture modes of SLM Ti-6Al-4V," *Materials Science and Engineering A*, vol. 616, pp. 1–11, 10 2014.

[19] A. Yadollahi, N. Shamsaei, S. M. Thompson, and D. W. Seely, "Effects of process time interval and heat treatment on the mechanical and microstructural properties of direct laser deposited 316L stainless steel," *Materials Science and Engineering A*, vol. 644, pp. 171–183, 9 2015.

[20] B. Torries, S. Shao, N. Shamsaei, and S. M. Thompson, "Effect of Inter-Layer Time Interval on the Mechanical Behavior of Direct Laser Deposited TI-6AL-4V," in *Proceedings of the 26th Annual International Solid Freeform Fabrication Symposium – An Additive Manufacturing Conference*, pp. 1272–1282, 2016.

[21] N. E. Uzan, R. Shneck, O. Yeheskel, and N. Frage, "Fatigue of AlSi10Mg specimens fabricated by additive manufacturing selective laser melting (AM-SLM)," *Materials Science and Engineering A*, vol. 704, pp. 229–237, 9 2017.

[22] E. Brandl, U. Heckenberger, V. Holzinger, and D. Buchbinder, "Additive manufactured AlSi10Mg samples using Selective Laser Melting (SLM): Microstructure, high cycle fatigue, and fracture behavior," *Materials and Design*, vol. 34, pp. 159–169, 2 2012.

[23] S. Romano, A. Brückner-Foit, A. Brandão, J. Gumpinger, T. Ghidini, and S. Beretta, "Fatigue properties of AlSi10Mg obtained by additive manufacturing: Defect-based modelling and prediction of fatigue strength," *Engineering Fracture Mechanics*, vol. 187, pp. 165–189, 1 2018.

[24] S. R. Ch, A. Raja, R. Jayaganthan, N. J. Vasa, and M. Raghunandan, "Study on the fatigue behaviour of selective laser melted AlSi10Mg alloy," *Materials Science and Engineering A*, vol. 781, p. 139180, 4 2020.

[25] M. Brandt, S. Sun, M. Leary, S. Feih, J. Elambasseril, and Q. Liu, "High-Value SLM Aerospace Components: From Design to Manufacture," *Advanced Materials Research*, vol. 633, pp. 135–147, 2013.

[26] R. Dehoff, C. Duty, W. Peter, Y. Yamamoto, W. Chen, C. Blue, O. Ridge National Laboratory, C. Tallman, and L. Martin Aeronautics Co, "Case Study: Additive Manufacturing of Aerospace Brackets," tech. rep., 2013.

[27] T. Persenot, A. Burr, R. Dendievel, J. Y. Buffière, E. Maire, J. Lachambre, and G. Martin, "Fatigue performances of chemically etched thin struts built by selective electron beam melting: Experiments and predictions," *Materialia*, vol. 9, 3 2020.

[28] B. Van Hooreweder and J.-P. Kruth, "Advanced fatigue analysis of metal lattice structures produced by Selective Laser Melting," *CIRP Annals*, vol. 66, pp. 221–224, 1 2017.

[29] B. Van Hooreweder, Y. Apers, K. Lietaert, and J. P. Kruth, "Improving the fatigue performance of porous metallic biomaterials produced by Selective Laser Melting," *Acta Biomaterialia*, vol. 47, pp. 193–202, 1 2017.

[30] Z. Dong, X. Zhang, W. Shi, H. Zhou, H. Lei, and J. Liang, "Study of size effect on microstructure and mechanical properties of AlSi10Mg samples made by selective laser melting," *Materials*, vol. 11, 12 2018.

[31] D. Kotzem, T. Arold, T. Niendorf, and F. Walther, "Damage tolerance evaluation of E-PBF-manufactured inconel 718 strut geometries by advanced characterization techniques," *Materials*, vol. 13, p. 247, 1 2020.

[32] M. Speirs, B. Van Hooreweder, J. Van Humbeeck, and J. P. Kruth, "Fatigue behaviour of NiTi shape memory alloy scaffolds produced by SLM, a unit cell design comparison," *Journal of the Mechanical Behavior of Biomedical Materials*, vol. 70, pp. 53–59, 6 2017.

[33] D. W. Rosen, "Design for Additive Manufacturing: A Method to Explore Unexplored Regions of the Design Space," in *18th Solid Freeform Fabrication Symposium*, pp. 402–415, 2007.

[34] M. K. Thompson, G. Moroni, T. Vaneker, G. Fadel, R. I. Campbell, I. Gibson, A. Bernard, J. Schulz, P. Graf, B. Ahuja, and F. Martina, "Design for Additive Manufacturing: Trends, opportunities, considerations, and constraints," *CIRP Annals*, vol. 65, pp. 737–760, 1 2016.

[35] H. Bikas, A. K. Lianos, and P. Stavropoulos, "A design framework for additive manufacturing," *The International Journal of Advanced Manufacturing Technology*, vol. 103, p. 3769– 3783, 2019.

[36] J.-H. Zhu, W.-H. Zhang, and X. Liang, "Topology Optimization in Aircraft and Aerospace Structures Design," *Archives of Computational Methods in Engineering*, vol. 23, pp. 595–622, 2016.

[37] C. Klahn, B. Leutenecker, and M. Meboldt, "Design for Additive Manufacturing – Supporting the Substitution of Components in Series Products," *Procedia CIRP*, vol. 21, pp. 138–143, 1 2014.

[38] B. Vayre, F. Vignat, and F. Villeneuve, "Designing for Additive Manufacturing," *Procedia CIRP*, vol. 3, pp. 632–637, 1 2012.

[39] M. Kamal and G. Rizza, "Design for metal additive manufacturing for aerospace applications," in *Additive Manufacturing for the Aerospace Industry*, ch. 4, pp. 67–86, Elsevier, 1 2019.

[40] Optomec Inc., "LENS Blisk Repair Solution," tech. rep., Albuquerque, USA, 2018.

[41] A. Kover, "Transformation In 3D: How A Walnut-Sized Part Changed The Way GE Aviation Builds Jet Engines," 2018.

[42] L. Magerramova, B. Vasilyev, and V. Kinzburskiy, "Novel designs of turbine blades for additive manufacturing," in *Proceedings of the ASME Turbo Expo*, vol. 5C-2016, American Society of Mechanical Engineers (ASME), 2016.

[43] L. Cheng, P. Zhang, E. Biyikli, J. Bai, S. Pilz, and A. C. To, "Integration of Topology Optimization with Efficient Design of Additive Manufactured Cellular Structures," 2015.

[44] EOS GmbH, "Certified for Universal Success: Additive Manufacturing of Satellite Components," tech. rep., EOS, Munich, Germany, 2018.

[45] D. Walton and H. Moztarzadeh, "Design and Development of an Additive Manufactured Component by Topology Optimisation," in *Procedia CIRP*, 2017.

[46] M. Süß, C. Schöne, and R. Stelzer, "Aerospace Case Study on Topology Optimization for Additive Manufacturing," in *Fraunhofer Direct Digital Manufacturing Conference DDMC*, 2016.

[47] M. Tomlin and J. Meyer, "Topology Optimization of an Additive Layer Manufactured (ALM) Aerospace Part," in *Proceeding of the 7th Altair CAE technology conference 2011*, 2011.

[48] D. Nagy, D. Zhao, and D. Benjamin, "Nature-Based Hybrid Computational Geometry System for Optimizing Component Structure," in *Humanizing Digital Reality*, pp. 167–176, Springer Singapore, 2018.

[49] L. He, M. Gilbert, and X. Song, "A Python script for adaptive layout optimization of trusses," *Structural and Multidisciplinary Optimization*, vol. 60, pp. 835–847, 8 2019.

[50] W. S. Dorn, R. E. Gomory, and H. J. Greenberg, "Automatic Design of Optimal Structures," *Journal de Mecanique*, 1964.

[51] L. He, M. Gilbert, T. Johnson, and T. Pritchard, "Conceptual design of AM components using layout and geometry optimization," *Computers and Mathematics with Applications*, vol. 78, pp. 2308–2324, 10 2019.

[52] H. Fairclough, M. Gilbert, A. Tyas, C. Thirion, and A. Tyas, "Balancing complexity and structural efficiency in the design of optimized trusses," tech. rep., 2018.

[53] Office of the Federal Register (OFR) and Government Publishing Office, "eCFR — Code of Federal Regulations," 2020.

[54] J. H. Heida and F. P. Grooteman, "Airframe inspection reliability using field inspection data Airframe inspection reliability using field inspection data," tech. rep., Nationaal Lucht-en Ruimtevaart-laboratorium, 1998.

[55] S. M. O Tavares and P. M. S T de Castro, "Introduction," in *Damage Tolerance of Metallic Aircraft Structures*, ch. 1, pp. 3–16, Springer, Cham, 2019.

[56] C.-y. Niu, *Airframe Structural Design*. Hong Kong: Conmilit Press, 1988.

[57] T. Swift, "Fail-Safe Design Requirements and Features, Regulatory Requirements," in *AIAA/ICAS International Air and Space Symposium and Exposition: The Next 100 Y*, (Dayton, Ohio), 2003.

[58] J. Schijve, *Fatigue of Structures and Materials*. Springer, 2009.

[59] H. K. Reddick, "Safe-Life and Damage-Tolerant Design Approaches for Helicopter Structures," in *Failure Analysis and Mechanisms of Failure of Fibrous Composite Structures*, (Hampton, VA, United States), pp. 129–152, 1983.

[60] S. J. Findlay and N. D. Harrison, "Why Aircraft Fail," *Materials Today*, vol. 5, no. 11, pp. 18–25, 2002.

[61] M. Jansen, G. Lombaert, M. Schevenels, O. Sigmund, M. Jansen, G. Lombaert, M. Schevenels, and O. Sigmund, "Topology optimization of fail-safe structures using a simplified local damage model," vol. 49, pp. 657–666, 2014.

[62] M. Zhou and R. Fleury, "Fail-safe topology optimization," *Structural and Multidisciplinary Optimization*, vol. 54, p. 1225– 1243, 2016.

[63] L. Huynh, J. Rotella, and M. D. Sangid, "Fatigue behavior of IN718 microtrusses produced via additive manufacturing," *Materials & Design*, vol. 105, pp. 278–289, 9 2016.

[64] F. Brenne, T. Niendorf, and H. J. Maier, "Additively manufactured cellular structures: Impact of microstructure and local strains on the monotonic and cyclic behavior under uniaxial and bending load," *Journal of Materials Processing Technology*, vol. 213, pp. 1558–1564, 9 2013.

[65] S. J. Li, L. E. Murr, X. Y. Cheng, Z. B. Zhang, Y. L. Hao, R. Yang, F. Medina, and R. B. Wicker, "Compression fatigue behavior of Ti-6Al-4V mesh arrays fabricated by electron beam melting," *Acta Materialia*, vol. 60, pp. 793–802, 2 2012.

[66] M. W. Wu, J. K. Chen, B. H. Lin, P. H. Chiang, and M. K. Tsai, "Compressive fatigue properties of additive-manufactured Ti-6Al-4V cellular material with different porosities," *Materials Science and Engineering A*, vol. 790, p. 139695, 7 2020.

[67] P. Köhnen, C. Haase, J. Bültmann, S. Ziegler, J. H. Schleifenbaum, and W. Bleck, "Mechanical properties and deformation behavior of additively manufactured lattice structures of stainless steel," *Materials & Design*, vol. 145, pp. 205–217, 5 2018.

[68] A. Zargarian, M. Esfahanian, J. Kadkhodapour, and S. Ziaei-Rad, "Numerical simulation of the fatigue behavior of additive manufactured titanium porous lattice structures," *Materials Science and Engineering: C*, vol. 60, pp. 339–347, 3 2016.

[69] S. Li, S. Zhao, W. Hou, C. Teng, Y. Hao, Y. Li, R. Yang, and R. D. Misra, "Functionally Graded Ti-6Al-4V Meshes with High Strength and Energy Absorption," *Advanced Engineering Materials*, vol. 18, pp. 34–38, 1 2016.

[70] S. Zhao, S. Li, S. Wang, W. Hou, Y. Li, L. Zhang, Y. Hao, R. Yang, R. Misra, and L. Murr, "Compressive and fatigue behavior of functionally graded Ti-6Al-4V meshes fabricated by electron beam melting," *Acta Materialia*, vol. 150, pp. 1–15, 5 2018.

[71] Q. Wang, S. Li, W. Hou, S. Wang, Y. Hao, R. Yang, and R. Misra, "Mechanistic understanding of compression-compression fatigue behavior of functionally graded Ti–6Al–4V mesh structure fabricated by electron beam melting," *Journal of the Mechanical Behavior of Biomedical Materials*, vol. 103, p. 103590, 3 2020.

[72] M. S. Pham, C. Liu, I. Todd, and J. Lertthanasarn, "Damage-tolerant architected materials inspired by crystal microstructure," *Nature*, vol. 565, pp. 305–311, 1 2019.

[73] A. Zargarian, M. Esfahanian, J. Kadkhodapour, S. Ziaei-Rad, and D. Zamani, "On the fatigue behavior of additive manufactured lattice structures," *Theoretical and Applied Fracture Mechanics*, vol. 100, pp. 225–232, 4 2019.

[74] A. Burr, T. Persenot, P. T. Doutre, J. Y. Buffiere, P. Lhuissier, G. Martin, and R. Dendievel, "A numerical framework to predict the fatigue life of lattice structures built by additive manufacturing," *International Journal of Fatigue*, vol. 139, p. 105769, 10 2020.

[75] S. I. Park, D. W. Rosen, S. k. Choi, and C. E. Duty, "Effective mechanical properties of lattice material fabricated by material extrusion additive manufacturing," *Additive Manufacturing*, vol. 1, pp. 12–23, 10 2014.

[76] M. Tang and P. C. Pistorius, "Oxides, porosity and fatigue performance of AlSi10Mg parts produced by selective laser melting," *International Journal of Fatigue*, vol. 94, pp. 192–201, 1 2017.

[77] O. H. Basquin, "The exponential law of endurance tests," in *Proc Am Soc Test Mater*, vol. 10, pp. 625–630, 1910.

[78] T. Persenot, A. Burr, G. Martin, J.-Y. Buffiere, R. Dendievel, and E. Maire, "Effect of build orientation on the fatigue properties of as-built Electron Beam Melted Ti-6Al-4V alloy," *International Journal of Fatigue*, vol. 118, pp. 65–76, 2019.

[79] M. T. Di Giovanni, J. T. O. de Menezes, G. Bolelli, E. Cerri, and E. M. Castrodeza, "Fatigue crack growth behavior of a selective laser melted AlSi10Mg," *Engineering Fracture Mechanics*, vol. 217, p. 106564, 8 2019.

[80] R. G. Forman and V. Shivakumar, "Growth Behavior of Surface Cracks in the Circumferential Plane of Solid and Hollow Cylinders," in *Fracture Mechanics: Seventeenth Volume* (J. H. Underwood, R. Chait, C. W. Smith, D. P. Wilhem, W. R. Andrews, and J. C. Newman, eds.), pp. 59–74, West Conshohocken, PA: ASTM International, 1 1986.

[81] K. Wang, F. Wang, W. Cui, T. Hayat, and B. Ahmad, "Prediction of short fatigue crack growth of Ti-6Al-4V," *Fatigue and Fracture of Engineering Materials and Structures*, vol. 37, no. 10, pp. 1075–1086, 2014.

[82] K. H. Kloos, A. Buch, and D. Zankov, "Pure Geometrical Size Effect in Fatigue Tests with Constant Stress Amplitude and in Programme Tests," tech. rep., 1981.

[83] D. El Khoukhi, F. Morel, N. Saintier, D. Bellett, P. Osmond, V. D. Le, and J. Adrien, "Experimental investigation of the size effect in high cycle fatigue: Role of the defect population in cast aluminium alloys," *International Journal of Fatigue*, vol. 129, 12 2019.

[84] D. Rhodes, "Fracture mechanics of multiple load path structure," *Theoretical and Applied Fracture Mechanics*, vol. 5, no. 2, pp. 97–100, 1986.

[85] T. Xu and R. Bea, "Load Shedding of Fatigue Fracture in Ship Structures," *Marine Structures*, vol. 10, pp. 49–80, 1997.

[86] R. W. Hertzberg and T. J. Pecorini, "An examination of load shedding during fatigue fracture," Tech. Rep. 6, 1993.

A
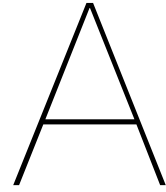
FEM Verification of Specimens

Before production, the designed specimens are verified using finite element modelling (FEM) in Abaqus. Aside from a full specimen analysis, the elliptical parts to introduce the load in the struts and the grips are modelled separately. This was done to design for the required stress concentrations and the equal displacement requirement.

A.1. Grip Analysis

The grip is modelled in a simplified two-dimensional way. A similar approach as shown by Huynh et al. is followed, where the top of the grip is extremely long to find the location where the iso-strain condition is reached [63]. One side of the grip was modelled as a 2D planar shell with thickness 1, which is possible due to symmetry. The 50 mm long solid part on the top of the grip was given zero displacement, while a shear load was applied at the flange that will be clamped in reality. A fictional elastic material with a modulus of $E = 200GPa$ and Poisson's ratio of $\nu = 0.3$ was used. These material properties are based on literature values for AM Inconel 718 and are used throughout all FEM analyses in this report. CPE4 plain strain elements were used to mesh the part.

With the given dimensions of the grip, the stress concentration factor resulting from the curvature is proven to be low enough. From the vertical displacement results in the model, it was found that 10 mm of solid material was needed to make sure the displacement is equal over the cross-section, as shown in figure A.1. From modelling with different material stiffnesses, it was found that the position where the equal strain requirement is satisfied, is independent of this parameter.

A.2. Ellipse Verification

For the ellipses, one quarter of the cross-section of a single strut is modelled because of symmetry. Furthermore, only half of the length is modelled, since the specimen are also symmetrical in the horizontal plane. The base is made long enough such that the stresses are constant at the bottom of the model. Due to the used length in the model, the stress was also evenly distributed at the end of the strut. For the three different diameters, a new model was created in Abaqus.

The models were created with a solid homogeneous section. C3D10 tetrahedral elements were used to mesh the partly cylindrical and curved part in a good fashion. Boundary conditions were applied in the form of symmetry constraints on the section planes of the model. The load is applied as a 0.1 mm vertical displacement constraint on the bottom of the base. The stress concentration factor is calculated from the maximum Von Mises stress in the model, which location was highlighted, and the total reaction forces at the applied symmetry constraint in the vertical direction. The models for different diameters showed similar results, with the maximum stress occurring at the point where the elliptical section and the cylinder meet. The maximum stress concentration factor was kept at $K_T = 1.011$.

In table A.1 the found stress concentration factors are shown. In figure A.2 the 9 mm diameter ellipse model is shown with the stresses, of which the maximum location is indicated. As can be seen, the stress concentration factors were kept low and the stress concentration is located at the expected location at the location where the test section and the ellipse meet.
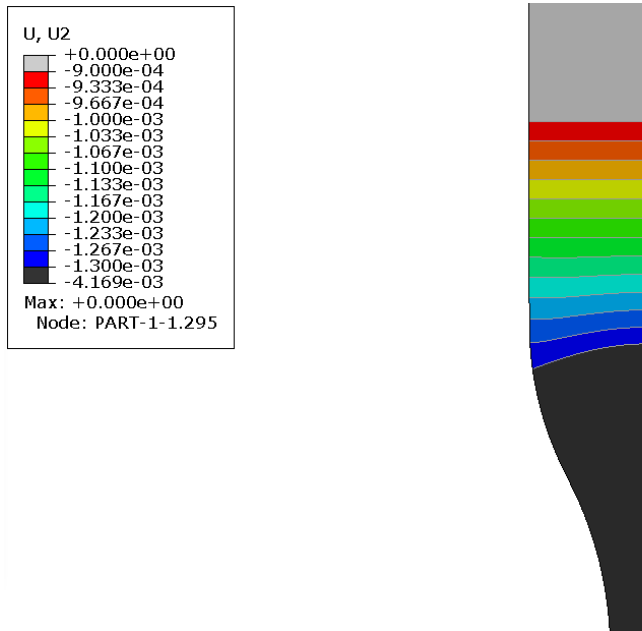
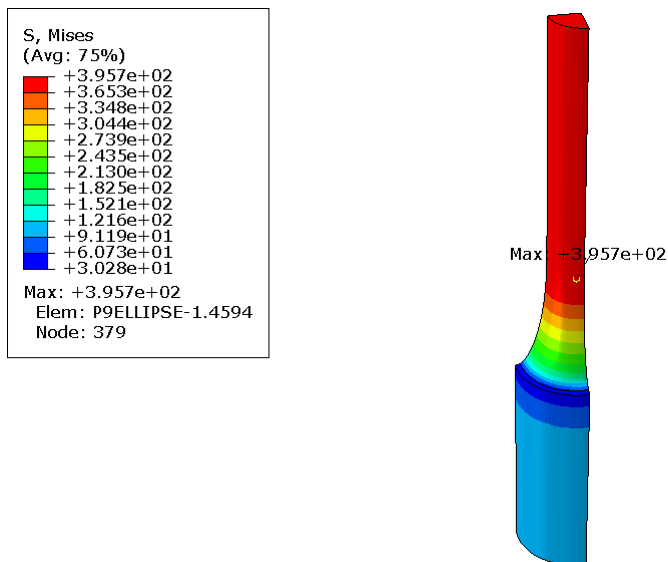Figure A.1: FEM result of vertical displacement modelling in the grip

Figure A.2: Stresses in the 9 mm FEM ellipse model

Table A.1: Results of the FEM analysis for ellipse models

d [mm]	1	3	9
Element size [mm]	0.1	0.3	0.8
K_T [-]	1.011	1.010	1.010

A.3. Full Specimen Analysis

The full specimens are subjected to a FEM analysis as a final check before production. The location and value of the maximum stresses and uniformity between the struts are the main points of attention. For modelling, the symmetry in the horizontal plane was used to model only half of the parts with a symmetry constraint. The same tetrahedral elements and the same material properties were used as for

the ellipses. The loading was applied as shear loads on the surfaces that are clamped, corresponding to the experimental situation.

In table A.2, the stress concentrations factors and location of these maximum stresses are shown. The results of the full FEM analyses were in good agreement with the estimated stress concentration factors found in the ellipse design. In figures A.3-A.5, the full results of the analyses for the multiple load path structures are given.

Table A.2: FEM results of full specimen analysis

	81-1mmØ	9-3mmØ	1-9mmØ
K_T	1.025	1.008	1.001
Location	Strut-ellipse interface	Strut-ellipse interface	Strut-ellipse interface
Ellipse K_T	1.011	1.010	1.010
Difference [%]	1.33	-0.19	-0.87
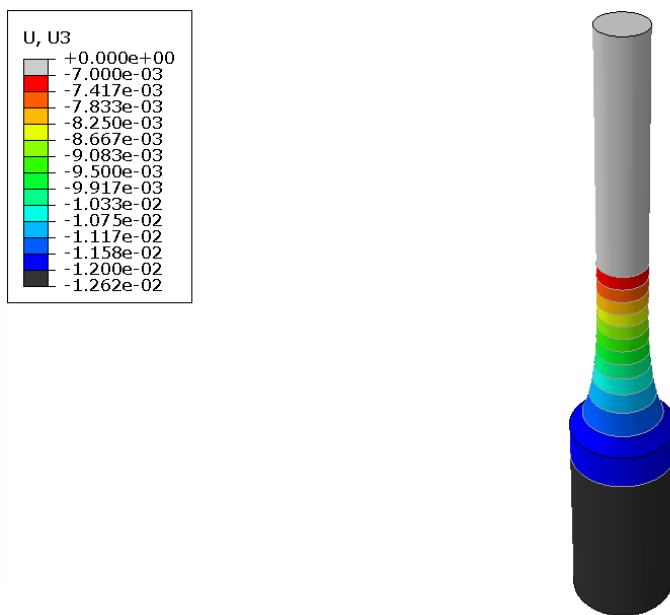
Figure A.3: Vertical displacement in 1-9mmØ specimen
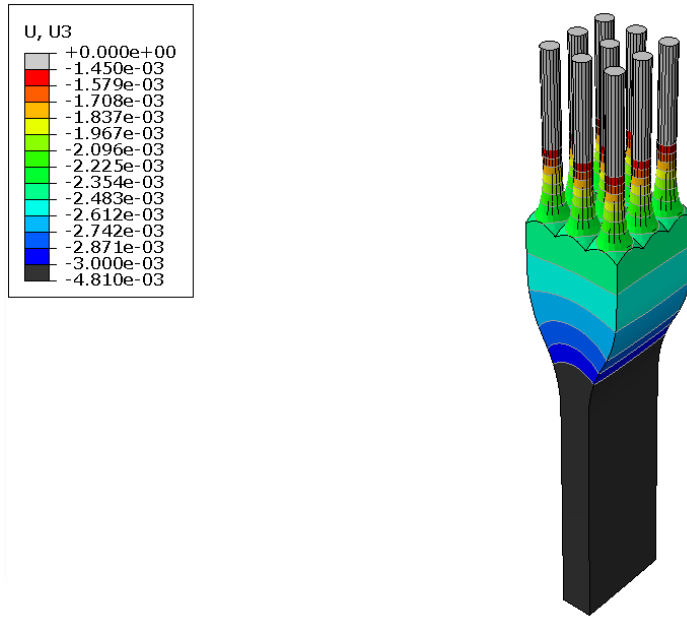
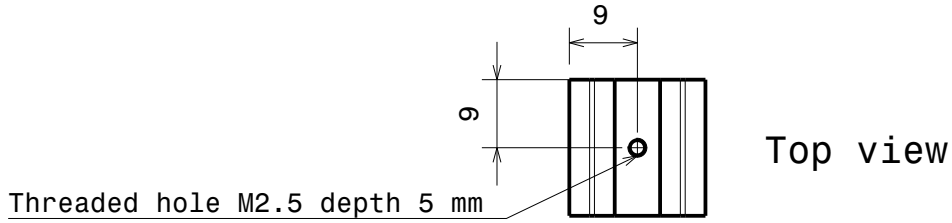Figure A.4: Vertical displacement in 9-3mmØ specimen
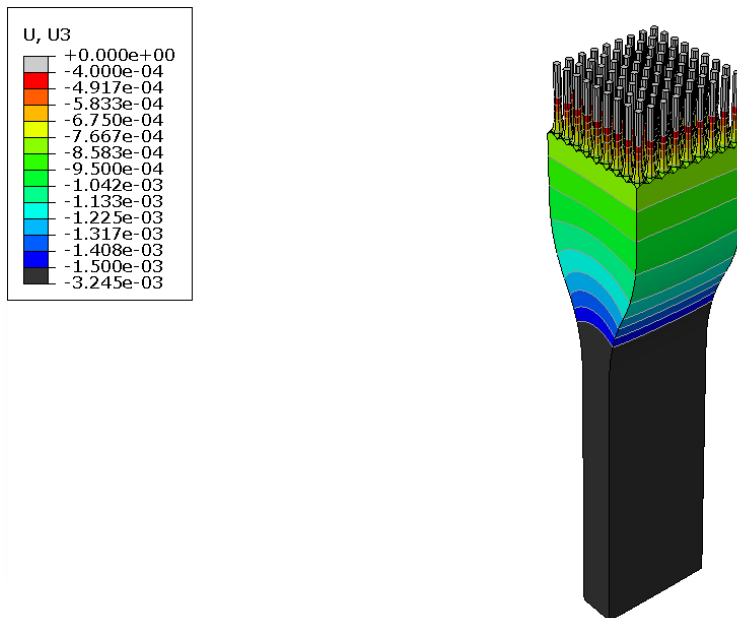
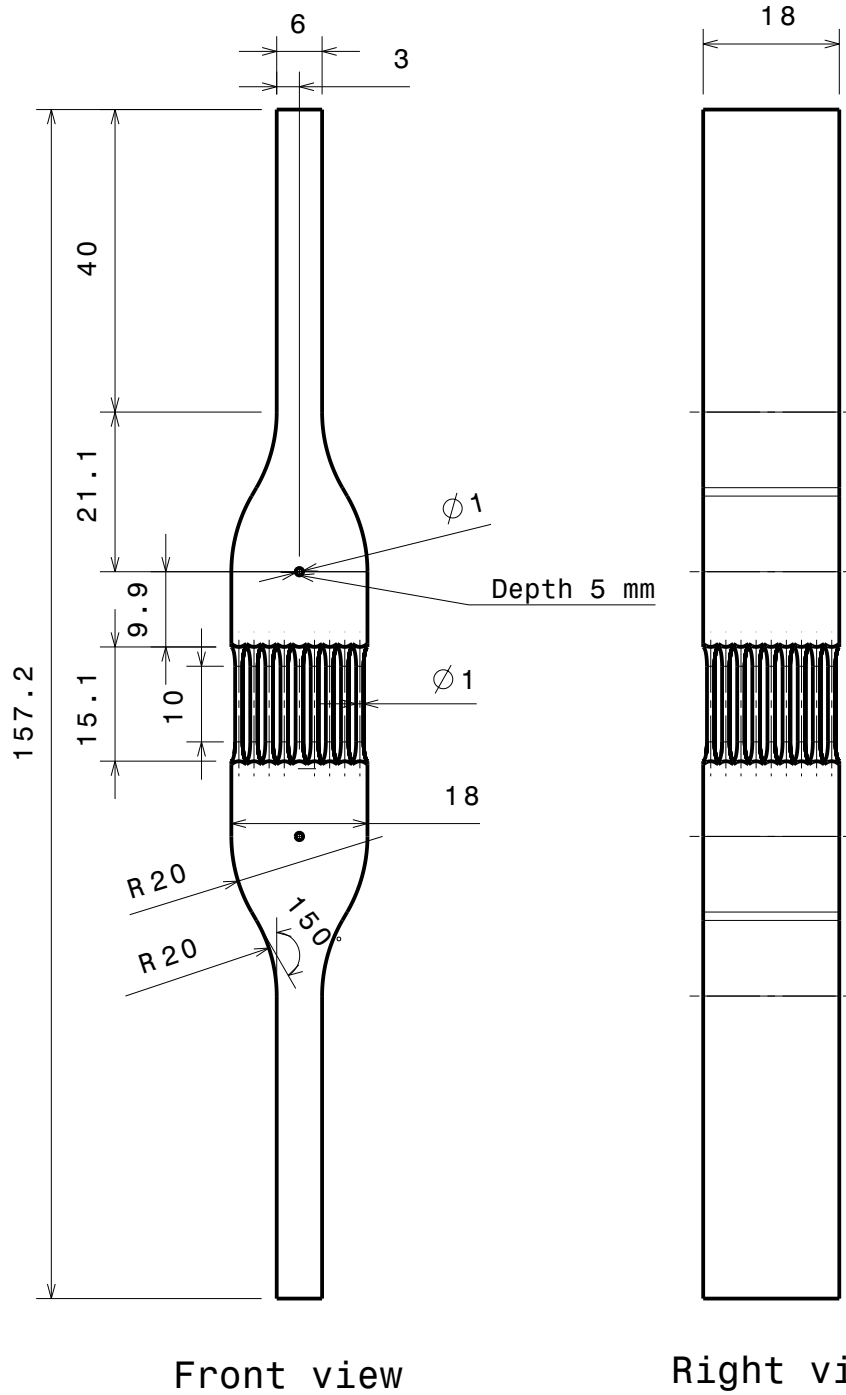Figure A.5: Vertical displacement in 81-1mmØ specimen

B

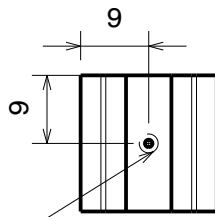# Technical Drawings of Specimens

Top view

9

9

Threaded hole M2.5 depth 5 mm

Isometric view

Scale 1:2

Front view

6

3

40

21.1

9.9

15.1

10

157.2

$\phi 1$

Depth 5 mm

$\phi 1$

18

R 20

R 20

150°

Right view

18
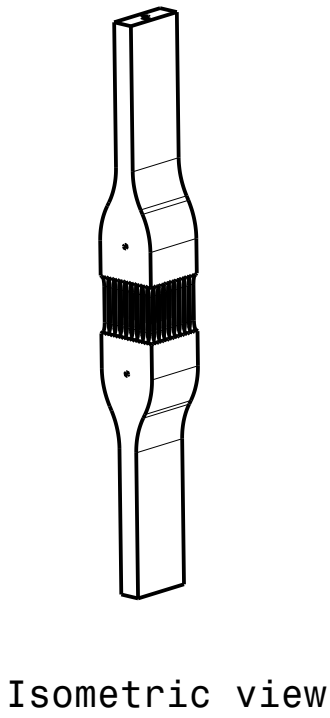
81 Struts Specimen with 1mm diameter struts
Material: AlSi10Mg
Scale 1:1
Size A4

9

Top view

9

M2.5 Threaded hole, 5 mm depth

6
3

40

21.1

ϕ1
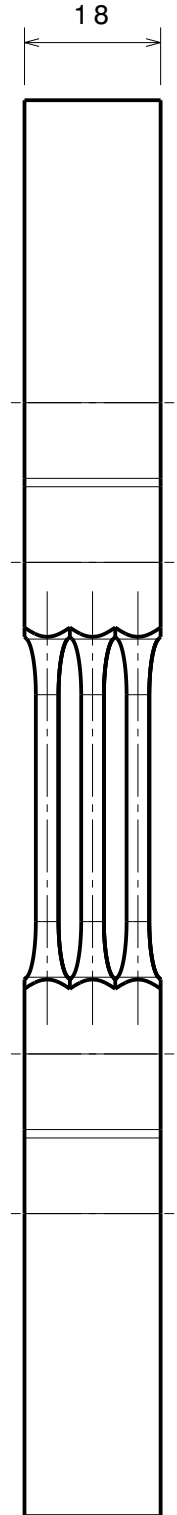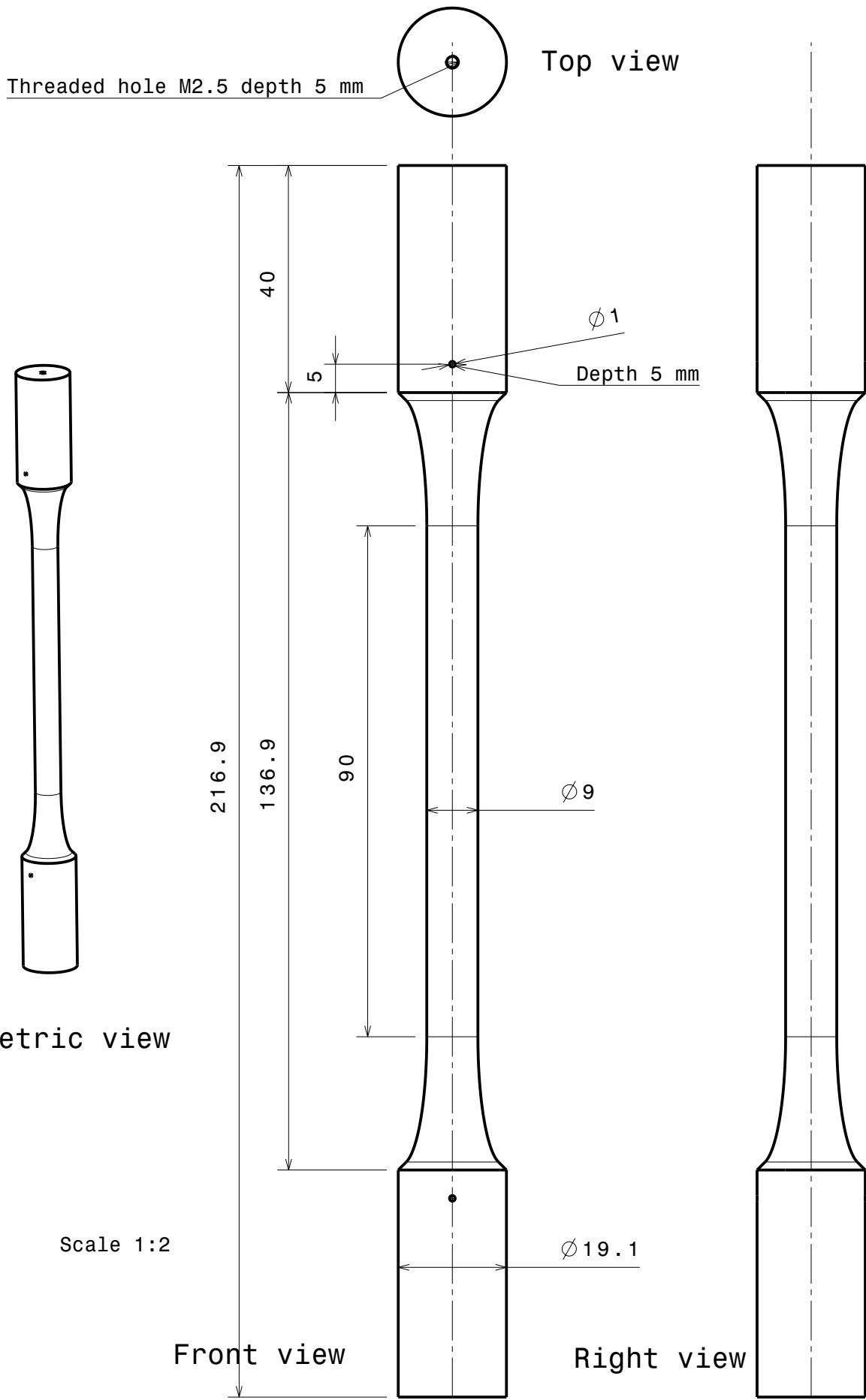5 mm depth

9.9

187.2

45.3

30

$\varnothing$3

18

R20

R20

150°

18
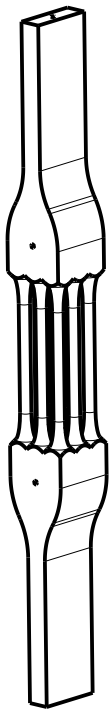
Isometric view
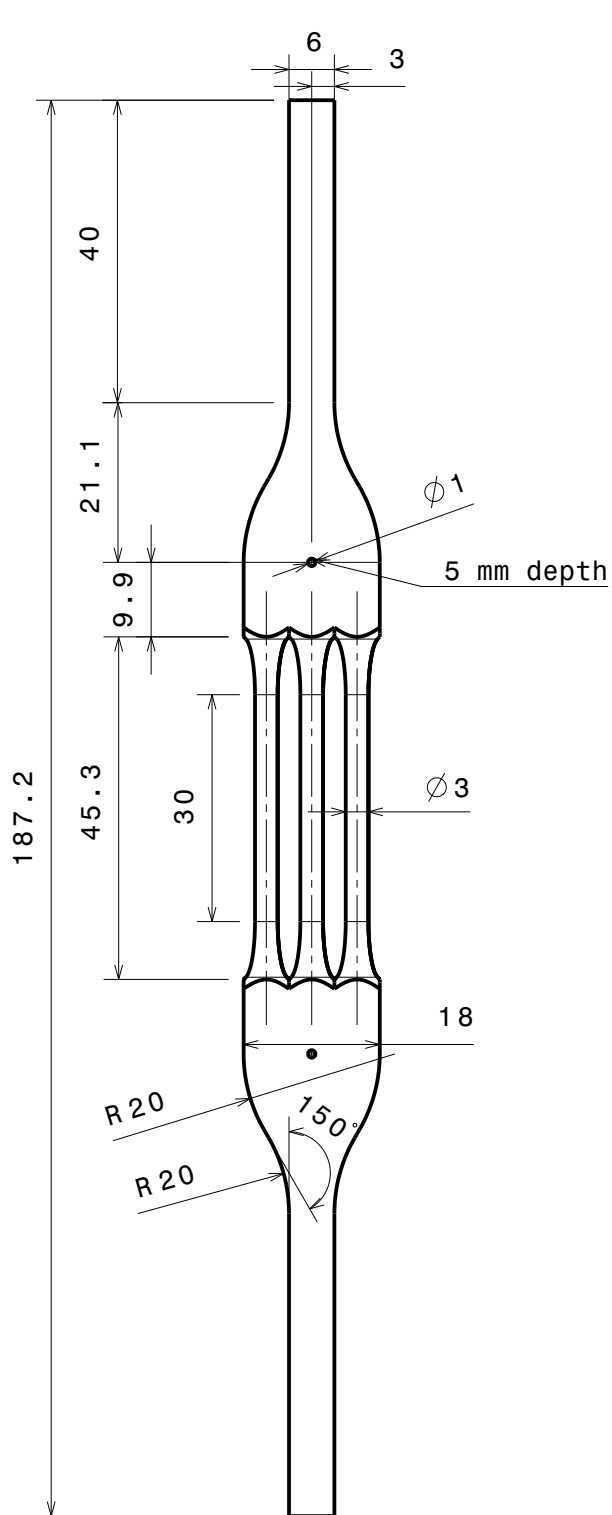
Scale 1:2

Front view

Right view

9 Struts Specimen with 3mm diameter struts
Material: AlSi10Mg
Scale 1:1
Size A4

Top view

Threaded hole M2.5 depth 5 mm

40

5

∅1

Depth 5 mm

216.9
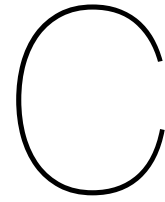
136.9

90

∅9

Isometric view

Scale 1:2

∅19.1

Front view

Right view

1 Strut Specimen with 9mm diameter
Material: AlSi10Mg
Scale 1:1
Size A4

C

Fatigue Test Data

Table C.1: Fatigue test results individual data points

Specimen type	S/YTS [-]	ID	N_{norm} [-]	GR [%]
1-9mmØ	0.63	03	53	
		06	67	
		08	59	
		09	70	
		10	82	
	0.88	01	11	
		02	12	
		04	6.0	
		05	8.9	
		07	11	
9-3mmØ	0.56	01	32.7	38
		02	52.4	5
		06	60.8	4
		08	52.5	6
		11	42.6	20
	0.69	15	15.2	11
	0.88	03	4.3	8
		04	5.4	5
		12	4.7	-
		13	5.2	-
		14	5.4	-
9-3mmØ-D	0.88	05	2.9	87
		09	2.2	81
		10	2.1	81
81-1mmØ	0.41	08	87	83
	0.47	09	32	48
		10	38	31
		11	28	51
		15	35	50
	0.63	03	4.9	45
		04	6.9	49
		05	6.2	43
		07	7.8	42
		12	7.2	46

Table C.2: Fatigue test results individual data points (continued)

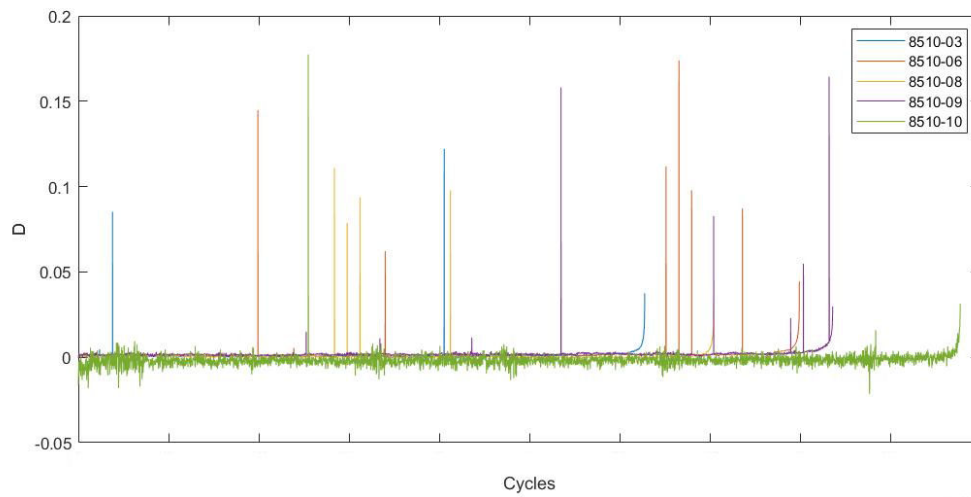| Specimen type	S/YTS [-]	ID	N_{norm} [-]	GR [%]
81-1mmØ	0.88	01	1.2	70
		02	1.5	40
81-1mmØ-D	0.63	06	5.4	51
		13	4.9	89
		14	54	69
1(9)-3mmØ	0.89	01	3.8	
		02	4.8	
		03	5.9	
		04	5.7	
		05	6.5	
		06	4.4	
		07	6.8	
		08	6.1	
		09	4.3	
1-3mmØ	0.88	01	6.9	
		02	8.8	
		03	9.5	
		04	9.3	
		05	8.5	
		06	6.1	
		07	8.8	
		08	8.3	
		09	8.6	
		10	8.7	
		11	9.6	
		12	6.2	
		13	9.4	
		14	7.0	
		15	7.4	
		16	9.9	

D
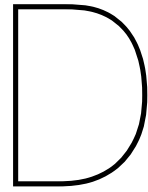
DCPD Results

Figure D.1: Calculated damage from DCPD output as function of cycles for 1-9mmØ specimens at 0.63 YTS
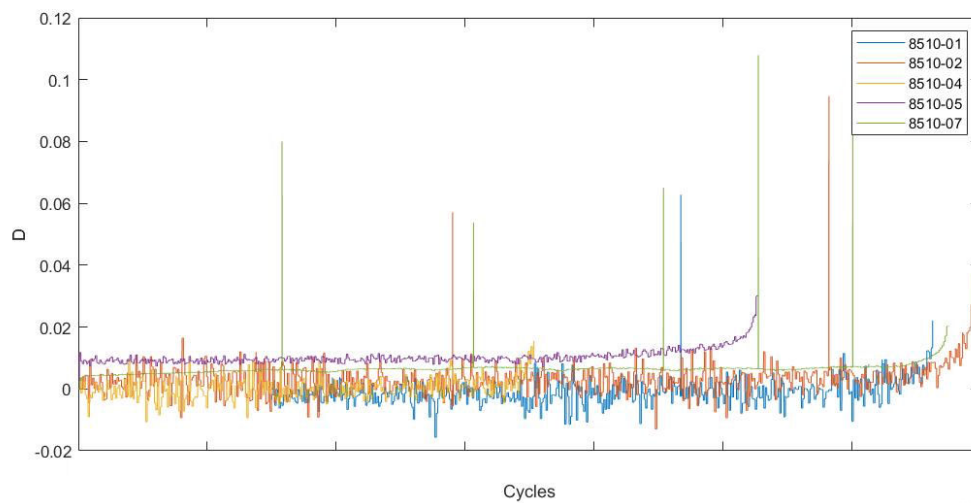

Figure D.2: Calculated damage from DCPD output as function of cycles for 1-9mmØ specimens at 0.88 YTS
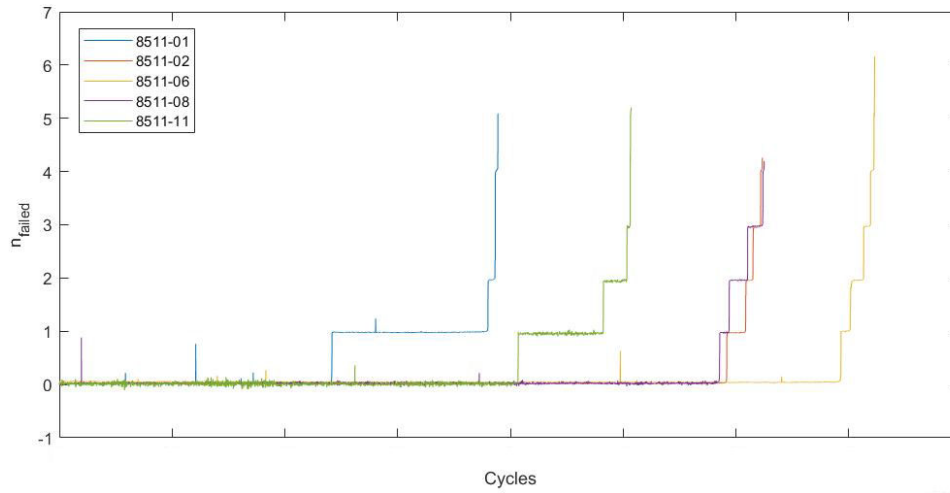
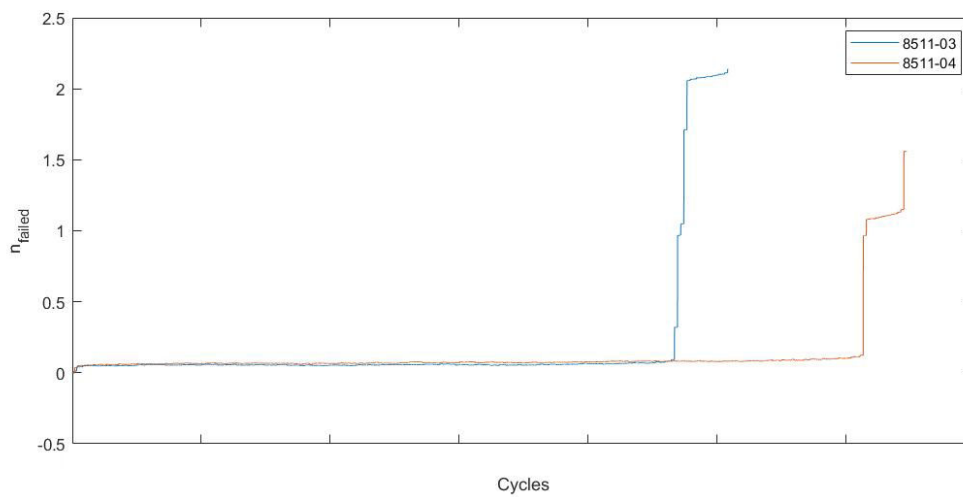Figure D.3: Calculated number of failed struts as function of cycles for 9-3mmØ specimens at 0.56 YTS

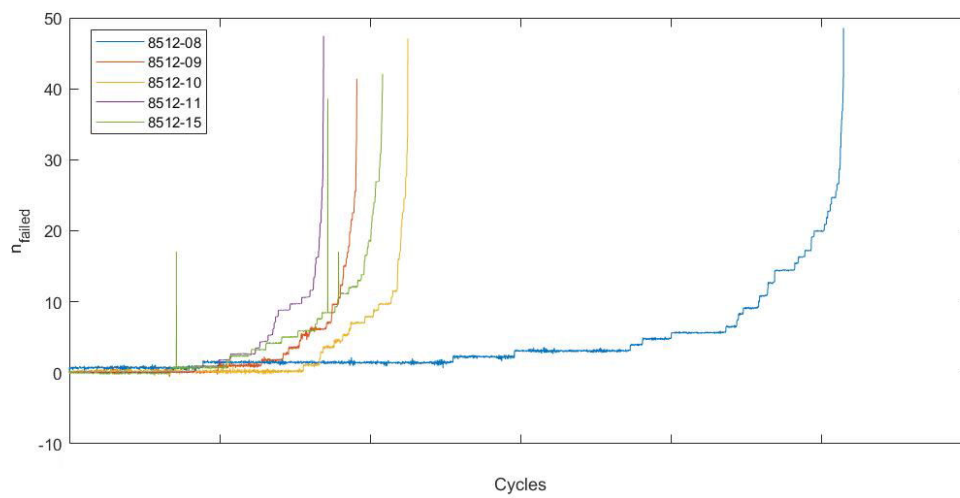Figure D.4: Calculated number of failed struts as function of cycles for 9-3mmØ specimens at 0.88 YTS

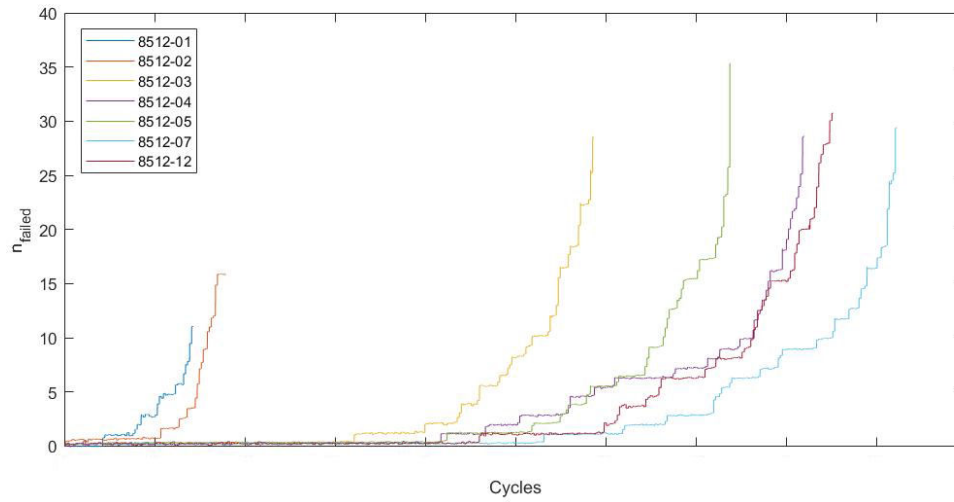Figure D.5: Calculated number of failed struts as function of cycles for 81-1mmØ specimens at 0.47 YTS

Figure D.6: Calculated number of failed struts as function of cycles for 81-1mmØ specimens at 0.63 YTS
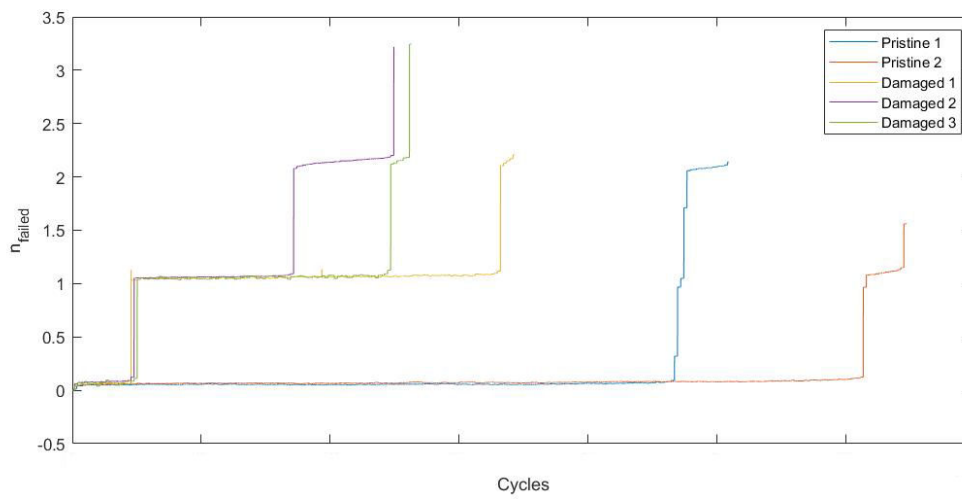

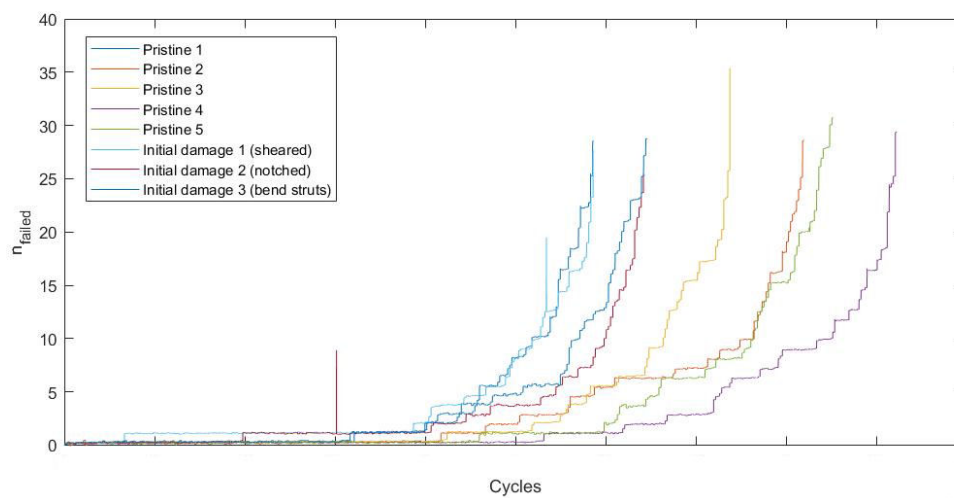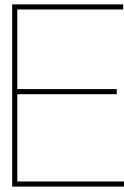Figure D.7: Calculated number of failed struts as function of cycles for 9-3mmØ with and without initial damage

Figure D.8: Calculated number of failed struts as function of cycles for 81-1mmØ with and without initial damage

E

MATLAB code

E.1. Cascading Damage

Input data points
```
% Input points to construct power law
Sinput = [160, 360];
Ninput = 10000*[40 50 55 80 100 ; 1.5 1.7 1.8 2 2.2];

% Data points for distribution and constant of the power law
DistrInput = 10000*[1.5 1.7 1.8 2 2.2].';
Sdistr = 360;
```

Model inputs
```
% Total amount of struts present
struts = 9;

% Amount of draws taken from the distribution
draws = 81;

% Test start stress level
Stest = 200;

% Ultimate tensile strength
UTS = 800;

% Number of samplings
M = 1000;
```

Crack growth inputs
```
includegrowth = true;

% Diameter and initial crack length
d = 9/sqrt(struts);
a0 = 0.5;

% Paris law parameters
Cparis = 6.0*10^-10;
m = 2.2;
```

Determine fatigue life distribution and load levels

```matlab
% Mean  of inputs for power law
Nmean = mean(Ninput.');

% Basquin relation from the mean input points
% Exponent
b = (log(Sinput(2))-log(Sinput(1)))/(log(Nmean(1))-log(Nmean(2)));

% Scale input distributed data to current input load
Ncorr = ((Sdistr/Stest)^(1/b))*DistrInput;

% Fit probability distribution
pd = fitdist(Ncorr,'wbl');

% Determine stress levels
S = ones(1, struts)*Stest;
for i = [1:struts]
    S(i) = S(i)*struts/(struts-i+1);
end

% Determine index of struts for UTS failure
Fail = find(S < UTS, 1, 'last' );
if isempty(Fail)
    Fail = 1;
end
```

Loop for M samplings

```matlab
% Outputs
Noutput = zeros(1,M);
GPoutput = zeros(1,M);
GRoutput = zeros(1,M);
events = zeros(M,Fail);
growthout = zeros(1,M);

for k = [1:M]
```

Construction of random variable matrix

```matlab
    % New matrix and first column with distributed fatigue life values
    Nmat = ones(draws,struts);
    Nmat(:,1) = random(pd,[draws,1]);

    % Remove negative lifes
    for l = [1:draws]
        if Nmat(l,1) < 0
            Nmat(l,1) = 0;
        end
    end

    % Modify matrix for multiple struts and multiple draws
    % Take lowest value of a certain set at every level and make integer
    sectionsize = fix(draws/struts);
    for i = [1:struts]
        Nmin = min(Nmat(((i-1)*sectionsize + 1):(i*sectionsize),1));
        Nmat(i,1) = Nmin;
    end
```

```
% Resize matrix
Nmat = Nmat(1:struts,:);

% Complete matrix by scaling to stress levels with basquin law
for i = [1:struts]
    for j = [2:struts]
        Nmat(i,j) = (S(1)/S(j))^(1/b)*Nmat(i,1);
    end
end
```

Additional parameters

```
N = 0;
level = 1;
D = zeros(struts,1);
growth = 0;
```

Loop for strut failures

```
while level <= Fail
    % Calculate min remaining life at this S per strut
    [nrem, index] = min(Nmat(:,level).*(ones(struts-level+1,1)-D));

    % Remove failed strut from model
    Nmat(index,:)= [];
    D(index) = [];

    % Add growth
    Ngrowth = Growth_Function(a0,d,S(level),Cparis,m);
    growth = growth + Ngrowth;
    nrem = nrem + includegrowth*Ngrowth;

    % Update D
    D = D + nrem*ones(struts-level,1)./Nmat(:,level);
    for i = [1:struts-level]
        if Nmat(i,level) <= 0
            D(i) = 1;
        end
    end

    % Add failure event
    if level ==1
        events(k,level) = nrem;
    else
        events(k,level) = events(k,level-1) + nrem;
    end

    % First failure
    if level == 1
        nremfirst = nrem;
    end

    % Add minimum remaining life to n, load level up
    N = N + nrem;
    level = level + 1;
end
```

Output

```matlab
    GP = N - nremfirst;
    GR = GP/N*100;

    % Add to lists
    Noutput(k) = N;
    GPoutput(k) = GP;
    GRoutput(k) = GR;
    growthout(k) = growth;

end
```

Process outputs to single mean (and std)

```matlab
% Final mean and std of outputs
Nf = mean(Noutput);
stdNf = std(Noutput);
GPf = mean(GPoutput);
GRf = mean(GRoutput);

% Total growth life output
Totgrow = mean(growthout);

% Mean of all failure events
meanevents = mean(events,1);
meanevents = [0 meanevents];
```

E.2. Crack Growth

```matlab
function N = Growth_Function(initial, diameter, maxstress,C,m)
```

Basic parameters

```matlab
    a = initial/1000;   %m, initial crack size
    b = diameter/1000;   %m, diameter of first analysed strut
    af = b;   % final crack size equal to full diameter

    % Stress amplitude
    S = 0.9*maxstress;       % MPa
```

Determine crack growth life

```matlab
    N = 0;

    % Loop
    while a < af
        % determine beta and K
      beta = (0.92*(2/pi)*sec(pi*a*0.5/b)*sqrt(tan((a*pi*0.5/b)/(0.5*pi*a/
b))))*(0.752+1.286*(0.5*pi*a/b)+0.37*(1-sin(0.5*pi*a/b))^3);
        K = beta*S*sqrt(pi*a);

        % growth rate
        da = C*K^m;

        % Update
        a = a+da;
        N = N+1;
    end

end
```